ROMA TRE
UNIVERSITÀ DEGLI STUDI

DOCTORATE IN APPLIED ELECTRONICS

XXIX OF DOCTORATE CYCLE

GNSS-based High integrity Positioning Systems for Railway Applications

PhD student Pietro Salvatori Pietro Salvatori

signature

Tutor Prof. Alessandro Neri

signature

Coordinator Prof. Enrico Silva

signature

ABSTRACT (ITALIAN VERSION)

Sistemi di Posizionamento ad Alta Integrità basati su GNSS per Applicazioni Ferroviarie

Il sistema di segnalamento è una delle componenti fondamentali del mondo ferroviario. I suoi compiti principali, infatti, sono la mitigazione delle problematiche che possono sorgere a causa di errore umano e l'allocazione della risorsa ferroviaria [1]. In Europa, per rispondere a tali necessità, è stato sviluppato lo standard di segnalamento ERTMS/ETCS (European Railway Traffic Management System/European Train Control System) [2]. Nel contesto ETCS, possono essere individuati tre livelli distinguibili in termini di livello di automazione: L1, L2 e L3. Una quarta situazione, chiamata ETCS Livello 0, si presenta nel caso in cui un treno compatibile con ETCS opera su una linea non equipaggiata con tale sistema. Allo stato attuale, solamente L1 e L2 sono operativi, mentre L3 è stato solamente concettualizzato. La principale differenza fra L1 e L2 è il canale di comunicazione fra sistema di controllo e la flotta ferroviaria. Per quanto riguarda la gestione del traffico, la linea viene suddivisa in sezioni chiamate blocchi, con l'assunto che un blocco non può essere occupato da più di un treno alla volta. Sia L1 che L2 si basano sull'approccio a "blocco fisso", una strategia che prevede blocchi di lunghezza fissa. Per determinare se un blocco è occupato da un treno, il sistema utilizza i circuiti di binario. La principale novità che verrà introdotta da L3 è una strategia di gestione del traffico più efficiente chiamata "blocco mobile". Questo approccio prevede la variazione dinamica delle lunghezze di blocco.

Questo lavoro di tesi riguarda lo studio di come la piattaforma ERTMS possa trarre beneficio dai sistemi di navigazione satellitare. Grazie a questa tecnologia, è possibile ridurre i costi di manutenzione e di esercizio. L'architettura di sistema prevede tre segmenti:

1. Segmento spaziale
2. Segmento di terra
3. Segmento utente

Il segmento spaziale include tutti i satelliti GNSS e SBAS. Il segmento di terra è costituito dalla rete di augmentation ed il segmento utente è rappresentato dalla flotta ferroviaria. Questo lavoro di tesi prevede lo studio sia di aspetti teorici legati alla navigazione satellitare che l'analisi di problematiche tipiche dell'ambiente e delle applicazioni ferroviarie. Il filone teorico ha avuto per oggetto principalmente il segmento di terra, con particolare riguardo all'augmentation ed al monitoraggio dell'integrità. Infatti, a causa degli stringenti requisiti che devono essere rispettati, un posizionamento standalone potrebbe non essere sufficiente a garantire le performance richieste. I moduli funzionali di augmentation e di monitoraggio dell'integrità assumono dunque un'importanza fondamentale nel sistema. Durante questo periodo di ricerca, sono state studiate architetture di reti e tecniche di monitoraggio dell'integrità. Per quanto riguarda lo studio delle problematiche legate al campo ferroviario, particolare enfasi è stata posta sul segmento utente. Il primo utilizzo di un sistema di controllo ferroviario basato su GNSS è la stima della posizione del treno lungo la linea (chilometrica progressiva). Questa operazione, come detto in [1], può essere effettuata tenendo in conto il fatto che il treno è vincolato a muoversi lungo una linea (i.e. il binario). In presenza di binari multipli, il processo di discriminazione del binario può essere separato dal processo di stima della chilometrica. In questo ambito, il focus principale della ricerca è lo studio di tecniche per determinare quale sia il binario occupato dal treno. Un altro aspetto importante descritto in questa tesi è la verifica dell'integrità del treno, una problematica importante che nasce se si considera l'introduzione di ETCS L3. In particolare, se per qualche motivo una porzione del convoglio si staccasse in una linea in cui sia in vigore l'approccio a blocco fisso, i circuiti di binario continuerebbero a rilevare la presenza di materiale rotabile nel blocco, dichiarandolo occupato. In questo modo, il treno che segue non entrerà nel blocco e non avverrà alcuna collisione. Qualora la stessa situazione avvenisse in una linea in cui sia in vigore l'approccio a blocco mobile, non sarebbe presente alcun circuito di binario a rilevare la presenza della sezione sganciata. Per questo motivo, la variazione dinamica della lunghezza del blocco prevede che il treno sia in grado di verificare autonomamente la propria integrità. Lo studio della soluzione della verifica dell'integrità del treno è stata effettuata sia nel caso di singola costellazione che nel caso di multipla costellazione. La presenza di un ambiente a multipla costellazione è stato considerato al fine dell'integrazione sia coerente che incoerente, evidenziando le prestazioni ottenibili con ciascuna tecnica. Uno dei problemi chiave dell'ambiente ferroviario è la presenza di aree in cui i segnali GNSS sono no disponibili oppure sono troppo degradati per poter dar luogo ad una soluzione affidabile. Per essere in grado di

operare in tali aree, si deve ricorrere a sistemi alternativi. Nella sezione finale della tesi, vengono illustrati una serie di concetti teorici su come sia possibile sfruttare sensori esterni quali unità inerziali per fornire continuità al sistema.

ABSTRACT (ENGLISH VERSION)

GNSS-based High integrity Positioning Systems for Railway Applications

The signaling system is one of the most important component of the railway world. In fact, its main tasks are the mitigation of issues due to human error and the allocation of the railway resource [1]. In Europe, to answer such a need, the standard ERTMS/ETCS (European Railway Traffic Management System/European Train Control System) has been deployed [2]. In the ETCS framework, three main levels, distinguishable among themselves in terms of system automation, can be individuated: L1, L2 and L3. A forth situation referred as ETCS Level 0 arises when an ETCS compliant train is moving on a non ETCS line. Up to now, only L1 and L2 are in operation while L3 has been only conceptualized. The main difference between L1 and L2 is in the communication link between the train control system and the train fleet. Concerning the traffic management, the line is divided in sections called blocks with the assumption that one block may be occupied by no more than one train at once. Both L1 and L2 rely on the "fixed block" approach, a strategy that foresees blocks of fixed length. To determine if a block is occupied by a train, the system makes use of track circuits. The main novelty that will be introduced by L3 is a more efficient traffic management strategy called "moving block". This approach foresees the dynamical tuning of the block lengths.

This work of thesis deals with the study on how ERTMS can benefit from satellite navigation. Thank to this technology, it is possible to reduce maintenance and operational costs. The overall system architecture foresees three segments:

1. Space segment
2. Ground segment
3. User segment

The space segment includes all the GNSS and the SBAS satellites. The Ground segment is constituted by the augmentation network and the User segment is represented by the train fleet. This work of thesis foresees the study of theoretical aspects related to satellite navigation as well as the analysis of typical issues related to railway environment and applications. The theoretical track has been mostly focused on the ground segment of the train control system

and, particularly, on augmentation and integrity monitoring. In fact, due to the stringent requirements that must be fulfilled, a standalone positioning could be not enough to guarantee the required performance. The augmentation and the integrity monitoring are therefore key modules of the system. During this research period, network architectures and integrity monitoring techniques have been studied. The study of typical issues related to the railway field has been mostly related to the user segment. The first use of the GNSS based train control system is the determination of the train position along the line (progressive mileage). This operation, according to [1], can be done explicitly accounting for the fact that the train is constrained to lie on a line (i.e. the track). In presence of multiple tracks, the track discrimination process can be separated from the mileage estimation process. In this framework, the main focus of the research is the study of techniques to determine the track occupied by the train. Another important aspect described in this thesis is the train integrity assessment, an important issue that arises considering the introduction of ETCS L3. Particularly, if for any reason a portion of a convoy is decoupled in a line equipped with the fixed block approach, the track circuits will continue to detect the presence of rolling stokes on the block, labelling it as occupied. In this way, the train that comes after will not enter in the block and there will be no collision. If the same situation happened in a line equipped with the moving block approach, there would be no track circuits to detect the parted section of the train. For this reason, the dynamical tuning of the block length foresees that the train is able to assess its own integrity. The study of the solution for the train integrity assessment has been carried out for both single constellation and multi-constellation framework. The presence of a multi-constellation environment has been considered for both coherent and incoherent integration, highlighting the performance achievable with each technique. One of the key problems of the railway environment is the presence of areas where the GNSS signals are either not present or too degraded to be used to provide a reliable solution. To operate in such areas, alternative system must be used. In the final section of this thesis, it is depicted a theoretical background on how it is possible to exploit external sensors like inertial units to provide system continuity.

ACKNOWLEDGMENTS

The work presented in this thesis is the outcome of the activities carried out during my three years of Ph.D. course at the University of Roma TRE.

The first person I would like to thank is my supervisor, Prof. Alessandro Neri, for all the help, the guidance and the advices received both before and during my Ph.D. studies.

I thank Ing. Rispoli for all the advices and for the great lessons on the importance of the applied research.

A special thanks goes to all the RadioLabs team (Agostino, Alessia, Andrea, Cosimo, Maurizio, Veronica), great colleagues and first of all great friends.

I would like to thank Prof Campisi, Prof. Carli and Prof.ssa Pascucci as well as all the COMLAB staff (Anna Maria, Emanuele, Federica, Federico, Massimo, Pradip, Yiwei) for all the help, the advices and the support during this period.

I am also grateful to Dr. Hill and Dr. Bonenberg from Nottingham Geospatial Institute for supporting me during my visit in Nottingham.

I would like to thank Sogei R&D Group and Ing. Capua for the advices and for have provided some of the data used for the simulation.

LIST OF PUBLICATIONS

Part of the activities carried out in this three years research period have been published in:

- Neri, F. Rispoli, and P. Salvatori, "A CENELEC SIL-4 compliant approach for discriminating railway parallel tracks based on EGNOS-GALILEO receivers", ENC-GNSS 2014, Rotterdam, The Netherlands.
- V. Palma, P. Salvatori, C. Stallo, A. Coluccia, A. Neri and F. Rispoli, "Performance Evaluation in terms of Accuracy Positioning of Local Augmentation and Integrity Monitoring Network for Railway Sector", IEEE International Workshop on Metrology for AeroSpace, 2014, Benevento, Italy.
- P. Salvatori, A. Neri, C. Stallo, V. Palma, A. Coluccia, and F. Rispoli, "AUGMENTATION AND INTEGRITY MONITORING NETWORK AND EGNOS PERFORMANCE COMPARISON FOR TRAIN POSITIONING", EUSIPCO 2014, Lisbon, Portugal.
- Neri, F. Rispoli, P. Salvatori and A.M. Vegni, "A Train Integrity Solution based on GNSS Double-Difference Approach", ION GNSS+ 2014, Tampa, FL, U.S.A.
- Neri, R. Capua, and P. Salvatori, "High Integrity Two-tiers Augmentation Systems for Train Control Systems", ION Pacific PNT 2015, Honolulu, HI, U.S.A.
- Neri, F. Rispoli, and P. Salvatori, "An analytical assessment of a GNSS based train integrity solution in typical ERTMS level 3 scenario", ENC 2015, Bordeaux, France.
- P. Salvatori, A. Neri, C. Stallo, and F. Rispoli, "Ionospheric Incremental Delay Models in Railway Applications", IEEE International Workshop on Metrology for AeroSpace, 2015, Benevento, Italy.
- A. Neri, F. Rispoli, P. Salvatori, “The perspective of adopting the GNSS for the evolution of the european train control system (ERTMS): a roadmap for standardized and certifiable platform“, ION GNSS+ 2015, Tampa, FL, U.S.A
- Neri, A.; Rispoli, F.; Salvatori, P., " A GNSS based solution for supporting virtual block operations in train control systems," IAIN 2015, 2015, 20-23 Oct. 2015
- A. Neri, S. Sabina, R. Capua, P. Salvatori, "Track Constrained RTK for Railway Applications", ION GNSS+ 2016, Portland, OR, U.S.A

CONTENTS

LIST OF FIGURES

LIST OF TABLES

LIST OF ABBREVIATIONS

Acronym	Description
AL	Alert Limit
ARAIM	Advanced RAIM
CHAIN	Cardinal Heading Aided Inertial System
COTS	Commercial Over The Shelf
DGNSS	Differential GNSS
DGPS	Differential GPS
DOP	Dilution Of Precision
ECEF	Earth Centred Earth Fixed
EGNOS	European Geostationary Navigation Overlay System
ENU	East North Up
ERTMS	European Railway Traffic Management System
ETCS	European Train Control System
GDOP	Geometric DOP
GNSS	Global Navigation Satellite System
GPS	Global Positioning System
GRA	Grande Raccordo Anulare
HDOP	Horizontal DOP
HFR	Hazardous Failure Rate
HMI	Hazardous Misleading Information
HMM	Hidden Markov Model
IMU	Inertial Measurement Unit
INS	Inertial Navigation System
IPP	Ionospheric Pierce Point
LAAS	Local Area Augmentation System
LDS	Location Determination System
LOS	Line Of Sight
MA	Movement Authority
MI	Misleading Information
OBU	On Board Unit

PDOP	Position DOP
PL	Protection Level
PPS	Precise Positioning Service
PTC	Positive Train Control
RAIM	Receiver Autonomous Integrity Monitoring
RBC	Radio Block Centre
RCM	Range Comparison Method
RS	Reference Station
RTK	Real Time Kinematic
SBAS	Satellite Based Augmentation System
SPS	Standard Positioning Service
SRM	Staff Responsible Mode
TAAN	Track Area Augmentation Network
TALS	Track Area Location Server
TDOP	Time DOP
TTA	Time To Alarm
URA	User Ranging Accuracy
URE	User Range Error
VDOP	Vertical DOP
WAAS	Wide Area Augmentation System
WMS	Wide area Master Station
WRS	Wide area Reference Station
WSN	Wireless Sensor Network

1 INTRODUCTION

In the transportation framework, one of the key point is represented by the precision localization. In the state of the art, there are many solutions and algorithms developed and standardized for the aeronautic field. Moreover, in the recent years some studies have been carried out on the possibility to extend such promising techniques also in the railway field. In this section, the framework, the key problems in the railway sector and the hint of the work will be presented, finally the thesis outline will be drawn.

1.1 FRAMEWORK

The object of this thesis is the study of solutions and algorithms for the high safety train localization systems. When it is referring to the railway environment, the main focus is the train control system. In fact, this entity plays one of the major role by ensuring the safety and by managing the traffic. In this way it is possible to grant an efficient access to the rail resource. As in [1], the main tasks of the signaling system are the allocation of the railway network resources and the mitigation of all those issues coming from human errors. Around the world, several train control systems have been developed and deployed; these systems are often based on national standard and this can create issues on the interoperability and on the cross-border traffic. In fact, if a convoy travels across three countries which have three different national train control standards, the train will have to be compliant with all those three systems. In Europe, to facilitate the operations they decided to create a unique standard known as ERTMS/ETCS (European Railway Traffic Management System/European Train Control System) [2]. Furthermore, this standard has been adopted by several countries even outside the European Union. In the ETCS framework there are three main levels distinguishable among themselves in terms of system automation. These levels are referred respectively as L1, L2 and L3. Beside these three levels, the situation under which an ETCS compliant train is moving on a non ETCS line is referred as ETCS Level 0. At this moment, only L1 and L2 are actually operational while L3 has only been conceptualized. The paradigms of L1 and L2 are depicted in Figure 1. L1 and L2 look very similar, the main difference between them is the communication link between the train control center and the fleet. In L1, the communications are realized by means of physical devices called Balises (known as “Eurobalises®”) deployed along the track while in L2 communications are performed by means of radio links. In order to

be able to move, the train must receive a MA (Movement Authority), a message containing data about the permission to proceed, maximum allowed speed, the next breaking point and so on; these instructions are then shown to the driver that has to follow them. In case of human error, the ride can be automatically corrected by the train system (e.g. slow down if exceeding the speed limit). As over-mentioned, the main novelty carried by L2 is the introduction of the radio link communication. In fact, the main limitation of L1 is that, despite the high safety standard that can be achieved, the efficiency of the rail resource management is lowered by effect of the discontinuous communication channel. An exemplum of such an issue can be found in [3]: "Let us look at this exemplum: the train has received a Moving Authority that states that next signal is red and so the driver expecting to stop the train before the signal reducing the speed; in the meanwhile the signal has come to green but the driver doesn't know this event until he has the signal in sight. This means that he can't increase the speed until the train catches a new balise obtaining the new moving authority". By having introduced a continuous communication channel, L2 has removed the bottleneck due to the latency of information. The main limitation in the traffic management under L2 is the so called “fixed block” approach. This approach foresees the partitioning of the rails in a set of fixed length sections called blocks imposing that no more than one train can occupy one specific block at the same time. In this way, the minimum separation of two consecutives trains is determined; in fact, a train cannot enter in a block until the previous train has cleared it. When L3 will have been introduced, also this limitation will be canceled out. In fact, L3 paradigm, shown in Figure 2, relies on the dynamical block length tuning according to the traffic and the line conditions. In this way it is possible to implement a more efficient resource access protocol. However, this approach (that is called “moving block”) requires a new method to determine the track occupancy.

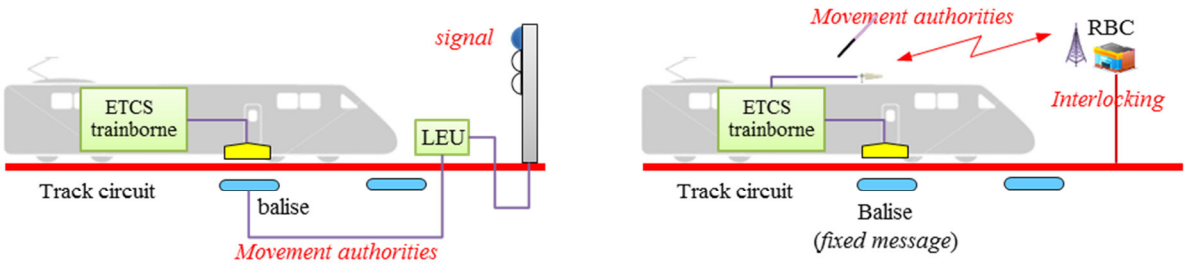

ETCS L1: On line signals, track circuits, via balises communications

ETCS L2: cabin signalling, track circuits, radio communications

Figure 1. ETCS L1 and L2 paradigms

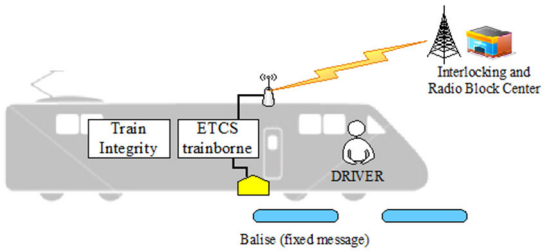

ETCS L3: cabin signalling, on-board train integrity assessment, radio communications

Figure 2. ETCS L3 paradigm

Nowadays, each block is equipped with track circuits, a well consolidated technology that is able to detect the presence of rolling stocks in a specific section. This technology fits perfectly with the fixed block approach, but its lack of flexibility doesn't allow the dynamical tuning of the block length. One possible solution is represented by the virtualization of the track circuit as authors have proposed in [4]. While working with L2 the track circuits can identify which block the train is lying on, developing the virtual track circuit, the main problem is to guarantee the safety in case of decoupled carriages occupying the track. In other words, one of the key functionalities offered by L3 is the so called "train integrity" assessment. This aspect will be described in details in section 6. Furthermore, the ETCS system foresees that a train is taken in charge by the RBC (Radio Block Center) when the train passes through the first group of balises; this means that, at the start of mission, the convoy must run in SRM (Staff Responsible Mode), implying very low average speed and accelerations [5]. If we were able to define a procedure to automatically identify the occupied track when the train is still standstill in the station platform, we would be able to reduce the time consumed by the start of mission. This could mean a higher efficiency of the traffic management (and so a benefit for the stakeholders and operators) and a lower risk linked with the shorter time interval in which the train is running in SRM (and so it is subjected to possible human errors). These considerations will be explained in more details in section 5. The migration from the traditional circuitries and devices like the balises or the track circuits to their virtual counterparties is object of several studies. One of the technology widely studied in this application is represented by the satellite navigation. In fact, according to [6] and [7], the satellite positioning system (together with hybrid telecommunication networks) will replace the traditional systems in the ERTMS. By means of GNSS (Global Navigation Satellite System) technology, it will be possible to reduce the costs associated with the maintenance and the deployment of the devices itself. However,

designing GNSS-aided train positioning system there are several issues that must be taken into account as it will be shown in the following sections.

1.2 HINT OF THE WORK

This work deals with the introduction of the GNSS technology into the ERTMS framework. As anticipated in the previous section, thank to this step charge innovation it will be possible to reduce the costs without decreasing the safety level achieved by traditional system. The market slice addressed by such an innovation is quite huge if it is considered that a big amount of the railway length in Europe is constituted by local, regional and low traffic lines where the traditional systems based on traditional devices would not be cost effective. The main challenge designing a GNSS-based LDS (Location Determination System) is the fulfillment of the stringent requirements SIL-4 imposed by the CENELEC specifications [8],[9],[10],[11]. The importance of meeting the requirements is crucial because it will guarantee the interoperability between the new GNSS-based modules with the other subsystems already in operation without impacting on the system performance, safety characteristics and architecture [1]. Due to the high accuracy and integrity required by the system, it is not possible to rely exclusively on standalone GNSS positioning. It is important to exploit augmentation data coming from an external network of Reference Stations properly deployed. In literature, there are two main augmentation network: wide area augmentation network and local augmentation network. In the first categories it is possible to find the SBAS (Satellite Based Augmentation System), fully operational systems widely used in the aeronautical field. However current SBAS is not providing multi-constellation capabilities even if the future extendibility in that direction is doable. In the meantime, local area augmentation network deployed for various operations can guarantee high performance even if the cost of deployment of local area networks in order to cover all the European railway network could be very expensive. In [12], authors conceptualized an hybrid solutions to take advantage of benefits offered by both architectures creating a “two-tier” augmentation network. In parallel to augmentation information, integrity data are sent to the on-board fleet to inform the trains about the presence of one or more faulty satellites that have to be discarded. The overall reference architecture is depicted in Figure 3. More in details, the system is composed by three segments: space segment, ground segment and user segment.

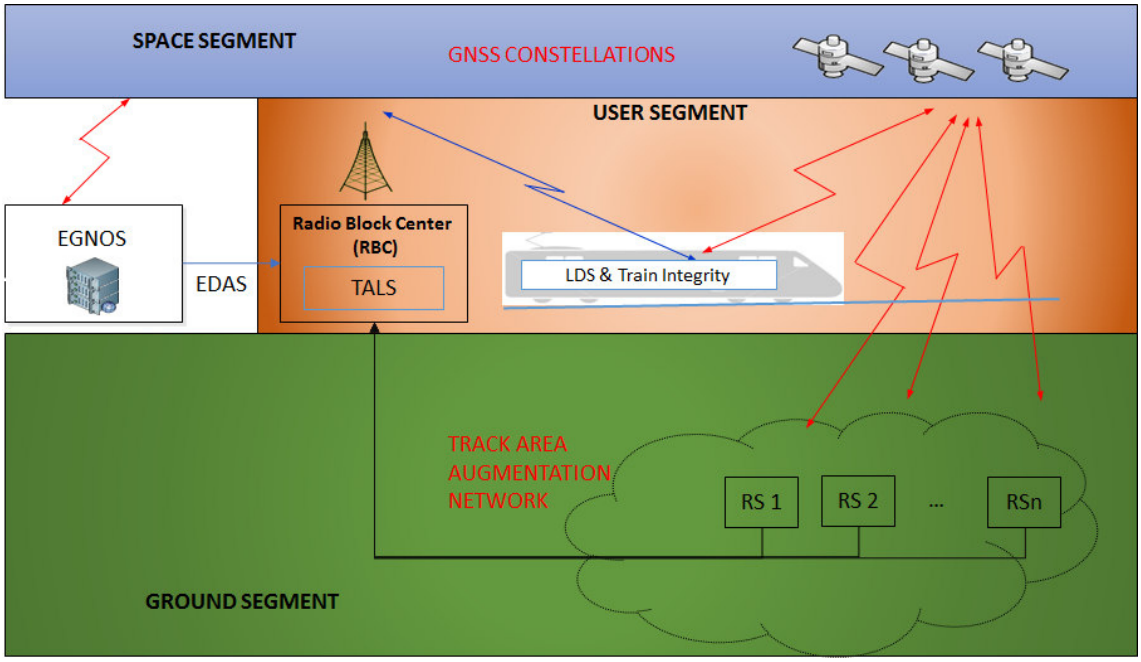

Figure 3. Reference Architecture

The space segment is constituted by the GNSS constellations as well as the geostationary satellites used for SBAS like EGNOS (European Geostationary Navigation Overlay System) in Europe. The Ground Segment is a dedicated Augmentation Network composed by a set of Reference Stations (RSs). The user segment is composed by the train fleet equipped with LDS On Board Units (OBUs) having in charge the position estimation as well as the train integrity assessment if required. The communications between the Ground Segment and the User Segment are performed by an entity called TALS (Track Area Location Server), a central unit that has in charge the data collection and processing. The TALS entity can be also part of the "two-tier" augmentation network having access to both data coming from the local network and from the SBAS system. Hint of this work of thesis is to review the system architecture focusing on both the ground segment and the user segment, analyzing algorithms and performance. Part of the results shown in this work have been published contributing to the state of the art in the train positioning sector.

1.3 Contribution and Thesis Outline

As introduced in the previous sub-sections, this work of thesis is inserted in the framework of the introduction of the GNSS technology into the train control system. The analysis carried out can be divided in two macroblocks: study of the satellite navigation

problems and study of specific problems that a train control system is devoted to solve. The activities carried out in the first group have been mostly focused on the analysis of augmentation and integrity monitoring approaches. The research focused on the study of the issues like the ionospheric delay modelling, the comparison between local and wide area architectures, the definition and the analysis of integrity monitoring algorithms and the design of a "2-tier" augmentation network. Moreover, I have had the opportunity to participate to most of the activities related to the on-field data acquisition. Concerning the on-board unit, my contribution has been mostly devoted on the study of typical railways situations like the track discrimination and the train integrity assessment. I contributed to the design and the validation of the approaches also by means of a simulator designed and developed in collaboration with the RadioLabs consortium. One of the main problems that must be faced designing a GNSS-based train control system is the lack of continuity of the ranging sources. Bridges, side walls, platform roofs and other obstacles can cover a portion of the sky, reducing the number of satellites in view. This situation is even worst in presence of tunnels were the sky is totally covered and there is no line of sight. An alternative navigation solution must be provided in those situations. During this research period, I had the opportunity to start the study of alternative navigation solutions, with particular emphasis on the inertial systems, and how it can be possible to use such technology in a railway environment. This part of the research has been carried out during my visit at the Nottingham Geospatial Institute (University of Nottingham) where I spent three months under the supervision of Prof. Hill. The thesis is organized in sections, each one describing a particular functionality of the system. Section 2 is dedicated to navigation principles and augmentation schemes. The aim of that section is to describe the problems related to satellite positioning and how it is possible to exploit reference stations to improve the performance. Both Local and Wide Area Augmentation schemes are presented and compared, leading to the definition of the "2-tier" augmentation network. Section 3 illustrates the integrity monitoring aspects describing all the activities carried out in that field. Algorithm design and performance assessment is presented for different approaches. Finally, a procedure to verify the Reference Station healthiness is analysed. Section 4 describes the train positioning aspects. The basic assumptions made in this section is the presence of one single track and the rigid body model used for the train. The approaches described in this chapter represent the state of the art in on board unit before the start of my Ph.D. program. I have partly contributed to the work presented in this section during a research period at RadioLabs consortium from May 2013 to December 2013. In section 5, the hypothesis of single track is

removed describing techniques to determine on which track the train is lying on. This functionality is crucial in the start of mission phase. Section 6 is devoted to the train integrity assessment. In this section, an approach to determine whether the train carriages are still coupled is presented. Performance analyses are carried out for single constellation and multi-constellation analysing both coherent integration and incoherent integration among the detectors. Section 7 introduces the multi-sensor platform. This section deals with the problem of operation in areas where the GNSS coverage is poor and therefore an alternative backup solution must be taken into account. The studies described in this section has been made during my visit at Nottingham Geospatial Institute. Finally, section 8 draws the conclusions and presents some future activities that can be carried out.

2 AUGMENTATION NETWORK ARCHITECTURES

In this section, the Stand Alone GNSS positioning as well as the differential GNSS techniques are introduced. Later on, the main augmentation network architectures are described. The performance analysis and assessment is presented and finally the "2-tier" augmentation network is introduced as the next frontier of the augmentation systems.

2.1 SINGLE CONSTELLATION STAND ALONE POSITIONING AND ERROR SOURCES

When GPS became operational in about 1990, the provided accuracies depended on the positioning used. Particularly the civilian users had access to the SPS (Standard Positioning Service) with a provided accuracy of about 100 meters (in that period the Selective Availability were still active) while the authorized users (typically military purposes) had access to the PPS (Precise Positioning Service) with a provided accuracy between 10 and 20 meters (95 percentile level) [13]. The receiver performs ranging measurements on the spread-spectrum signals transmitted by the satellites. Let t^i be the measured travel time of the signal from the i-th satellite to the user. The pseudorange ρ^i can be defined as the conversion of the travel time in meters:

$$\rho^i = t^i \cdot c \tag{1}$$

Where c represents the signal propagation speed (*i.e.* speed of light in the vacuum). ρ^i differs from the true range r^i because of several phenomena that affects the t^i measurement process [13]. The pseudorange measurement from the i-th satellite to the n-th receiver at the k-th epoch can be written as:

$$\rho_n^i[k] = r_n^i[k] + c\left(\delta t_n[k] - \delta t_i^{sat}[k]\right) + c\Delta\tau_{i,n}^{ion}[k] + c\Delta\tau_{i,n}^{trop}[k] + \upsilon_n^i[k] \tag{2}$$

Where:

$\rho_n^i[k]$ is the measured pseudorange for the i-th satellite by the n-th receiver at the k-th

epoch;

$r_n^i[k]$ is the true range between the i-th satellite and the n-th receiver at the k-th epoch;

$\delta t_n[k]$ is the n-th receiver clock offset at the k-th epoch;

$\delta t_i^{sat}[k]$ is the clock offset of the i-th satellite at the k-th epoch;

$c\Delta\tau_{i,n}^{ion}[k]$ is the ionospheric incremental delay on the Line of Sight between the i-th satellite and the n-th receiver at the k-th epoch;

$c\Delta\tau_{i,n}^{trop}[k]$ is the tropospheric incremental delay on the Line of Sight between the i-th satellite and the n-th receiver at the k-th epoch;

$\upsilon_n^i[k]$ is the error on the Line of Sight between the i-th satellite and the n-th receiver at the k-th epoch that has not been explicitly expressed. This term contains the receiver thermal noise, multipath, interferences and so on.

A receiver interested on estimating its own position will perform the so called PVT (Position Velocity and Time) estimation. Analysing more deeply the over mentioned components it is possible to identify some of the error sources that can affect the pseudorange measurement.

TRUE RANGE

The term related to the true range between the satellite and the receiver is one of the key elements of the estimation. It actually depends on both the receiver position (the one that is object of estimation) and the satellite position. The position of the space craft is retrieved by the ephemeris broadcasted by the satellite by means of an orbital propagator [13],[14]. For sake of compactness, the time dependency of the quantities is neglected.

$$r_n^i = \left\| \mathbf{X}_n - \mathbf{X}^i \right\| = \sqrt{\left(x_n - x^i\right)^2 + \left(y_n - y^i\right)^2 + \left(z_n - z^i\right)^2} \tag{3}$$

Where the tern $\mathbf{X}_n = \left(x_n, y_n, z_n\right)$ represents the unknown receiver position at the reception time epoch while the tern $\mathbf{X}^i = \left(x^i, y^i, z^i\right)$ represents the satellite position at the transmission time.

Receiver Clock Offset

The receiver clock offset cannot be predicted with a sufficient accuracy. According to [13], user clocks have stability of one part in 10^7. Anyway, this quantity can be estimated by the pseudorange measurements leading the number of required equation to four.

Satellite Clock Offset

The satellite clock offset can be estimated by means of parameters broadcasted by the satellites. The receiver clock bias is about 1.5 meters [13].

Ionospheric Incremental Delay

The ionosphere delays the signal in space by as much as 30 meters (this value is evaluated according the worst-case scenario of solar storm and solar maximum, in the afternoon and at low elevation angle) [13]. Typical value of the ionospheric incremental delay is between 4 and 10 meters. About 50% to 75% of this error can be removed by using standard model [13],[15]. Moreover, adverse space weather can cause ionospheric storm which can introduce large pseudorange errors [16]. Due to the importance of the impact of the ionosphere, this aspect will be described in more details in section 2.6.

Tropospheric Incremental Delay

The tropospheric effect is related to the index of refraction of the lower atmosphere. A simple model can predict most of the effect even if the unmodelled error can reach 2 to 3 meters at about 5 degrees elevation [13].

Error Budget

Table 1 summarizes the pseudorange errors in a standalone GPS solution. As it is possible to see, most of the errors are biases that can be drastically reduced by using a reference station.

Table 1. Pseudorange Error in Standalone GPS

Source	Bias errors [m]	Random errors 1-σ [m]
Ephemeris Data	4.0	0.0
Satellite Clock Data	1.5	0.7
Ionosphere	4.0	0.0
Troposphere	0.0	0.5
Multipath	0.0	1.0
User Receiver	0.0	1.5

The reference station can be used in a Differential GNSS positioning mode or in Relative positioning mode. The first approach uses the reference station to estimate the slowly varying components of the errors broadcasting them as corrections [13]. In the relative positioning approach, the reference station (called Master) provides its own raw measurements (i.e. pseudorange or carrier phase cycles) to allow the rover to estimates the baseline between itself and the Master. This approach requires a communication link that is able to transfer all the required data. In both approach all the biases introduced by the satellite are cancelled out; moreover, by using the double difference technique (in the relative positioning scheme) it is possible to cancel out also the common mode errors introduced by the reference and the user receivers. In addition to these benefits, the use of a reference station located near to the user can strongly reduce the impact of the local effect such as the atmospheric incremental delays.

SINGLE EPOCH STANDALONE POSITIONING

When the receiver is performing the PVT estimation, it has to solve a system in four unknowns. If the number of observed satellite is higher than four, the surplus equations can be used to increase the system performance. Typically, a single epoch estimator performs a LSE (Least Squares Estimation) trying to minimize the sum of the squares of the errors on the single equation solutions. In practice the goal is to solve a linearized equation system with respect to an approximated receiver position $\underline{\mathbf{X}}_r = \begin{pmatrix} X_r & Y_r & Z_r \end{pmatrix}^T$.

Let $\Delta\rho_n^i[k]$ be the reduced pseudorange defined as:

$$\Delta\rho_n^i[k] = \rho_n^i[k] - \hat{r}_n^i[k] + c\delta\hat{t}_i^{sat}[k] - c\Delta\hat{\tau}_{i,n}^{ion}[k] - c\Delta\hat{\tau}_{i,n}^{trop}[k] \quad (4)$$

Where:

$\rho_n^i[k]$ is the measured pseudorange for the i-th satellite by the n-th receiver at the k-th epoch;

$\hat{r}_n^i[k]$ is the estimated geometric distance between the i-th satellite and the n-th RS at the k-th epoch estimated by means of the navigation message and the receiver position (coordinates of the linearization point);

$\delta\hat{t}_i^{sat}[k]$ is the estimated clock offset of the i-th satellite at the k-th epoch by using the navigation message;

$c\Delta\hat{\tau}_{i,n}^{ion}[k]$ is the estimated ionospheric incremental delay on the Line of Sight between the i-th satellite and the n-th RS at the k-th epoch estimated by means of the klobuchar model;

$c\Delta\hat{\tau}_{i,n}^{trop}[k]$ is the estimated tropospheric incremental delay on the Line of Sight between the i-th satellite and the n-th RS at the k-th epoch estimated by means of the tropospheric model.

For sake of compactness the time dependency is removed in the following equations. The system is defined as follows:

$$\Delta\underline{\rho} = \mathbf{H}\underline{X} + \underline{\upsilon} \tag{5}$$

The known terms vector $\Delta\underline{\rho}$ is obtained by rearranging column-wise the reduced pseudorange measured by the i-th receiver:

$$\Delta\underline{\rho} = \left(\Delta\rho_n^1 \quad \Delta\rho_n^2 \quad \cdots \quad \Delta\rho_n^{N_{Sat}}\right)^T \tag{6}$$

The four component unknown vector $\underline{X}$ is composed by the corrections to be applied either to the linearization point coordinates and to the receiver clock offset. Each row of the design matrix $\mathbf{H}$ is composed by the three cosines of the line of sight between the satellites and the receiver plus a four component fixed and equal to 1.

$$\mathbf{H}=\begin{pmatrix} \frac{X_r-X^1}{\rho_r^1} & \frac{Y_r-Y^1}{\rho_r^1} & \frac{Z_r-Z^1}{\rho_r^1} & 1 \\ \frac{X_r-X^2}{\rho_r^2} & \frac{Y_r-Y^2}{\rho_r^2} & \frac{Z_r-Z^2}{\rho_r^2} & 1 \\ \cdots & \cdots & \cdots & \cdots \\ \frac{X_r-X^{N_{Sat}}}{\rho_r^{N_{Sat}}} & \frac{Y_r-Y^{N_{Sat}}}{\rho_r^{N_{Sat}}} & \frac{Z_r-Z^{N_{Sat}}}{\rho_r^{N_{Sat}}} & 1 \end{pmatrix} \tag{7}$$

The least square solution can be achieved as:

$$\hat{\underline{\mathbf{X}}}_n=\left(\mathbf{H}^T\mathbf{H}\right)^{-1}\mathbf{H}^T\Delta\underline{\rho} \tag{8}$$

DILUTION OF PRECISION

According to [17], the covariance matrix of the estimation is:

$$R_{\hat{\mathbf{X}}_n}=\frac{\hat{\underline{e}}^T\hat{\underline{e}}}{m-n}\left(\mathbf{H}^T\mathbf{H}\right)^{-1}=\hat{\sigma}_0^2\left(\mathbf{H}^T\mathbf{H}\right)^{-1} \tag{9}$$

Where $\mathbf{H}$ is the design matrix, m is the number of observation and n is the number of unknown and the error vector $\underline{e}$ can be represented as:

$$\underline{e}=\Delta\underline{\rho}-\mathbf{H}\hat{\underline{X}} \tag{10}$$

Either in the stand alone or differential positioning, $R_{\hat{\mathbf{X}}_n}$ is a positive defined 4 by 4 matrix. Such a value can be linked to the geometric configuration of satellites with respect to the user location. In fact, when the satellites are well spaced the carries more information in terms of the Fisher information matrix. Because the Fisher matrix is the inverse of the estimation covariance matrix, the better is the geometry the higher is the information and then the smaller is the covariance matrix. In fact, intuitively, a smaller covariance matrix represents a lower level of uncertainty on the estimation. Taking the covariance matrix of the least square problem, it can be written as:

$$R_{ECEF} = \begin{pmatrix} \sigma_x^2 & \sigma_{x,y} & \sigma_{x,z} & \sigma_{x,cdt} \\ \sigma_{y,x} & \sigma_y^2 & \sigma_{y,z} & \sigma_{y,cdt} \\ \sigma_{z,x} & \sigma_{z,y} & \sigma_z^2 & \sigma_{z,cdt} \\ \sigma_{cdt,x} & \sigma_{cdt,y} & \sigma_{cdt,z} & \sigma_{cdt}^2 \end{pmatrix} \tag{11}$$

The 3 by 3 matrix block related to the space coordinates can be converted in a ENU (Earth North Up) frame obtaining:

$$R_{ENU} = \begin{pmatrix} \sigma_e^2 & \sigma_{e,n} & \sigma_{e,u} \\ \sigma_{n,e} & \sigma_n^2 & \sigma_{n,u} \\ \sigma_{u,e} & \sigma_{u,n} & \sigma_u^2 \end{pmatrix} = \mathbf{F}^T \begin{pmatrix} \sigma_x^2 & \sigma_{x,y} & \sigma_{x,z} \\ \sigma_{y,x} & \sigma_y^2 & \sigma_{y,z} \\ \sigma_{z,x} & \sigma_{z,y} & \sigma_z^2 \end{pmatrix} \mathbf{F} \tag{12}$$

Where $\mathbf{F}$ is the transformation matrix defined as follows:

$$\mathbf{F} = \begin{pmatrix} -\sin\lambda & -\sin\varphi\cos\lambda & \cos\varphi\cos\lambda \\ \cos\lambda & -\sin\varphi\sin\lambda & \cos\varphi\sin\lambda \\ 0 & \cos\varphi & \sin\varphi \end{pmatrix} \tag{13}$$

In (13), φ and λ indicate respectively the latitude and latitude coordinates. The GDOP (Geometric DOP), PDOP (Position DOP), HDOP (Horizontal DOP), VDOP (Vertical DOP) and TDOP (Time DOP), the indicators that express the quality of the geometry of the system, are then defined as follows:

$$\begin{aligned} GDOP &= \sqrt{\frac{\sigma_e^2 + \sigma_n^2 + \sigma_u^2 + \sigma_{cdt}^2}{\sigma_0^2}} \\ PDOP &= \sqrt{\frac{\sigma_e^2 + \sigma_n^2 + \sigma_u^2}{\sigma_0^2}} \\ HDOP &= \sqrt{\frac{\sigma_e^2 + \sigma_n^2}{\sigma_0^2}} \\ VDOP &= \sqrt{\frac{\sigma_u^2}{\sigma_0^2}} \\ TDOP &= \sqrt{\frac{\sigma_{cdt}^2}{\sigma_0^2}} \end{aligned} \tag{14}$$

2.1.1 Observation Combinations

A linear combination of pseudorange measurement (concerning the carrier phase it is possible to define an equivalent relationship) can be defined as:

$$\rho_n^{i,comb} = \alpha\rho_n^{i,L1} + \beta\rho_n^{i,L2} \tag{15}$$

Where:

$\rho_n^{i,comb}$ is the measured pseudorange for the i-th satellite by the n-th receiver after combination;

$\rho_n^{i,L1}$ is the measured pseudorange for the i-th satellite by the n-th receiver on L1 frequency;

$\rho_n^{i,L2}$ is the measured pseudorange for the i-th satellite by the n-th receiver on L2 frequency;

α, β are the coefficients of the combination;

The coefficients for the most used observation combinations are shown in Table 2. The coefficients for the geometry free combination have opposite signs depending on whether it is evaluated on pseudoranges (code) or on carrier phase measurement due to the opposite impact of the ionosphere (phase anticipation and code delay).

Table 2. Coefficients of observation combinations

Combination Name	α	β
Iono-free	$f_1^2 / \left(f_1^2 - f_2^2\right)$	$-f_2^2 / \left(f_1^2 - f_2^2\right)$
Geometry Free (on code)	-1	+1
Geometry Free (on phase)	1	-1
Wide Lane	$f_1 / \left(f_1 - f_2\right)$	$-f_2 / \left(f_1 - f_2\right)$
Narrow Lane	$f_1 / \left(f_1 + f_2\right)$	$f_2 / \left(f_1 + f_2\right)$

2.2 MULTI-CONSTELLATION LEAST SQUARE SOLUTION

The analysis carried out in the previous paragraph is valid whichever constellation is used (apart from applying the proper orbital propagator and satellite clock model). However, when more than one constellation is used, there are three possibilities of data processing:

1) creating a unique hybrid virtual constellation containing all the satellites in view
2) performing position estimations constellation by constellation
3) performing position estimations by using subsets of satellites not necessarily belonging to the same constellation

In the first case (the most widely used), it is possible to increase the number of satellites used in the estimation algorithm increasing the availability [18]. Moreover, the accuracy is higher than in the single constellation case because of the better geometry of the system. This configuration will be referred as coherent integration because the data fusion is the pseudorange domain. The second situation, because the position estimation is performed separately constellation by constellation it is referred as incoherent integration. In fact, the data fusion is performed in the position domain. It is possible to demonstrate how this approach is less prone to integrity issues. In fact, in case of a not properly identified faulty satellite, by using the coherent integration its measurement will affect the entire system, while, by using the incoherent estimation, it will affect only the sub-estimation in which it is involved (i.e. a faulty GPS satellite will compromise only the GPS system, not the GLONASS or GALILEO ones). If more than two estimators are present it is possible to identify which subset contains the faulty one. The third case is a hybrid solution performing an incoherent integration of data obtained by a coherent integration. This situation will not be analysed in this work. When mixing satellites coming from different constellations in the pseudorange domain (so both in the first and in the third case) the bias between the different constellations must be taken into account. In fact, when performing a position estimation in a single constellation receiver, all the common mode errors for the entire constellation will affect only the receiver clock offset estimation. When considering two independent constellations, there is a bias called Inter Constellation Bias between them. From a mathematical point of view, this implies that for each new constellation used the number of unknown to be estimated in the LSE system is increased by one. Generalizing to the case of N independent constellations, there are $N-1$ biases to be taken

into account. Let $\mathbf{H}$ be the design matrix in the single constellation scenario defined by (7). For each constellation added, a new column must be added to $\mathbf{H}$. The i-th element of this new column will be 1 or 0 depending on whether the i-th satellite belongs to that constellation or not. To better understand such a configuration, let five be the number of satellites in view: satellites 1 to 3 belong to the first constellation and satellite 4 and 5 belong to the second one. In this case the design matrix $\mathbf{H}'$ will be:

$$\mathbf{H}' = \begin{pmatrix} \frac{X_r - X^1}{\rho_r^1} & \frac{Y_r - Y^1}{\rho_r^1} & \frac{Z_r - Z^1}{\rho_r^1} & 1 & 0 \\ \frac{X_r - X^2}{\rho_r^2} & \frac{Y_r - Y^2}{\rho_r^2} & \frac{Z_r - Z^2}{\rho_r^2} & 1 & 0 \\ \frac{X_r - X^3}{\rho_r^3} & \frac{Y_r - Y^3}{\rho_r^3} & \frac{Z_r - Z^3}{\rho_r^3} & 1 & 0 \\ \frac{X_r - X^4}{\rho_r^4} & \frac{Y_r - Y^4}{\rho_r^4} & \frac{Z_r - Z^4}{\rho_r^4} & 1 & 1 \\ \frac{X_r - X^5}{\rho_r^5} & \frac{Y_r - Y^5}{\rho_r^5} & \frac{Z_r - Z^5}{\rho_r^5} & 1 & 1 \end{pmatrix}$$

2.3 Differential GNSS and Augmentation Systems

2.3.1 Differential Positioning

In principles, a DGPS (Differential GPS) system, or more generally a DGNSS (Differential GNSS) system, exploit a local reference station located at a known position. This station is able to estimate the slowly varying components of the satellite range measurement errors and transmit them to the final user as corrections [13]. In Figure 4 it is shown the functional scheme of the DGNSS approach. The achievable performances are strongly influenced both by the distance between the user and the reference station and by the elapsed time between the correction generation and their use. These effects are respectively due to the spatial decorrelation and the temporal decorrelation of the range errors. According to [13] users located near the station can achieve accuracy of 2 to 8 meters. In essence, the Reference Station (called Master) knows its own location and then it is able to predict the geometric range between itself and the satellite. This range is not necessarily the true range because it is affected by the ephemeris error.

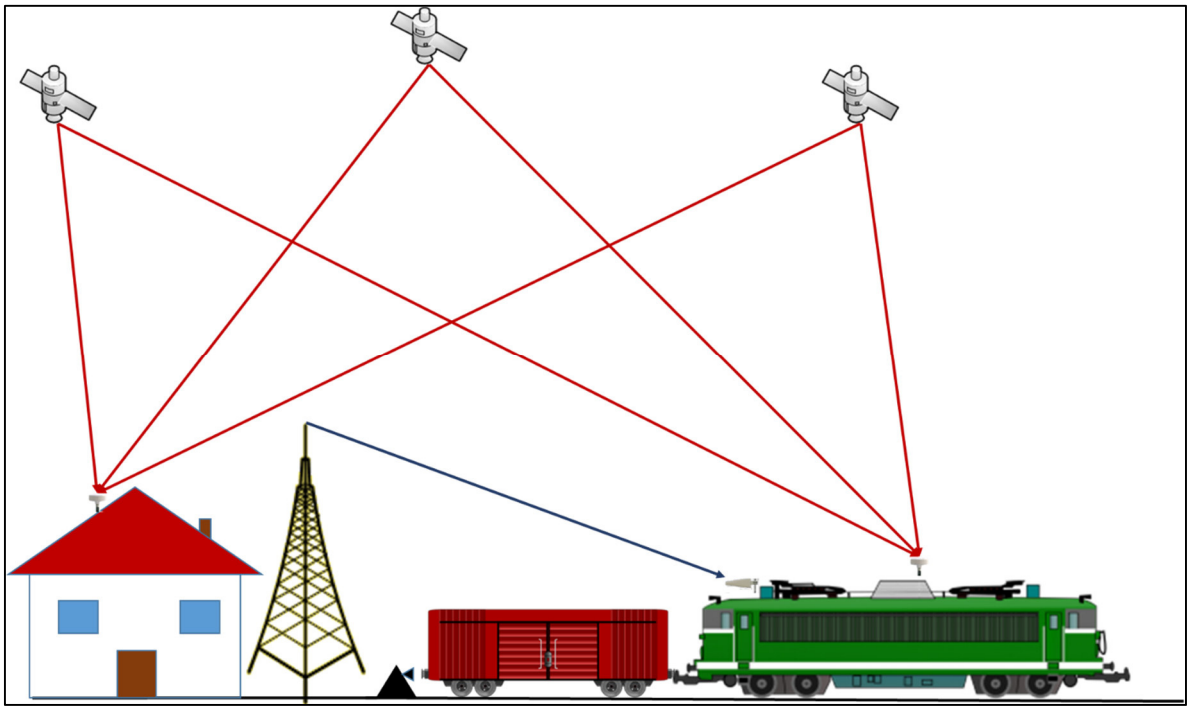

Figure 4. DGNSS principles

The differential correction for the i-th satellite $\Delta\tilde{\rho}_m^i$ is obtained as the difference between the expected range and the measured pseudorange:

$$\Delta\tilde{\rho}_m^i = \rho_m^i - \hat{r}_m^i = c\left(\delta t_m - \delta t_i^{sat}\right) + \psi_m^i \tag{16}$$

Where:

$\hat{r}_m^i$ is the estimated geometric distance between the i-th satellite and the Master estimated by means of the navigation message and the known receiver position;

ρ_m^i is the measured pseudorange for the i-th satellite by the Master;

δt_m is the clock offset of the Master;

δt_i^{sat} is the satellite clock offset of the i-th satellite;

ψ_m^i is the sum of atmospheric incremental delays and the other unmodelled components in the pseudorange domain;

The differential correction is then applied to the pseudorange measured by the Rover:

$$\rho_r^i - \Delta\tilde{\rho}_m^i = \hat{r}_r^i + c\left(\delta t_r - \delta t_i^{sat}\right) + \psi_r^i - c\left(\delta t_m - \delta t_i^{sat}\right) - \psi_m^i = \hat{r}_r^i + c\left(\delta t_r - \delta t_m\right) + \psi_r^i - \psi_m^i \quad (17)$$

As it is possible to see in equation (17), the corrected pseudorange is no more affected by the satellite clock offset and, if Master and Rover are close to each other (due to the high correlation of the atmospheric delays) is generally characterized by a smaller residual pseudorange error. Anyway the corrected pseudorange is affected by the difference of clock offset between Master and Rover. The DGNSS is the basis for the Local Area Augmentation system. According to [14], because the pseudorange errors may vary epoch by epoch, to enable the user to compensate for pseudorange error rate, the pseudorange rate correction may also be transmitted by the Master station. By multiplying this value for the temporal gap between the current time instant and the time in which the corrections have been issued, the user is able to compensate better the time variant component of the pseudorange error.

2.3.2 Local Area Augmentation Network

A Local Area Augmentation System (LAAS) is a local differential GPS system [19]. These kind of systems was born in the avionic sector. Particularly, its main task is to serve the precision approach in flight operations. The basic architecture foresees a set of GNSS receivers at known and surveyed location on the airport property. By using a radio data link, the reference measurement (or the corresponding corrections) are broadcasted to approaching aircrafts. By applying this information, the on board receiver can achieve sub-meter accuracy [19]. Together with the corrections, quality indicators and warns about any eventual system malfunctions can be broadcasted to grant the safety operation. The main architecture of a LAAS system is shown in Figure 5. Differently to SBAS, LAAS can be considered a DGPS system because it forms a single correction for each satellite (scalar corrections). In fact, the wide area systems, as it will be shown in the next paragraph, having more stations deployed in a large area, form multiple corrections for each satellite (vector corrections). Scalar corrections, are better for highly demanding application in local areas [19], because they can mitigate errors due to local effect that can be revealed only nearby the end user (i.e. the airplane that is going to land). In contrast, the vector ones are better for wide area coverage because they have the possibility to catch not only the local errors, but also their spatial gradients. The importance to have more than one reference receivers even in LAAS application is related to the redundancy; in fact, having more than one observation related to the same satellite it is possible to perform integrity checks to

detect faulty measurements before they can influence the broadcasted correction [19]. This consideration becomes crucial if it is considered the hypothesis of faulty Reference Station.

2.3.3 Wide Area Augmentation Network

A Wide Area Augmentation System (WAAS) is constituted by a ground network that is able to compute and to transmit GPS integrity and correction data to the user [20]. Moreover, in a SBAS (Satellite Based Augmentation System) those data are broadcasted by geostationary satellites whose signals can be used as additional ranging ones. The ground segment foresees a set of receivers, known as WRSs (Wide area Reference Stations), deployed in precisely known locations in a wide area region. WRSs monitor the GPS satellites and send their raw measurement to the WMSs (Wide area Master Stations). By jointly processing all these received measurements, the WMS is able to determine four corrections (three for satellite location and one or the clock offset) for each of the monitored satellites. Furthermore, the WMS can also estimate a set of corrections for the ionospheric delays. An integrity warning flag can be arisen in case of troublesome satellite detected. In essence, a WAAS system can improve accuracy in two main ways: by reducing the user pseudorange measurement error to approximatively 1 or 2 meters (1σ) and by adding new ranging signals that can improve the geometry.

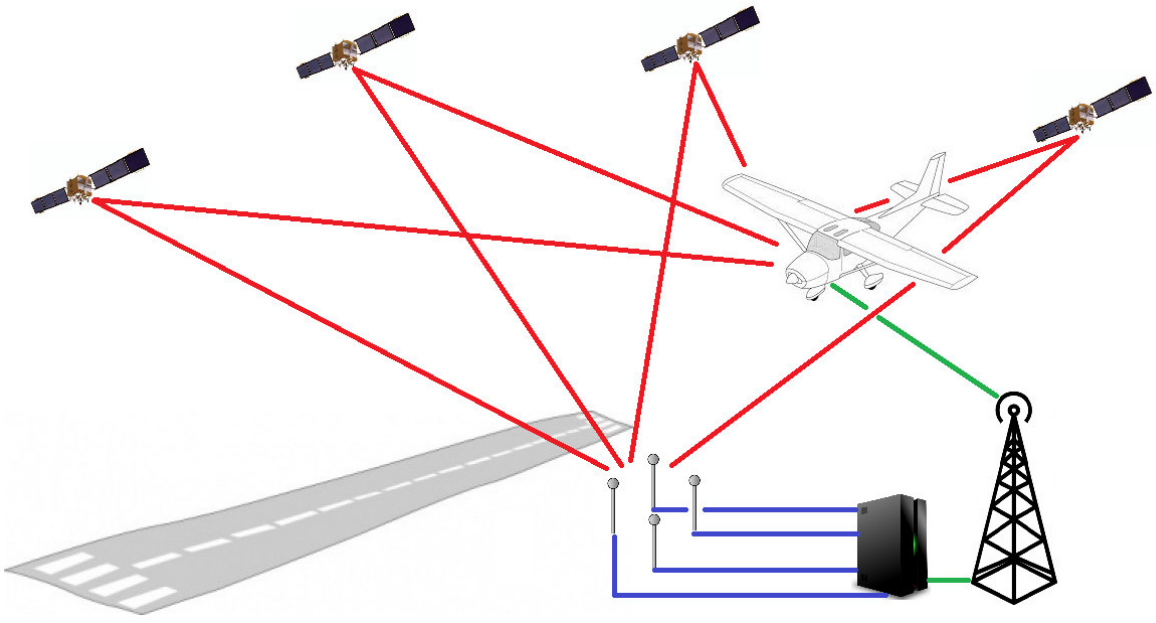

Figure 5. LAAS scheme

2.4 AIMN AND SBAS FOR TRAIN POSITIONING: PERFORMANCE ANALYSIS

As shown in section 1, the use of an external augmentation network is highly recommended to provide both accuracy and integrity. In [21], authors performed a comparison performance analysis between a LDS system that makes use of SBAS corrections and one that makes use of a proper local Area Integrity Monitoring Network (AIMN). As it has been shown in the previous subsections, the principle of a local area network relies in the high spatial correlation of the local errors; on the other hand, the wide area network is able to identify all those non-local issues in which a wider network can provide better analysis. To perform this analysis, it has been designed an architecture (shown in Figure 6) that is able to acquire data both from the local AIMN and from the SBAS system (i.e. EGNOS). More in details, the local network is realized by a set of Reference Stations equipped with COTS (Commercial Over The Shelf) GNSS receivers and a TALS that jointly process data coming from those stations. In parallel to this first entity, it has been designed an EGNOS adapter that is responsible to acquire the SBAS message and convert retrieved data in the same format of the local AIMN (i.e. differential correction). The last component of the ground segment is a switch to commutate between SBAS and AIMN mode. The train fleet is equipped with OBUs that exploit augmentation and integrity data to perform the PVT estimation. The presence of multiple independent chains in the OBU could be introduced to exploit the redundancy to mitigate integrity issues. The OBU section will be described in more details in section 4. In the performance assessment phase, the EGNOS message has been retrieved by EDAS (EGNOS Data Access Service), a service to provide EGNOS data on internet either in real-time or in post processing without the need of establishing a direct link with the geostationary satellites. This solution has the benefit to be usable in all those situations in which the signals are blocked or disturbed by interference. The limitation of using EDAS instead the ordinary satellite link is the non-possibility to exploit the SBAS signals for ranging purposes. The dataset used in the simulation has been acquired during a measurement campaign in Rome. There have been deployed two Reference Station each of them has been equipped with 2 receivers (NVS NV08C-CSM and U-BLOX NEO-6P) and two antennas (Tallysman TW-241O). To emulate a train travelling on route, a car moving along a highway equipped with the same devices of the reference has been used.

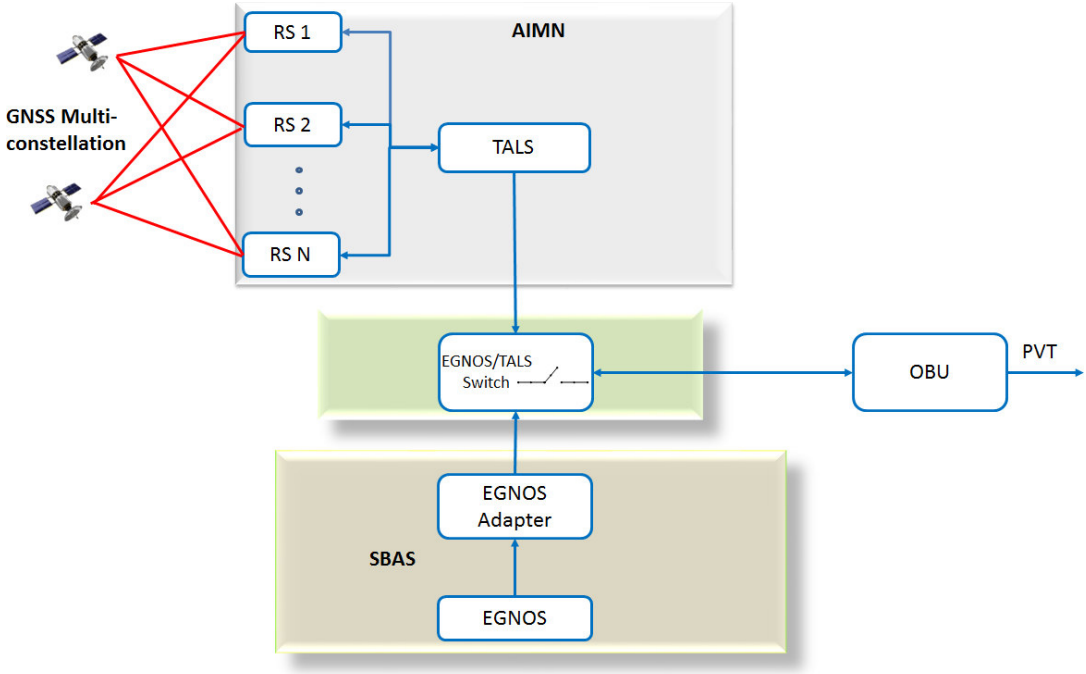

Figure 6. Hybrid Augmentation Network

In the simulations, the position (in terms of curvilinear abscissa of the track[1]) and speed errors have been respectively evaluated. To realize the GroundTruth a high grade GNSS multi-frequency and multi-constellation receiver has been adopted. Figure 7 shows the position estimate of the train w.r.t. the ground truth when using either AIMN data (above) or EGNOS corrections (below) to augment the position estimation. When using the wide area approach, the position error is generally lower than the case of the AIMN, except in some specific epochs where there are errors a little higher than the other case. Anyway, the local network has been implemented by using low cost components, so the positioning error obtained is completely in line with the expectations. As concern the speed analysis, the speed error trend is depicted in Figure 8. The speed computation has been obtained by exploiting the Doppler shift measurement provided by the receivers. Results described in this sections, encouraged the next step of hybrid augmentation network architecture that in [12] authors have called "2-tier" augmentation network. In authors perspective, the future integrity of ERTMS system will result from the integration of the evolved wide area networks together with the local area augmentation networks. In the next sub-section, the "2-tier" architecture will be described in more details.

[1] The position is estimated by taking into account the track constraint as it will be shown in section 4

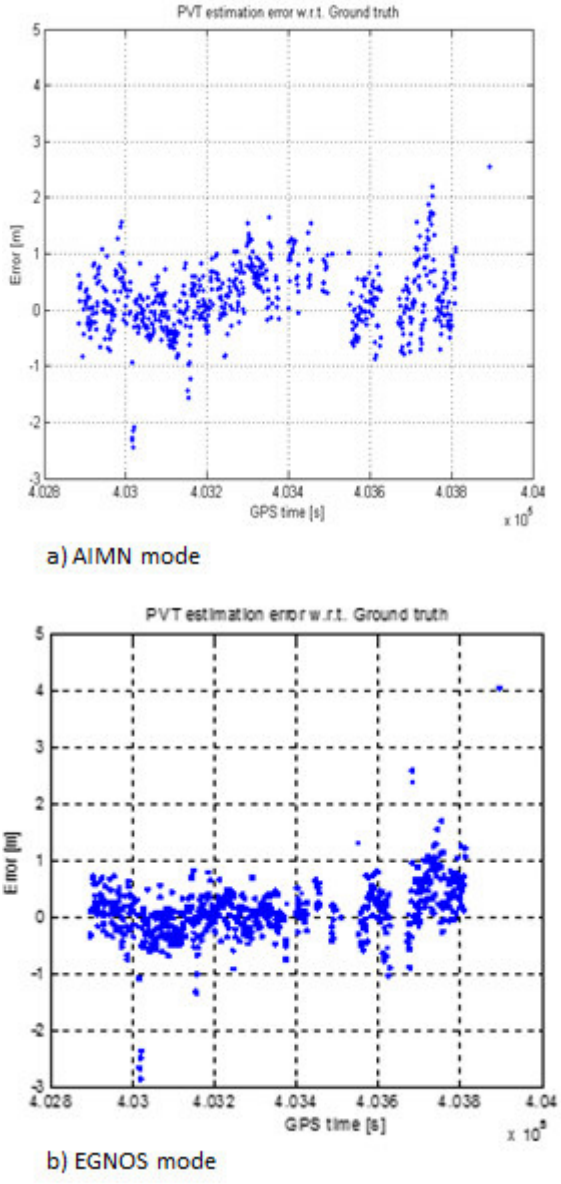

Figure 7. Position error w.r.t. GroundTruth AIMN vs. EGNOS

2.5 "2-TIER" AUGMENTATION NETWORK SCHEME

The "2-tier" augmentation network has been designed as a hybrid system that takes the benefit of having both a wide area augmentation system and a local augmentation network. According to [12], the first tier essentially consists of the evolved Wide Area Augmentation networks complemented with specific Applications for Railway. This layer provides integrity data about the monitored satellites and constellations together with all those data required to compute the confidence interval of the estimated positions. The second tier is a local AIMN distributed along the railway.

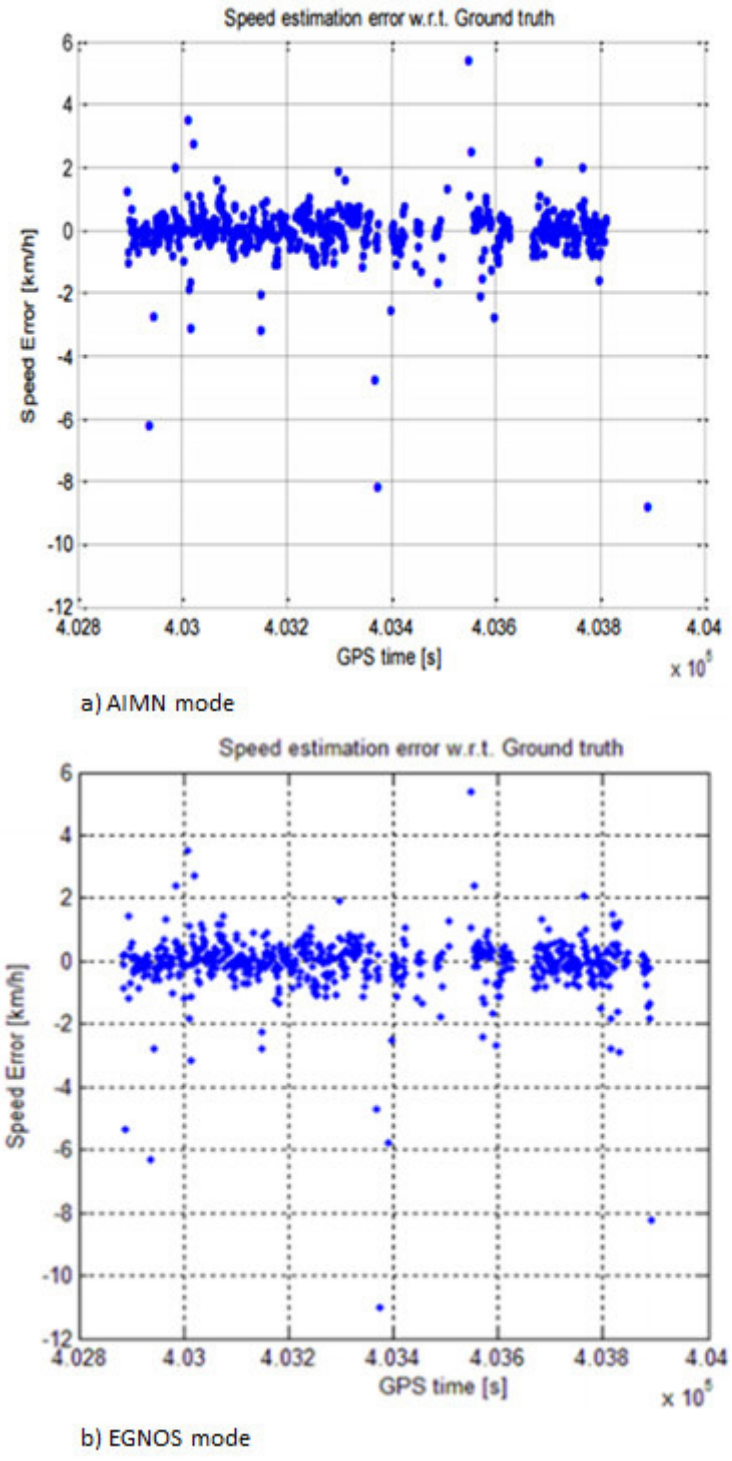

Figure 8. Speed error w.r.t. GroundTruth AIMN vs. EGNOS

This layer consists in a set of Reference Station with both Ranging and Integrity Monitoring functionalities. To complete the scheme, it is also foreseen the presence of a central processing unit that is able to monitor the healthiness of the Local Stations and to compute the augmentation data to be provided to the OBUs. The overall architecture is depicted in Figure 9.

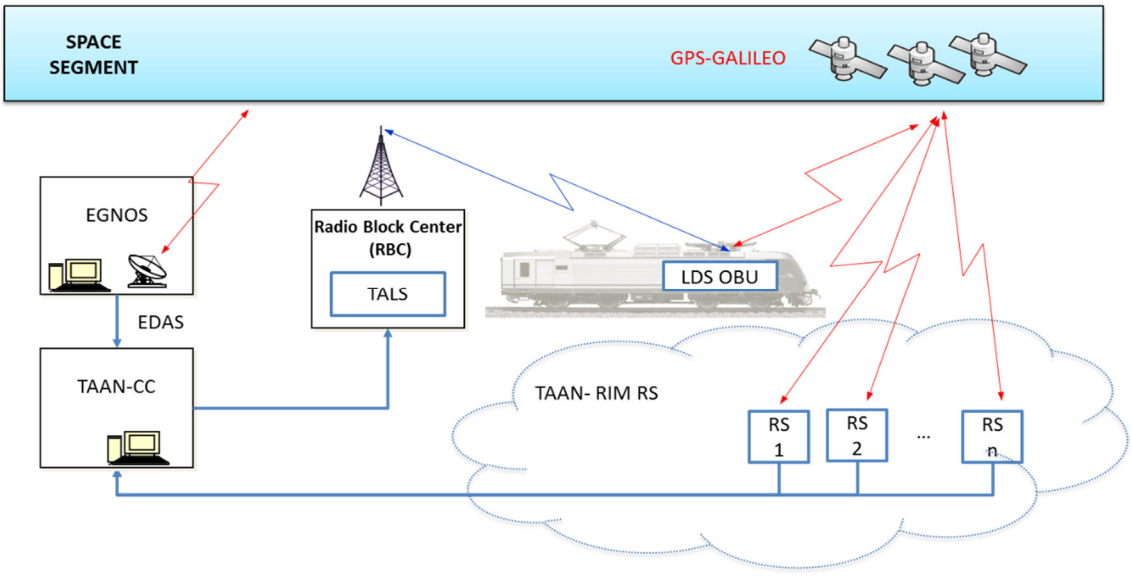

Figure 9. "2-tier" overall architecture

The second tier network, called TAAN (Track Area Augmentation Network), developed in the framework of the European Union Horizon 2020 Galileo-2014-1 ERSAT Project [12], will provide augmentation information as well as integrity information in order to fulfill the safety requirements imposed by SIL4. The TAAN is able to communicate with the TALS entity that has in charge the communications with the train fleet. This architecture can work in a multi-constellation framework and it is able to perform also the Reference Station integrity check. As it will be shown in section 3, the "2-tier" network has the ability to identify and to exclude a faulty RS from the augmentation and integrity monitoring network. In this way, the measurements originated by that faulty stations shall not affect anymore the augmentation data.

2.6 IONOSPHERIC INCREMENTAL DELAY MODELLING

In this paragraph, the issue related to the ionosphere modelling. As introduced in section 2.1, the ionospheric delay is one of the most difficult to model, and the impact of the model residuals represents the largest error for AIMN users in terms of reliability and availability [14],[21],[22],[23],[24]. In a Differential GNSS configuration, the Ground Segment exploits the spatial correlation of the atmospheric delays to mitigate their impact into the Rover position determination. To model the ionosphere, several model have been introduced in the past. Among the others, the model proposed by Klobuchar [25][25] is the most commonly used and it is able to compensate up to approximately 50% of the disturb [24]. Moreover, the Klobuchar

model is the default for GPS standard users. With the introduction of GALILEO, the European navigation system, a different model called NeQuick will be introduced. This model has been developed by the International Centre for Theoretical Physics (ICTP) in Trieste and the University of Graz and exploit a three dimensional electron content distribution model for the ionosphere [26]. To understand better the impact of the ionosphere on the signals broadcasted by the satellites, it is important to start from a physic point of view. As in [23], we can consider the ionosphere as a shell that surrounds the Earth at an height between 50 km to more than 1000 km. A wide number of free electrons (negative charged particles) and positive ions are the result of the ultraviolet sun radiation; when an electromagnetic signal passes through this shield, it undergoes an effect that depends on the wavelength. In the GNSS signals frequencies, according to the amount of free electrons, the effect is an increase of the speed of the carrier wave. The total effect is obtained by integrating the electron density along the LOS (Line Of Sight) and, on a practical point of view, consists in phase advance and the delay of the message carried by the signal [24].

2.6.1 Single Frequency Users

To predict and so to compensate the ionospheric effect, single frequency users can rely on the Klobuchar model by means a set of eight parameters broadcasted by the GPS satellites. This model considers the electron content as if they were concentrated on a thin layer located at a height of about 350 km. Under this assumption, the model refers to IPP (Ionospheric Pierce Point) as the intersection between the thin layer and LOS between the satellite and the user receiver. It is possible then to apply a transformation to evaluate the slant delay from the vertical delay. The approach foreseen by Klobuchar model consists on a constant dc component (5 ns) for the night time and a cosine curve with the peak at 14:00 local time. Amplitude and period of the cosine are both modelled as third degree polynomial functions of the geomagnetic latitude. Polynomial coefficients are broadcasted in the navigation message [15]. With the advent of GALILEO, users may use a new ionospheric model known as NeQuick. This model divides the ionosphere in three regions:

1) $height < 100km$
2) $100km \le height \le h_{\max}^{F_2}$

3) $height > h_{\max}^{F_2}$

The GALILEO version of the NeQuick algorithm foresees a new parameter called Level of Effective Ionization A_Z because the original version provide TEC values by using monthly data, not daily, on solar activity [24]. This parameter is expressed as a second order polynomial function whose coefficients are broadcasted in the navigation message [27],[28].

2.6.2 Dual Frequency users

A user that is operating with a dual frequency GNSS receiver can combine the measurements either to remove the first order of the ionospheric incremental delay (iono-free combination). This happens because at two different frequencies respectively labelled as f_1 and f_2, the ratio between the delays at the two frequencies is constant and equal to the square of the ratio of the two frequencies:

$$\frac{\Delta\tau_{i,n}^{ion}\big|_{f_1}}{\Delta\tau_{i,n}^{ion}\big|_{f_2}} = \frac{f_2^2}{f_1^2} \tag{18}$$

In the iono-free combination, as it has been shown in section 2.1.1, the coefficients are defined as follow:

$$\begin{cases} \alpha_{IF} = \dfrac{f_1^2}{f_1^2 - f_2^2} \\ \beta_{IF} = -\dfrac{f_2^2}{f_1^2 - f_2^2} \end{cases} \tag{19}$$

Having a double frequency receiver, it is also possible to realize a geometry free combination; this latter is not affected by the satellite geometry and the clocks [24],[38]. In the geometry free combination, the coefficients are defined as follow:

$$\begin{cases}\alpha_{IF}=1\\ \beta_{IF}=-1\end{cases} \tag{20}$$

It is possible to identify how all the components that do not depend on the frequency are cancelled out by this combination:

$$\begin{aligned}&\rho_n^{j,GF}=\rho_n^{j,L1}-\rho_n^{j,L2}=\\&=r_n^i+c\left(\delta t_n-\delta t_i^{sat}+\Delta\tau_{i,n}^{ion,L1}+\Delta\tau_{i,n}^{trop}\right)+\upsilon_n^{j,L1}-\left[r_n^i+c\left(\delta t_n-\delta t_i^{sat}+\Delta\tau_{i,n}^{ion,L2}+\Delta\tau_{i,n}^{trop}\right)+\upsilon_n^{j,L2}\right]=\\&=c\Delta\tau_{i,n}^{ion,L1}-c\Delta\tau_{i,n}^{ion,L2}+\upsilon_n^{j,L1}-\upsilon_n^{j,L2}\end{aligned} \tag{21}$$

Where:

r_n^i is the geometric range between the receiver and the satellite;

c is the speed of the light in the vacuum;

δt_n is the n-th receiver clock offset;

δt_i^{sat} is the clock offset of the i-th satellite at the k-th epoch;

$\Delta\tau_{i,n}^{ion,Lj}$ is the ionospheric incremental delay on the Line of Sight between the i-th satellite and the n-th receiver at the j-th frequency (j=1,2);

$\Delta\tau_{i,n}^{trop}$ is the tropospheric incremental delay on the Line of Sight between the i-th satellite and the n-th receiver;

$\upsilon_n^{i,Lj}$ is the error on the Line of Sight between the i-th satellite and the n-th receiver at j-th frequency (j=1,2) that has not been explicitly expressed. This term contains the receiver thermal noise, multipath, interferences and so on.

The ionospheric delay on the L1 frequency can then be evaluated as:

$$c\Delta t_{i,n}^{ion,L1}\cong\rho_n^{i,GF}\left(\frac{f_{L2}^2}{f_{L2}^2-f_{L1}^2}\right) \tag{22}$$

In [24], authors have shown a comparison analysis between Klobuchar and NeQuick for two satellites. The Ground Truth has been realized by means of the geometry free technique.

Klobuchar model has been estimated by means of the parameters broadcasted in the navigation message, while for the NeQuick model online data (forecasted TEC map) has been exploited to estimate the three coefficients. In Figure 10 there is the comparison on the PRN1 satellite while in Figure 11 the comparison is performed on PRN2 satellite. In both cases, NeQuick model (as expected) performed better than the Klobuchar one.

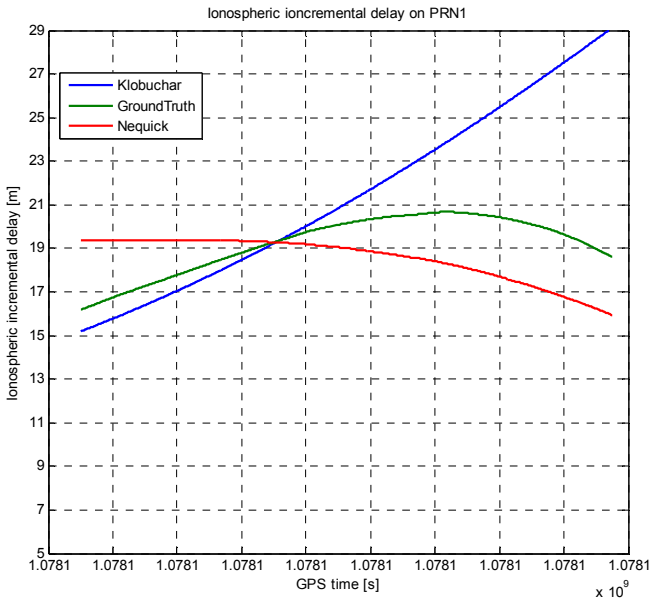

Figure 10. NeQuick and Klobuchar models comparison for PRN1 Satellite

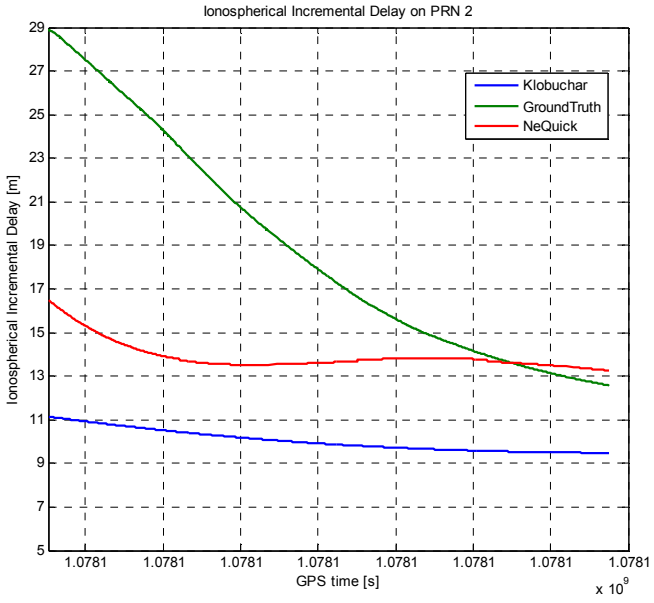

Figure 11. NeQuick and Klobuchar models comparison for PRN2 Satellite

3 SIGNAL IN SPACE AND RS INTEGRITY MONITORING

In this section the algorithms and techniques concerning the integrity monitoring will be described. Firstly, the basics definition of integrity will be introduced, then algorithms to assess SIS (Signal In Space) integrity will be described. Finally, an algorithm to assess the RS healthiness in a "2-tier" augmentation network architecture will be described.

3.1 DEFINITIONS

Designing a navigation system, there are some definitions that must be taken into account. The requirements are expressed in terms of Accuracy, Integrity, Continuity and Time Availability. According to [19] and [20], the Accuracy can be defined as the position error at the 95% level in the absence of system failures. On the other hand, Integrity and Continuity characterize the system response to failures or rare natural events. The system must be able to detect and possibly to fix the threats in a timely fashion. Let AL (Alert Limit) be the error tolerance that for a given parameter measurement must not to be exceeded without issuing an alert and let TTA (Time To Alarm) be the maximum allowable interval between the time in which the Alert Limit has been overpassed and the time in which the alert is arisen. As in [19], an integrity failure occurs when the position error is greater than the *Alert Limit* and this event is not notified within the proper *time to alarm*. It is possible to define another indicator called *Integrity Risk* that represents the probability that an Integrity failure could occurs. In contrast to *Integrity Risk*, the *Continuity Risk* is defined as the probability that the navigation system will fail during the operation given that it was available at the beginning of the operation. It appears obvious that continuity and integrity are competing requirements. In fact, a sensitive integrity detection procedure will guarantee a low integrity risk, but it could generate false alarm that affect the system continuity. If, on the other hand, the procedure is determined in order to have a low false alarm rate (to increase the continuity) some events could be miss detected leading to integrity failures. A trade-off between integrity and continuity is on the basis of navigation systems. In addition to these parameters, the time availability is the fraction of time in which the system is operational [19]. This parameter, differently by continuity and integrity, is not an instantaneous measure of the safety. During operational phase, the position error is not known. In this situation is not possible to evaluate whether that error is greater than AL. To measure the risk that the AL threshold have been exceeded by the position error, a

statistical bound of such a quantity, referred as Protection Level (PL), must be computed. In real time the system will evaluate the PL and it will compare this value with the AL. If PL is greater than the threshold, then the system is labelled as unreliable, otherwise, if the statistical bound is below the AL, the system is considered as trustworthy. In post processing, if a ground truth has been acquired, it is possible to evaluate the actual position error by comparing the estimated rover position and the real rover position. In this way, it is possible to verify, epoch by epoch, whether the PL bounded the estimation error; this information is usually shown in the so called "Staford Plot". The Stanford Plot is a 2D histogram where the bins are identified by the couples of estimation error (in the abscissa axis) and correspondent PL (in the ordinate axis). The occurrence number is represented by means of a chromatic logarithmic scale. An exemplum of Stanford Diagram is shown in Figure 12. The bisector of the first quadrant identify the sets of point in which the PL is exactly equal to the estimation error. In the Stanford plot there are other two main lines: the line with constant error equal to AL and the line with constant PL equal to the AL.

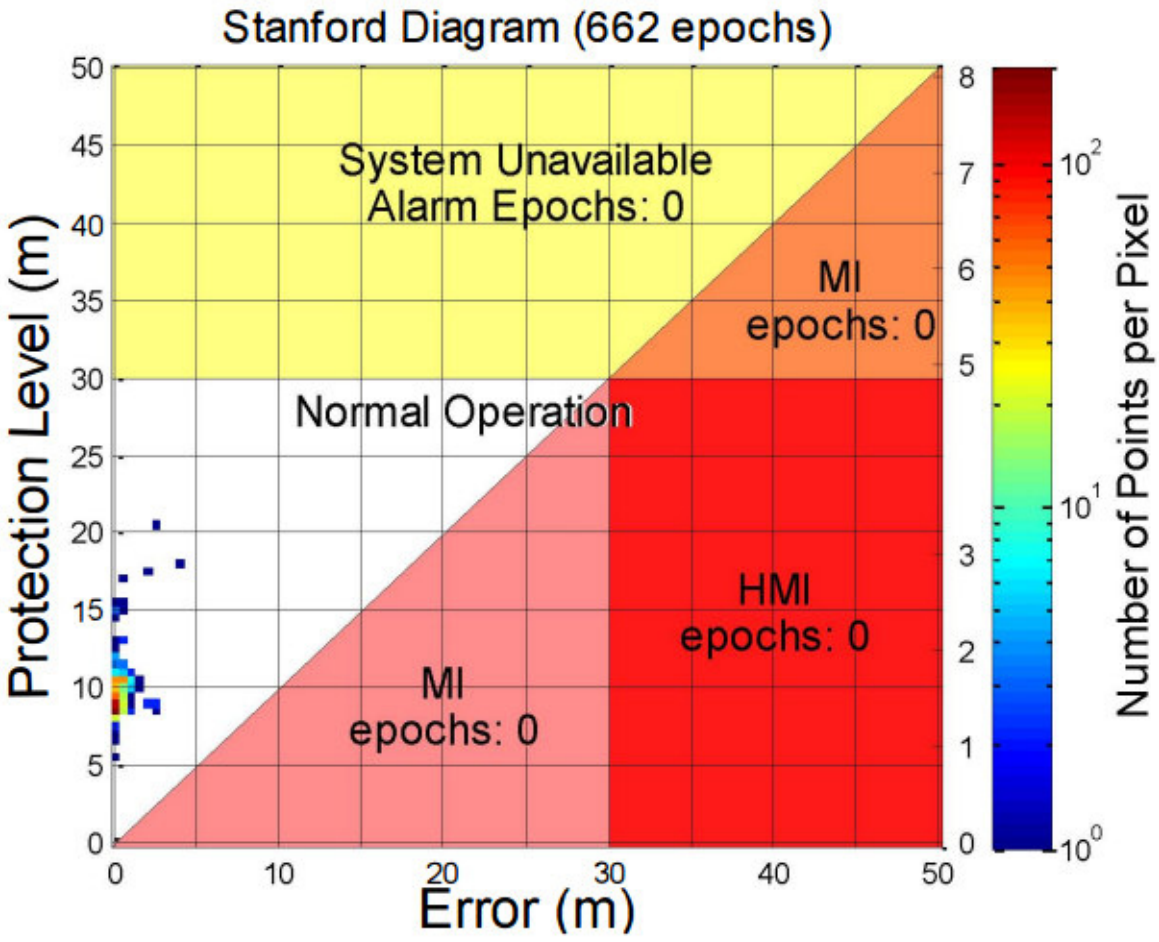

Figure 12. Stanford Plot with AL = 30m

When the position error is greater than PL, the bounding has not worked properly. This situation is called MI (Misleading Information). The MI, by its own, not necessarily corresponds to an integrity failure. In fact, it could happen that, even if error is greater than PL, both of them are greater than AL. In this case the system is labelled as unreliable, so the corrupted position estimation is not used. The area corresponding to such a situation is represented by the orange triangle in the Stanford Plot. Moreover, if the error is higher than PL but both of them are below the AL the system is operating in safe conditions (even if this situation is not desirable). This second case of MI is represented by the pink triangle in the Stanford Plot. The real integrity issue happens when only the position error is higher than AL. In this case the system is considered available while it should be declared as not reliable. This situation is called HMI (Hazardous Misleading Information) and it is represented by the red area. In the case of error smaller than the PL, there are two main circumstances depending on whether PL is greater than AL. In fact, if that happens, the system is not used and declared not available (yellow area). Points belongs to this area are related to continuity issues. On the other hand, if PL is below the decision threshold and bounds correctly the estimation error the system is operating in normal conditions (white area). Looking at Figure 12, because all the points are in the white region far from the diagonal, it is possible to affirm that the system has good performance in terms of both integrity and continuity.

3.2 SIS INTEGRITY FUNDAMENTALS

As anticipated in section 1, the augmentation of GNSS data is highly recommended to fulfil the stringent requirements imposed by SIL-4. Another important factor to take into account is the SIS integrity assessment. A position solution retrieved by keeping into account a measurement either affected by a satellite fault or strongly prejudiced by atmospheric or local effect can lead to a misleading information. In literature, integrity monitoring solutions have been studied both in terms of RAIM (Receiver Autonomous Integrity Monitoring) approaches ([16],[30],[33],[34],[35],[42]) and in terms of IMN (Integrity Monitoring Network) algorithms ([8],[12],[36],[37],[38]). The first category is represented by all those techniques that can be implemented directly on the Rover. On the other hand, the IMN algorithms rely on a network of Reference Stations deployed in known position. In this way, it is possible to evaluate theoretical pseudoranges for all the satellites in view and to compare them with the measured raw data. When the actual data are not close enough to the expected data, such measurements

are labelled as faulty. A faulty measurement can depend by three factors: receiver malfunctioning, transmitter malfunctioning (including errors in the navigation message) and propagation effects. It is obvious that, if the monitor receiver has a malfunctioning, this can produce a misleading integrity assessment either in terms of false alarms or miss detection. From this consideration, arise the necessity of RS integrity assessment. In [12] authors provided a technique to identify and exclude a faulty RS from the Network. Concerning the transmitter issues, many factors could be the source of errors; however, only those regarding the navigation message will be considered. In the propagation phase, errors can be caused by ionospheric storms or scintillation. Anyway that issue is not described in this work. In nominal conditions, SPS users can consider the reliability of each broadcast navigation message and that the URE (User Range Error) is at meter level or even sub-meter level [39]. When anomalies happen, UREs can reach higher values and in some cases can lead the SPS user to generate a hazardous misleading position solution. In [39], a list of potential SIS anomalies is presented; some of these situations, especially the ones depending by the satellite clock offset, can be at kilometre level. Authors proposed a method to evaluate SIS UREs in post processing by comparing the broadcasted ephemeris with the precise post processed ones. In the navigation there is a parameter called URA (User Ranging Accuracy) that is intended to be a conservative representation of the standard deviation of the URE at the worst case location on Earth [39]. In this work of thesis, the RAIM approaches will be only introduced while the IMN techniques will be described in more details.

3.2.1 Ephemeris faults

Concerning the ephemeris faults, there are two main categories to be taken into account. According to [38], ephemeris fault can be categorized in two types, A and B, depending on whether the fault is associated with a satellite manoeuvre. Particularly, a type A fault is associated with a satellite manoeuvre while in the type B fault the satellite is broadcasting anomalous ephemeris, that can produce wrong satellite position estimation when they are used in the orbital propagator, without any satellite manoeuvre involved. To mitigate the type B ephemeris fault, the LGF has a monitor that stores validated ephemeris from the previous days and perform a predictive estimate of the ephemeris to be compared with the ones received in the navigation message [38],[40],[41]. The type A faults, despite they are rarer than the B ones, are more difficult to be mitigated. When a scheduled movement is performed, an unhealthy flag

is broadcasted by the satellite in order to inform the user not to use that satellite; when the operation is correctly concluded, the flag is toggled to healthy status and the signal coming from that space craft can be used again to perform the PVT estimation. The information carried by means of the status flag can be used by the Type B fault monitor. Ephemeris anomalies involving satellite manoeuvre can be further subdivided in two categories: A1 and A2. The A1 class is represented by all those faults that occur after the satellite manoeuvre. The operation is intentional and scheduled and followed by the broadcasting of erroneous ephemeris data. The A2 class is represented by all those issues that are present during the satellite movement. This faults occurs if the healthy flag remains improperly set to "healthy" (type A2a ephemeris fault) or if there is an unintentional manoeuvre due to unplanned events such as propellant leakage or other similar situations (type A2b ephemeris fault).

3.2.2 RAIM techniques

RAIM is a GPS integrity monitoring scheme that makes use of redundant signals to detect a satellite failure that can lead to large range error [42]. The RAIM aim is to detect the presence of a malfunctioning satellite and the identification of which satellite is malfunctioning. One simple RAIM method, shown in [42], is the RCM (Range Comparison Method). Under this approach, the receiver estimates its own position by using all the satellites in view and then, by exploiting its estimated position, perform the satellites pseudorange prediction. By comparing these values with the measured ones, the receiver is able to perform an integrity decision by means of a proper threshold. This technique is similar to the approaches used in IMN approaches with the difference that in reference stations the position is well known and not estimated. The mathematical model will be described in the IMN section. The main drawbacks of RAIM technique are the use of a single constellation, the use of single frequency and the single fault detection capability [33]. The ARAIM (Advanced RAIM) approach has been so designed to be multi-constellation, double frequency with a multiple fault detection capability [33].

3.3 IMN BASED SIS INTEGRITY ASSESSMENT

3.3.1 Pseurorange Residual Definition

The IMN based integrity assessment approaches are the focus of this work. As introduced in the previous paragraph, an integrity monitoring network is constituted by a set of reference stations deployed in well-known georeferenced locations. By knowing their own positions, each station is able to evaluate the satellite reduced pseudorange[2] $\Delta\rho_n^i[k]$ as:

$$\Delta\rho_n^i[k] = \rho_n^i[k] - \hat{r}_n^i[k] + c\delta\hat{t}_i^{sat}[k] - c\Delta\hat{\tau}_{i,n}^{ion}[k] - c\Delta\hat{\tau}_{i,n}^{trop}[k] \tag{23}$$

where:

$\rho_n^i[k]$ is the measured pseudorange for the i-th satellite by the n-th RS at the k-th epoch

$\hat{r}_n^i[k]$ is the estimated geometric distance between the i-th satellite and the n-th RS at the k-th epoch estimated by means of the navigation message and the known receiver position

c is the speed of the light in the vacuum

$\delta\hat{t}_i^{sat}[k]$ is the estimated clock offset of the i-th satellite at the k-th epoch by using the navigation message

$c\Delta\hat{\tau}_{i,n}^{ion}[k]$ is the estimated ionospheric incremental delay on the Line of Sight between the i-th satellite and the n-th RS at the k-th epoch estimated by means of the ionosphere model (e.g. Klobuchar) in meters

$c\Delta\hat{\tau}_{i,n}^{trop}[k]$ is the estimated tropospheric incremental delay on the Line of Sight between the i-th satellite and the n-th RS at the k-th epoch estimated by means of the troposphere model in meters

By considering the reduced pseudorange shown in equation (23), it is possible to observe how it depends on biases introduced by the Reference Station as the receiver clock offset. More in details, the reduced pseudorange can be expressed as:

[2] See section 2.1

$$\Delta\rho_n^i[k] = c\delta t_n[k] + \varepsilon r_n^i[k] - c\left(\varepsilon\delta t_i^{sat}[k]\right) + c\varepsilon\Delta\tau_{i,n}^{ion}[k] + c\varepsilon\Delta\tau_{i,n}^{trop}[k] + \upsilon_n^i[k] = \\ = c\delta t_n[k] + \zeta_n^i[k] \tag{24}$$

where:

c is the speed of the light in the vacuum

$\delta t_n[k]$ is the receiver clock offset of the n-th RS at the k-th epoch

$\varepsilon r_n^i[k]$ is the estimation error on the geometric distance between the i-th satellite and the n-th RS at the k-th epoch

$\varepsilon\delta t_i^{sat}[k]$ is the estimation error on the clock offset for the i-th satellite at the k-th epoch

$c\Delta\hat{\tau}_{i,n}^{ion}[k]$ is the residual ionospheric incremental delay on the Line of Sight between the i-th satellite and the n-th RS at the k-th epoch not compensated by the ionosphere model (e.g. Klobuchar) in meters

$c\Delta\hat{\tau}_{i,n}^{trop}[k]$ is the residual tropospheric incremental delay on the Line of Sight between the i-th satellite and the n-th RS at the k-th epoch not compensated by the troposphere model in meters

$\upsilon_n^i[k]$ is the error on the Line of Sight between the i-th satellite and the n-th receiver at the k-th epoch that has not been explicitly expressed. This term contains the receiver thermal noise, multipath, interferences and so on.

$\zeta_n^i[k]$ is the pseudorange residual defined as:

$$\zeta_n^i[k] = \varepsilon r_n^i[k] - c\left(\varepsilon\delta t_i^{sat}[k]\right) + c\varepsilon\Delta\tau_{i,n}^{ion}[k] + c\varepsilon\Delta\tau_{i,n}^{trop}[k] + \upsilon_n^i[k] \tag{25}$$

In case of multi-constellation processing, the inter-constellation biases due to the different time offset between the constellations must be taken into account as it has been explained in section 2.2. For sake of compactness, these terms will be considered as estimated and compensated, neglecting them from the following. For each satellite, two hypotheses can be defined: H0 (healthy) or H1 (faulty). Assuming the RS as healthy, in the H0 hypothesis, $\zeta_n^i[k]$ can be modelled as a Gaussian zero mean random variable with variance $\sigma_{i,n}^2$. In the H1

hypothesis (the satellite is affected by a fault), $\zeta_n^i[k]$ is still Gaussian distributed, but the expectation is $\mu_n^i(\beta)$ where β is modelled in terms of a wrong satellite position. In case of fault of different sources, β will represent an effective satellite position error that would have produced an error on the estimated receiver position of equal entity. The pseudorange residual is a widely used indicator to monitor ephemeris and satellite faults. In [36] authors defined an approach to monitor satellite ephemeris errors, while in [37] authors used a least squares residual approach to identify and exclude multiple satellite faults.

3.3.2 Single Difference Squared L2 norm

Performing the Single Difference between two reduced pseudorange referring to two different satellites observed by the n-th RS it is possible to observe how all the biases introduced by the RS itself can be removed.

$$\begin{aligned}\Delta\rho_n^{i,j}[k] &= \Delta\rho_n^i[k] - \Delta\rho_n^j[k] = c\delta t_n[k] + \zeta_n^i[k] - c\delta t_n[k] - \zeta_n^j[k] = \\ &= \zeta_n^i[k] - \zeta_n^j[k] = \zeta_n^{i,j}[k]\end{aligned} \tag{26}$$

Evaluate the single difference on two reduced pseudorange corresponds to perform the single difference among the pseudorange residuals associated to them. It is possible to build for each RS and for each satellite a vector $\underline{\xi}_n^i[k]$ whose elements are the single differences of the residual pseudoranges by using the n-th RS and the i-th satellite as pivot:

$$\underline{\xi}_n^i[k] = \left(\zeta_n^{i,1}[k] \quad \zeta_n^{i,2}[k] \quad \cdots \quad \zeta_n^{i,N_{sat}}[k]\right)^T \tag{27}$$

In case of fault on one or more satellites, all the singe differences involving that satellite will be affected by that event. In [12], authors evaluated the squared L2 norm of $\underline{\xi}_n^i[k]$ for all the satellite in view. Authors compared the maximum of those evaluated values with a threshold; if that maximum is over the threshold, the corresponding satellite is labelled as faulty, and the process is repeated excluding it. This process is repeated until there are no more satellites to be checked or the maximum value is within the threshold. Figure 13 depicts a

schematic of the algorithm that is able to exclude more than one faulty satellite. The most important part is the threshold tuning. The procedure followed is based on the Neyman-Pearson criterion. According to this approach, the threshold is evaluated by imposing the desired false alarm probability that becomes a system requirement. The miss detection probability is then evaluated as a performance indicator. Let the indicator y_n^i be the squared L2 norm of the single difference vector $\underline{\xi}_n^i$; for sake of compactness the time dependency is neglected.

$$y_n^i = \left(\underline{\xi}_n^i\right)^T \underline{\xi}_n^i \tag{28}$$

As shown in the previous paragraph, the pseudorange residual observed by the n-th Rs for the i-th satellite is a Gaussian distributed random variable with standard deviation $\sigma_{i,n}^2$ and expectation $\mu_n^i(\beta)$ where β is the effective satellite position error that would have produced an error on the estimated receiver position of equal entity. If no fault occurs, such a random variable can be considered as zero mean. The single difference residuals, can be then considered again as Gaussian distributed with variance $\sigma_{i,n}^2 + \sigma_{j,n}^2$ and a mean value respectively equal to zero in the fault free scenario, and equal to $\mu_n^i(\beta^i)$ if the i-th is affected by a fault and the j-th is healthy and, more generally, equal to $\mu_n^i(\beta^i) - \mu_n^j(\beta^j)$ in the case of both faulty satellites.

1. For each RIM n of the 2nd tier:
   a. Initialize the set $S_n^{H,SD}$ of healthy satellites to the set of visible satellites with elevation greater than the elevation mask.
   b. Repeat
      - for each satellite in $S_n^{H,SD}$ compute the quantity y_n^i
      c. Select the satellite with the largest y_n^i

      $$\hat{i} = Arg\left\{\underset{i \in S_n^{H,SD}}{Max}\left[y_n^i\right]\right\}$$

      d. If $y_n^{\hat{i}}$ exceeds a predefined threshold $\gamma_{y_n^{\hat{i}}}$
         - remove $\hat{i}$ from the healthy set $S_n^{H,SD}$
         - and mark the satellite as *unreliable*.

      until $y_n^{\hat{i}} > \gamma_{y_n^{\hat{i}}}$ and S_H is non empty.

Figure 13. Single Different Squared L2 Norm SIS integrity assessment algorithm

If the elements of the vector $\underline{\xi}_n^i$ were Gaussian distributed independent and identically distributed random variables, y_n^i would follow the chi square distribution with a number of degrees of freedom equal to the number of elements that would have been summed (satellites number excluding the pivot one). However, being obtained by means of differencing, the elements of $\underline{\xi}_n^i$ are correlated, thus means that y_n^i follows the generalized chi square distribution with $N_y = N_{sat} - 1$ degrees of freedom. The distribution is centred or not centred depending on whether the SIS is healthy or not. According to Neyman Pearson criterion the exclusion threshold γ can be evaluated as:

$$\gamma = D^{-1}_{\chi^2_{G,Ny}}\left(1 - P_{fa}\right) \tag{29}$$

Where:

$D^{-1}_{\chi^2_{G,N_y}}(\bullet)$ is the generalized chi square inverse cumulative distribution with N_y degrees of freedom

P_{fa} is the desired false alarm probability

As a consequence, the miss detection probability will be retrieved as:

$$P_{md} = D^{nc}_{\chi^2_{G,Ny}}\left(\gamma, \lambda\right) \tag{30}$$

Where:

$D^{nc}_{\chi^2_{G,Ny}}(\bullet)$ is the generalized chi square non centred cumulative distribution with N_y degrees of freedom

λ is the parameter of non centrality

For the assessment of the performance of the of this algorithm, a GNSS simulator developed by RadioLabs in the framework of the ESA Artes-20 3InSat and H2020 ERSAT projects has been employed. Data have been provided by Sogei GRDNet (GNSS R&D

Network) [68]. According to [12], the single difference of residuals pseudorange in nominal conditions have a trend similar to the ones depicted in Figure 14. Data shown in Figure 14 leads to y_n^i indicators shown in Figure 15. In order to verify the algorithm, 3 scenarios are taken into account:

i. absence of SIS fault (i.e. nominal conditions);
ii. injection of fitting errors in the pseudoranges of a single satellite as due to wrong satellite clock parameters broadcasted by the satellite;
iii. injection of white noise to all pseudoranges of one RS.

Data used in the i) test are real data GPS only measurement acquired on field. In that occasion all the satellites were healthy. As shown in Figure 16, the algorithm correctly labelled as healthy all the satellite in view. To emulate a satellite fault used in case ii), an adulterated clock offset bias parameter for PRN23 satellite has been introduced in the ephemeris file. In this way, the receiver has been forced to estimate the satellite clock offset by means of a wrong second order polynomial. In order to verify the correct identification, a fault free window of about 1 hour has been left in the centre of the observation.

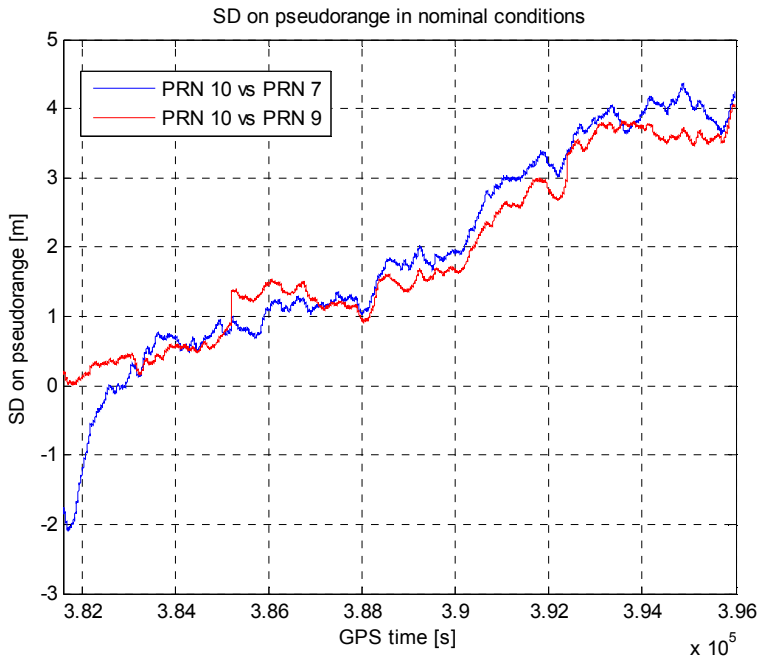

Figure 14. Single Difference pseudorange residuals trend in nominal conditions

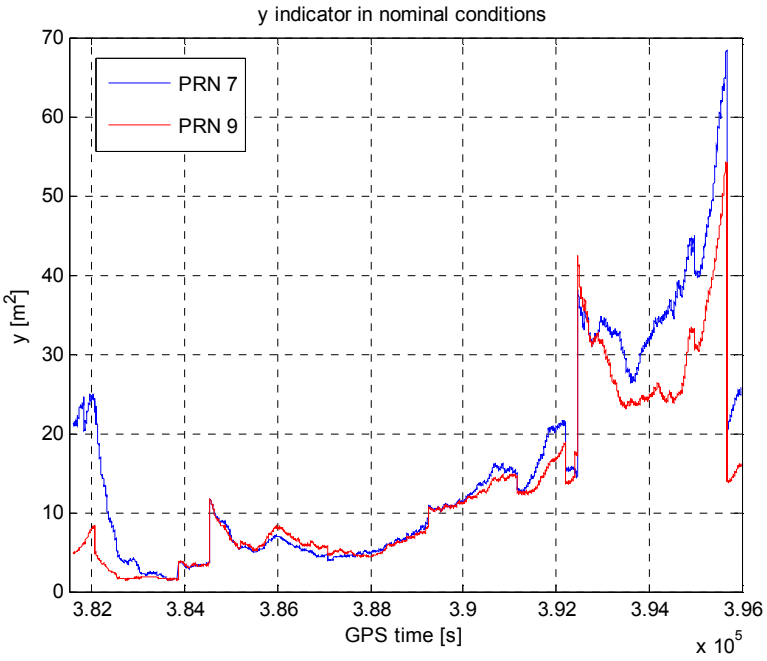

Figure 15. y indicator in nominal conditions

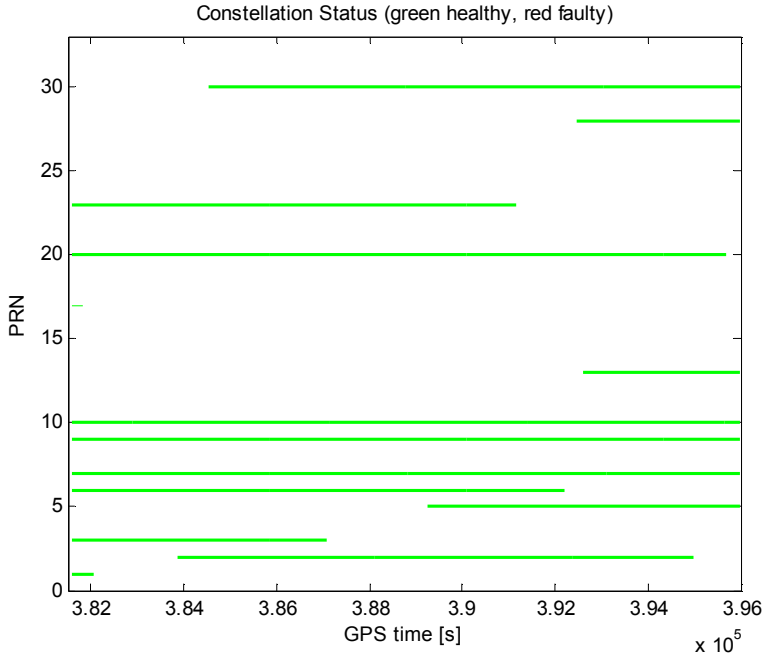

Figure 16. GPS constellation status in nominal conditions

Finally, in the case of scenario iii), a white Gaussian noise with standard deviation of 2.5 meters has been added to all the pseudorange measured by the RS in the observation window. As shown in Figure 18, all the satellites have been identified as faulty. In this scenario it becomes clear how is important to identify malfunctioning RS in order to exclude them from the SIS assessment procedure.

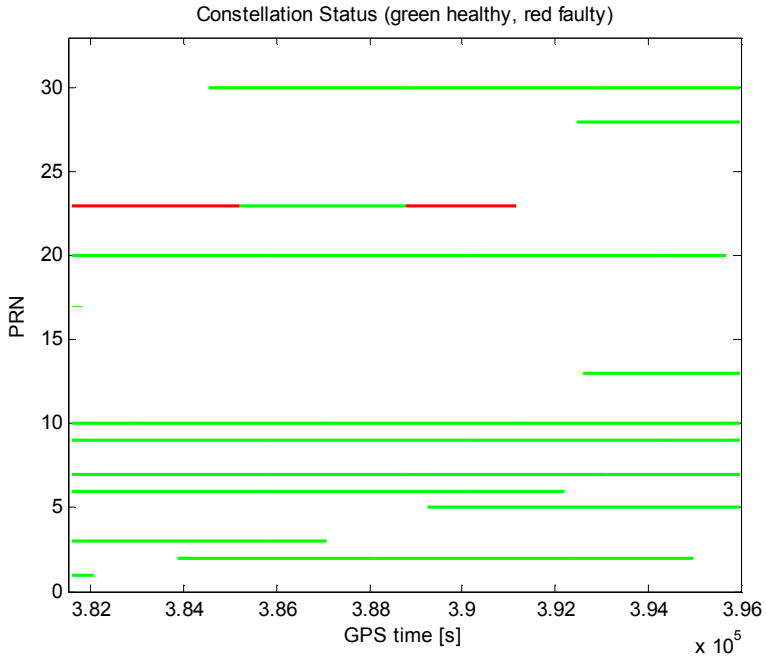

Figure 17. GPS constellation status with one injected fault

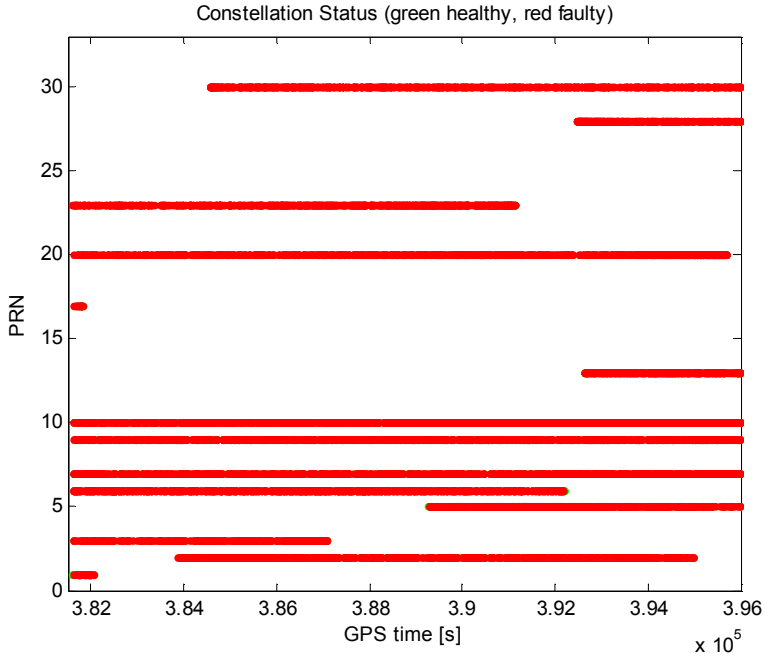

Figure 18. GPS constellation status in case of malfunctioning RS

3.3.3 Multi-Station pseudorange residual squared L2 norm

The procedure described in the section 3.3.2 is applicable to every Reference Station; this RS can be either a single Reference Station (like in the DGNSS approach) or a station that

belongs to a network. The further step for the SIS integrity assessment is the jointly processing of data coming from all the station that view a specific satellite. Following an approach depicted in [8], a procedure to identify and exclude faulty satellites can be based on the jointly processing of pseudorange residual estimated by the RSs. In the following the time dependency is neglected for sake of compactness. Let w^i indicator be defined as:

$$w^i = \sum_{n=1}^{N_{RS}} \frac{\left(\hat{\zeta}_n^i\right)^2}{\left(\sigma_{i,n}\right)^2} \tag{31}$$

Where:

$\hat{\zeta}_n^i$ is the estimated pseudorange residual for the i-th satellite by the n-th RS at the k-th epoch

N_{RS} is the number of Reference Station that contribute to the indicator evaluation

$\sigma_{i,n}$ is the standard deviation of the $\hat{\zeta}_n^i$

w^i can be considered as the weighted L2 norm square of the vector $\underline{\hat{\zeta}^i}$ defined as:

$$\underline{\hat{\zeta}^i} = \left(\hat{\zeta}_1^i \quad \hat{\zeta}_2^i \quad \cdots \quad \hat{\zeta}_{N_{RS}}^i\right)^T \tag{32}$$

The procedure compares the w^i indicator of each satellite with the an exclusion threshold. The satellites whose indicator is greater than the threshold are labelled as faulty. Assuming that the residual are Gaussian distributed, with expectation equal to zero in case of healthy satellite and equal to $\mu_n^i(\beta)$ in case of satellite fault, following the same approach defined in the previous sections it is possible to define the system performance. In the H0 hypothesis, w^i follows a centred chi-square distribution with $N_w = N_{RS} - 1$ degrees of freedom, while in the H1 hypothesis follows a non-centred chi-square distribution with N_w degrees of freedom and a parameter of non-centrality $\lambda(\beta)$. According to Neyman Pearson criterion, the exclusion threshold γ can be set as:

$$\gamma = D^{-1}_{\chi^2_{Nw}}\left(1-P_{fa}\right) \tag{33}$$

Where:

$D^{-1}_{\chi^2_w}(\bullet)$ is the chi square inverse cumulative distribution with N_w degrees of freedom

P_{fa} is the desired false alarm probability

As a consequence, the miss detection probability will be retrieved as:

$$P_{md} = D^{nc}_{\chi^2_{Nw}}(\gamma,\lambda) \tag{34}$$

Where:

$D^{nc}_{\chi^2_{Nw}}(\bullet)$ is the chi square non centred cumulative distribution with N_w degrees of freedom

λ is the parameter of non-centrality

3.3.4 Multi-Station pseudorange residual double difference squared L2 norm

In [12], authors proposed a multiple fault detection algorithm based on L2 square norm of Double Difference pseudorange. The suggested approach has been designed to identify and exclude faulty RS and will be presented in section 3.4. The same approach can be used to identify and exclude faulty satellites. Let $\zeta_m^{i,j}$ and $\zeta_n^{i,j}$ be the single difference residual with respect to the satellites i-th and j-th evaluated respectively by the m-th and the n-th reference station. The double difference pseudorange residual $\zeta_{m,n}^{i,j}$ can be defined as:

$$\zeta_{m,n}^{i,j} = \zeta_m^{i,j} - \zeta_n^{i,j} = \zeta_m^i - \zeta_m^j - \zeta_n^i + \zeta_n^j \tag{35}$$

This value is no more affected by clock offset errors. Following a methodology similar to the one followed for the other approaches, let $\underline{\psi}_{m,n}^i$ be the double difference pseudorange residual vector:

$$\underline{\psi}_{m,n}^{i} = \begin{pmatrix} \zeta_{m,n}^{i,1} & \zeta_{m,n}^{i,2} & \cdots & \zeta_{m,n}^{i,N_{SAT}} \end{pmatrix}^{T} \tag{36}$$

Let the satellite fault indicator z^i the squared L2 norm of the double difference pseudorange residual defined as:

$$z^{i} = \sum_{m=1}^{N_{RS}} \sum_{n=1}^{N_{RS}} \left(\underline{\psi}_{m,n}^{i} \right)^{T} \underline{\psi}_{m,n}^{i} \tag{37}$$

Supposing all satellites in view to be healthy in the initialization phase, the z^i indicator is evaluated for each satellite belonging to healthy list. If the maximum indicator is greater than the exclusion threshold, the corresponding satellite is identified as faulty. The anomalous satellite is then excluded and the process is repeated without that satellite. The procedure ends when the maximum is below the threshold or there are no more satellites in the healthy list. In Figure 19 a schematic of the algorithm is shown. Being the double difference pseudorange residuals correlated and Gaussian distributed, in the H0 hypothesis (nominal conditions) z^i follows a generalized chi square distribution with $N_z = \left(N_{sat} - 1\right)\left(N_{RS} - 1\right)^2$ degrees of freedom. While in the H1 hypothesis (satellite fault) z^i follows a non-central generalized chi square distribution with $N_z = \left(N_{sat} - 1\right)\left(N_{RS} - 1\right)^2$ degrees of freedom and parameter of non-centrality λ.

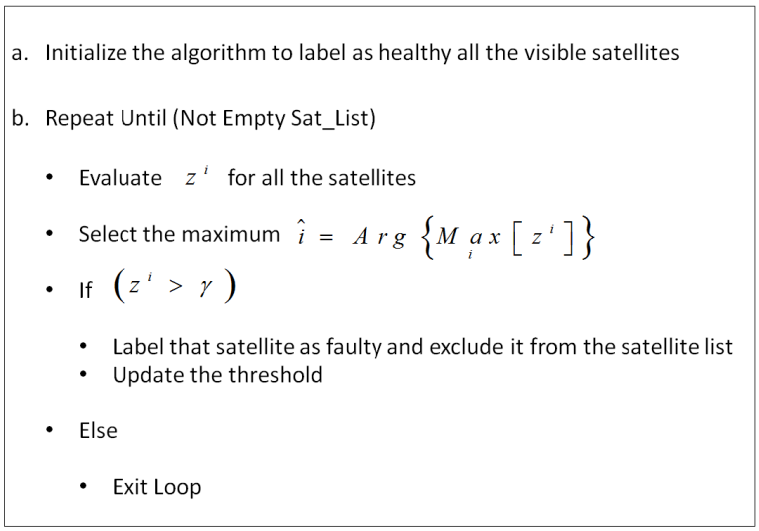

Figure 19. Double difference residual L2 square norm algorithm workflow7

According to Neyman Pearson criterion the exclusion threshold γ can be evaluated as:

$$\gamma = D^{-1}_{\chi^2_{G,Nz}}\left(1-P_{fa}\right) \tag{38}$$

Where:

$D^{-1}_{\chi^2_{G,N_z}}(\bullet)$ is the generalized chi square inverse cumulative distribution with N_z degrees of freedom

P_{fa} is the desired false alarm probability

As a consequence, the miss detection probability will be retrieved as:

$$P_{md} = D^{nc}_{\chi^2_{G,Nz}}(\gamma,\lambda) \tag{39}$$

Where:

$D^{nc}_{\chi^2_{G,Nz}}(\bullet)$ is the generalized chi square non centred cumulative distribution with N_z degrees of freedom

λ is the parameter of non-centrality

3.3.5 Final considerations

Considering the methods presented in this section, the main limitation of the single difference pseudorange residual approach is represented by the single station operation. Anyway that method could be used, as proposed in [12], for the preliminary integrity assessment. Trying to put together data coming from more than one station, the approach take makes use of the pseudorange residuals has the advantage of being compact and easy to be implemented. However, its main drawback is the dependence of the system by the receiver clock offset estimation. In fact, the residual estimation process is affected by the error in the receiver clock offset estimation. In fact, a faulty satellite that has not been excluded can lead to a wrong receiver clock offset estimation and then afflicting the pseudorange residual of all the

other satellites. Anyway this method can be applied on a network of RS that has a preliminary SIS integrity check as the one presented in section 3.3.2. This limitation has been removed in the approach presented in 3.3.4. In fact, dealing with the double difference, all the issues related to clock offsets have been cancelled out. On the other side of the coin, we have the impossibility to detect and exclude satellite faults due to satellite clock. The other advantage of using the double difference approach instead of the one in 3.3.2 is the possibility to reveal more efficiently the presence of multiple satellite fault. The main limitation of the double difference squared L2 norm approach is represented by the computational cost in the evaluation of the exclusion threshold.

3.4 RS INTEGRITY MONITORING

In the previous section, it has been introduced the problem of dealing with a malfunctioning Reference Station. The faulty RS can lead to wrong differential correction or to problems in the SIS integrity assessment. These problems can be related to the false exclusion of healthy satellites or to the miss detection of a faulty satellite. The first event can create a continuity issue while the second can lead to misleading information or even to an integrity failure. The use of a "2-tier" architecture as shown in section 2.5, can strongly mitigate all those issues related to a faulty RS. One of the task foreseen by that architecture is identification of a malfunctioning reference receiver. In [12] author make use of raw data provided by the 1st tier RS and analyse the statistics on the double difference residuals. Furthermore, the approach can be easily extended by performing the double difference among the RS belonging to the 2nd tier only. The double difference pseudorange residual $\zeta_{m,n}^{i,j}$ can be defined as in equation (35) by double differencing the reduced pseudorange. Performing the double difference of reduced pseudorange is equivalent to perform double difference of pseudorange residuals. This value is no more affected by clock offset errors. Following a methodology similar to the one followed for the other approaches, let $\underline{\vartheta}_n^{i,j}$ be the double difference pseudorange residual vector:

$$\underline{\vartheta}_n^{i,j} = \begin{pmatrix} \zeta_{n,1}^{i,j} & \zeta_{n,2}^{i,j} & \cdots & \zeta_{n,N_{RS}}^{i,j} \end{pmatrix}^T \tag{40}$$

Let the satellite fault indicator z_n the squared L2 norm of the double difference

pseudorange residual defined as:

$$z_n = \sum_{i=1}^{N_{Sat}} \sum_{j=1}^{N_{Sat}} \left(\underline{g}_n^{i,j} \right)^T \underline{g}_n^{i,j} \tag{41}$$

Supposing all the RSs to be healthy in the initialization phase, the z_n indicator is evaluated for each RS in the healthy list. If the maximum indicator is greater than the exclusion threshold, the corresponding station is identified as faulty and excluded. The process is repeated until the maximum is below the threshold or there are no more RS in the healthy list. In Figure 20 a schematic of the algorithm is shown. For the performance assessment the approach followed is similar to the ones presented in the SIS integrity algorithms section. Since the double difference pseudorange residuals are correlated and Gaussian distributed, in the H0 hypothesis (nominal conditions) z_n follows a generalized chi square distribution with $N_{z_n} = N_{RS} \cdot N_{Sat} \cdot \left(N_{Sat} - 1 \right)$ degrees of freedom. While in the H1 hypothesis (receiver fault) z_n follows a non-central generalized chi square distribution with N_{z_n} degrees of freedom and parameter of non-centrality λ. According to Neyman Pearson criterion the exclusion threshold $\gamma_{z_n^{Tier\,2}}$ can be evaluated as:

$$\gamma_{z_n^{Tier\,2}} = D^{-1}_{\chi^2_{G,Nz_n}} \left(1 - P_{fa} \right) \tag{42}$$

Where:

$D^{-1}_{\chi^2_{G,Nz_n}} (\bullet)$ is the generalized chi square inverse cumulative distribution with N_{z_n} degrees of freedom

P_{fa} is the desired false alarm probability

As a consequence, the miss detection probability will be retrieved as:

$$P_{md} = D^{nc}_{\chi^2_{G,Nz_n}} \left(\gamma_{z_n^{Tier\,2}}, \lambda \right) \tag{43}$$

1. Initialize the set R_{Tier2}^{H} of healthy RSs to the set of TAAN RSs.
2. Repeat
   - for each RS n in R_{Tier2}^{H} compute the quantity z_n
   - Select the RS in R_{Tier2}^{H} with the largest z_n

$$\hat{n} = Arg\left\{ \underset{i \in R_{Tier2}^{H}}{Max}\left[z_n \right] \right\}$$

   - If $z_{\hat{n}}$ exceeds a predefined threshold $\gamma_{z_n^{Tier2}}$
     - remove $\hat{n}$ from the healthy set R_{Tier2}^{H}
     - and mark the RS as *faulty*.

   until $z_{\hat{n}} > \gamma_{z_n^{Tier2}}$ and S_H is non empty.

Figure 20. Schematic RS fault detection algorithm

Where:

$D_{\chi^2_{G,Nz_n}}^{nc}(\bullet)$ is the generalized chi square non centred cumulative distribution with N_{z_n} degrees of freedom

λ is the parameter of non-centrality

To verify the correct behaviour of the algorithm, in [12] authors considered a network of 8 RS. Data have been provided by Sogei GRDNet (GNSS R&D Network) [68]. Particularly, two scenarios have been taken into account:

i absence of faults (i.e. nominal conditions);

ii simulated fault on RS #6 corresponding to an increase of the measurement noise, (i.e. $\mathbf{R}_{\Delta\rho_n} = \sigma_{\Delta\rho_n}^2 \mathbf{I}$ with $\sigma_{\Delta\rho_n} = 2.5m$.

In Figure 21 and in Figure 22 are depicted respectively the temporal trend of the z_n indicator in case of short (50 km) and long baseline (500 km) length. The double differences have been evaluated with single frequencies observations. In both cases two data sets have been plotted: the nominal conditions z_n (case *i*) and the corresponding corrupted one (case *ii*). As expected, with the increase of the baseline, the spatial decorrelation of the atmospheric delays

leads to an incomplete cancellation of the ionospheric and tropospheric delay terms when computing the Double Differences. This effect, according to [12], generates an increment in the equivalent measurement noise affecting the single differences with the baseline length. Although the z_n indicator performs the RS integrity assessment even in presence of large baselines, baseline increases the sensitivity of the detector w.r.t. the magnitude of the RS fault.

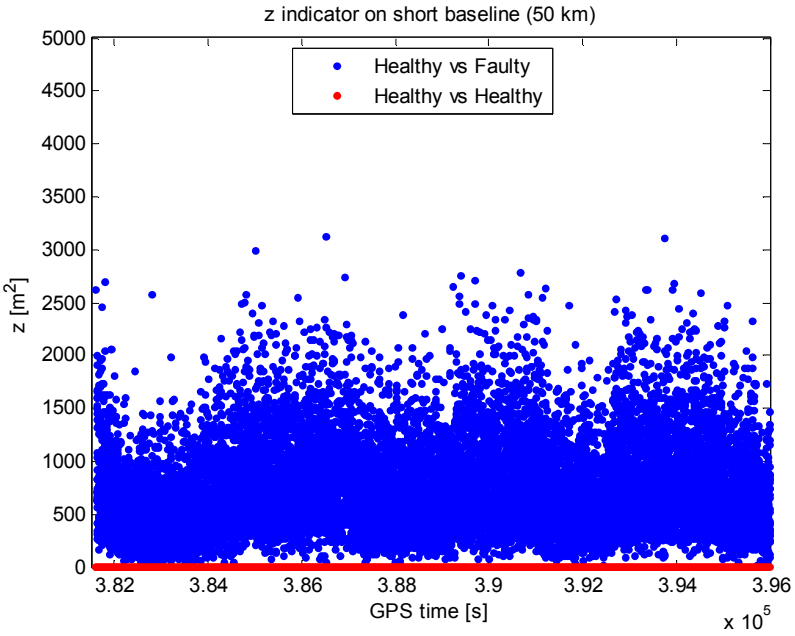

Figure 21.Temporal trend of z indicator on short baselines

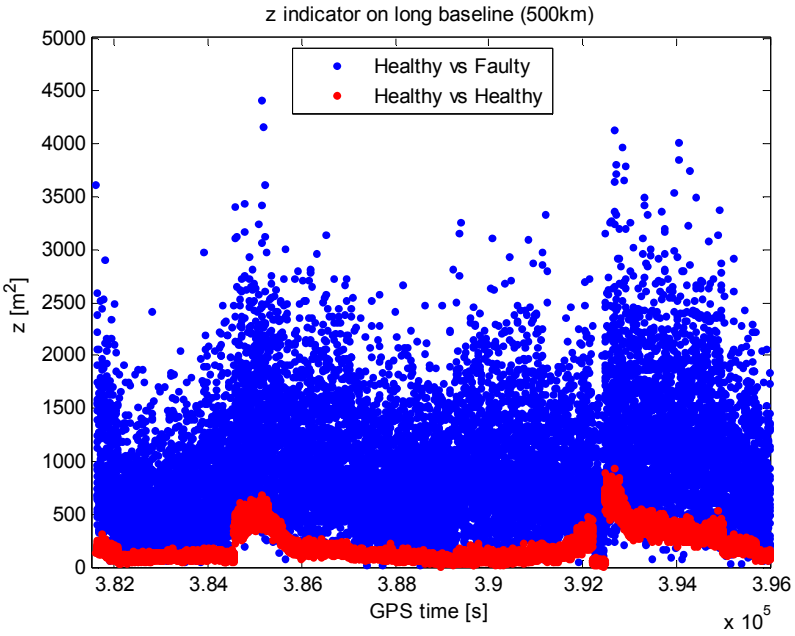

Figure 22. Temporal trend of z indicator on long baselines

In the *i* case, all the RS were healthy and how is it possible to see in Figure 23, the algorithm correctly labelled all the stations as healthy. In the case *ii* a fault on RS#6 has been simulated and, how it is shown in Figure 24, even in this case the procedure correctly identify and exclude only the faulty RS.

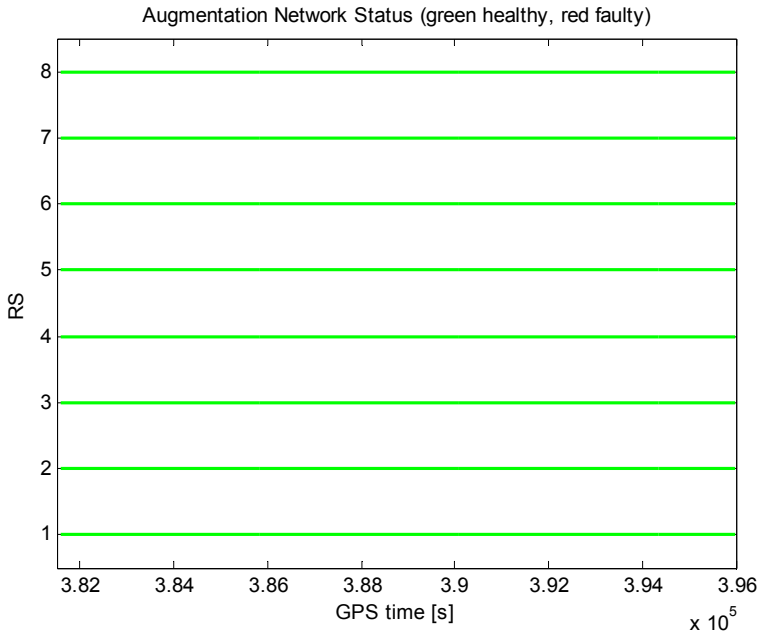

Figure 23. Augmentation Network with all healthy RS

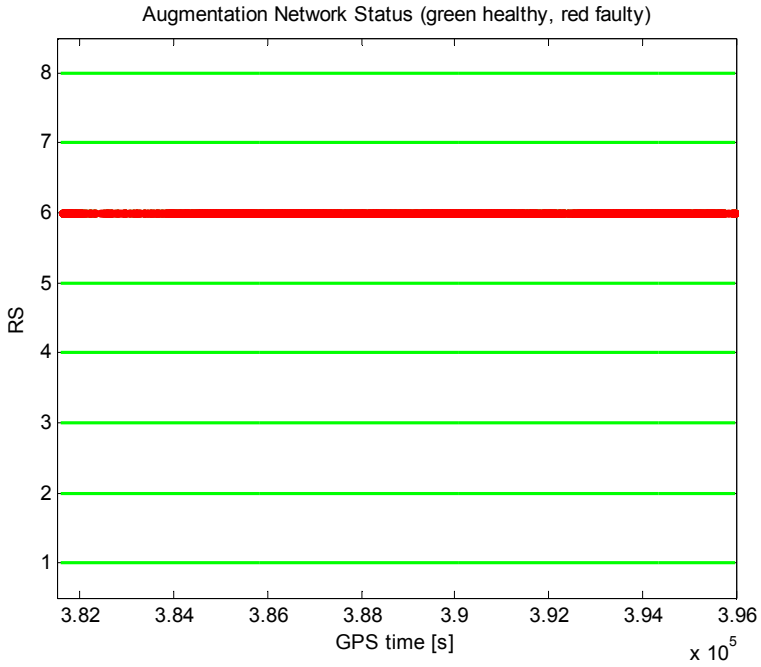

Figure 24. Augmentation Network with one faulty RS

4 GNSS TRAIN POSITIONING

In this section, the main algorithms and approaches designed for the GNSS based train positioning will be introduced. The analysis carried out in this section foresees two main assumptions: the presence of one single track, the train is modelled as a rigid body. The approach in presence of multiple track will be described in section 5.

4.1 INTRODUCTION

As introduced in section 1, the ERTMS is the European standard for train signalling. As in [43], GNSS represents a strategic technology for the evolution of the ERTMS platform; at this aim, a roadmap has been adopted to include the GNSS-based systems into the ERTMS specifications by 2017. With a huge market slice, the introduction of satellite navigation into satellite positioning is a key innovation allowing a drastically reduction of maintenance and operational costs. The highly demanding SIL-4 requirements imposed by the CENELEC specifications ([8],[9],[10],[11]) represent the main challenge in the GNSS-based systems. In fact, the new modules must provide the same level of safety already granted by the traditional ones. Moreover, the requirements fulfillment will guarantee the interoperability between the new GNSS-based modules with the other subsystems already in operation without impacting on the system performance, safety characteristics and architecture [1]. The augmentation and integrity assessment are crucial for the development of a high safety standard for train control systems. In this section the focus will be represented by the On Board Unit. As in [7], the OBU is responsible to provide the PVT estimation together with the associated confidence interval. Each GNSS LDS OBU is equipped with:

- One (or more) GNSS receiver;
- A database for the track (Track DB);
- a local processor performing the PVT by exploiting the GNSS observables, the Track DB, the augmentation data received from the TALS server;

To increase the integrity and availability [7], the OBU can make use of:

- multiple GNSS antennas;
- two or more different GNSS receivers developed by separate manufacturers to avoid common modes of failure;
- multiple independent processing chains;
- a complementary set of integrity mechanisms (e.g. self check).

According to [44], dealing with a train localization system, five distinct categories can be identified:

1) Detection of position along the track
2) Train speed and braking distance estimation
3) Track detection in presence of multitrack
4) Detection of turnout direction
5) Train Integrity

In this section only the first problem will be considered while the track detection and the train integrity issues will be discussed respectively in section 5 and in section 6.

4.2 POSITION ALONG THE TRACK: THE TRACK CONSTRAINT

Considering the train positioning, for sake of compactness, the first assumption made deals with the train model. A train is a set of vehicles linked by mechanical couplings, in the following the train is assumed as a unique rigid body. Under this hypothesis, the train position can be described by the position of one point. The position of every other points of the train can be then obtained by rigid translation. This assumption will be slightly relaxed in section 6 when the train integrity issue will be considered. A key consideration dealing with the train positioning is the so called track constrain ([1],[7]). In fact, during its ride the train is constrained to lie along the track. This means that, given the track on which the train is lying on, the absolute train position is given by the associated mileage expressed in terms of curvilinear abscissa of the track. Operatively, this operation is equivalent to a change of random variable. In fact, instead of estimating a 3D random variable (receiver geographic coordinates) the system estimates a 1D variable (curvilinear abscissa). This transformation, in principles, leads to the reduction of the number of satellites needed to perform the estimation. In fact, by

exploiting the track constraint technique it is possible to estimate the train location even when only two satellites are in view. However, the effective reduction in the number of required satellites to make a fix when track constraint is applied depends on track-satellite geometry [7]. By geometrical consideration, satellites whose line of sight is aligned with the track carries more information than the ones at the cross-over. Following the weighted least square approach, the observations in excess can be used to increase accuracy, availability or even the integrity. Let $s(t)$ be the curvilinear abscissa of a train reference point at time t. Without loss of generality, let the centre of the antenna of the GNSS receiver be the train reference point. In the following the ECEF (Earth Centred Earth Fixed) frame is selected to express the absolute position. The same approach can be alternatively performed in a local ENU (East North Up) coordinates system. In fact, the range (or better a pseudorange) is the L2 norm of the distance between the receiver and the satellite. Since L2 norms are invariant with respect to changes of orthonormal basis, the measurement equations can be equivalently expressed in any orthonormal basis [7]. For sake of compactness the time dependency is neglected in the following. Under the track constraint imposition, the train position can be expressed as:

$$\mathbf{X}^{Train}(x,y,z)=\mathbf{X}^{Train}(s)=\left[X_x^{Train}(s)\quad X_y^{Train}(s)\quad X_z^{Train}(s)\right]^T \tag{44}$$

Thus implies that the geometric distance between the receiver and the train can be expressed as function of the curvilinear abscissa s

$$r_{Train}^{i}=\left\|\mathbf{X}^{i}-\mathbf{X}^{Train}(x,y,z)\right\|=\left\|\mathbf{X}^{i}-\mathbf{X}^{Train}(s)\right\| \tag{45}$$

4.3 TRACK CONSTRAINT IN STAND ALONE OR DIFFERENTIAL POSITIONING

In a Stand Alone or in a Differential positioning, when the track constraint is imposed, there are two unknown: curvilinear abscissa and receiver clock offset. The system solution can be obtained by an iterative approach around a linearization point. The approach presented in the following is compliant with both Stand Alone or Differential Positioning techniques. The navigation equation system solving approach is based on the first order Taylor's series expansion around a train curvilinear abscissa estimation. The initial estimate, following [7], is obtained by performing a track free PVT estimation and then selecting the nearest track point

as the initial point for the iterations. Let $\underline{z}^{(m)}$ be the unknown vector at the m-th step. $\underline{z}^{(m)}$ can be written as:

$$\underline{z}^{(m)} = \begin{pmatrix} \Delta s^{(m)} \\ \Delta \delta t_n{}^{(m)} \end{pmatrix} \tag{46}$$

Where:

$\Delta s^{(m)}$ is the correction to be applied to the mileage estimated at the m-th step

$\Delta \delta t_n{}^{(m)}$ is the correction to be applied to the receiver cock offset estimated at the m-th step

Let $\Delta\underline{\rho}^{(m)}$ be the vector obtained by rearranging column-wise the reduced pseudorange measured by the OBU at the m-th iteration:

$$\Delta\underline{\rho}^{(m)} = \left(\Delta\rho^{1}_{Train}{}^{(m)} \quad \Delta\rho^{2}_{Train}{}^{(m)} \quad \cdots \quad \Delta\rho^{N_{Sat}}_{Train}{}^{(m)} \right)^T \tag{47}$$

In case of differential positioning approach, the differential corrections are considered as compensated in the reduced pseudorange evaluation. Let $\mathbf{H}^{(m)}$ be the design matrix at the m-th step that would have been evaluated in case of unconstrained PVT estimation. According to section 2, $\mathbf{H}^{(m)}$ can be expressed as:

$$\mathbf{H}^{(m)} = \begin{pmatrix} e^{1}_{Train,x}{}^{(m)} & e^{1}_{Train,y}{}^{(m)} & e^{1}_{Train,z}{}^{(m)} & 1 \\ e^{2}_{Train,x}{}^{(m)} & e^{2}_{Train,y}{}^{(m)} & e^{2}_{Train,z}{}^{(m)} & 1 \\ \cdots & \cdots & \cdots & \cdots \\ e^{N_{Sat}}_{Train,x}{}^{(m)} & e^{N_{Sat}}_{Train,y}{}^{(m)} & e^{N_{Sat}}_{Train,z}{}^{(m)} & 1 \end{pmatrix} \tag{48}$$

Where the first three elements of each row of the $\mathbf{H}^{(m)}$ represents the three directors cosines of the line of sight between the corresponding satellite and the OBU:

$$\mathbf{e}^{i}_{Train}{}^{(m)} = e^{i}_{Train,x}{}^{(m)} \cdot \hat{x} + e^{i}_{Train,y}{}^{(m)} \cdot \hat{y} + e^{i}_{Train,z}{}^{(m)} \cdot \hat{z} \tag{49}$$

Let $\mathbf{D}^{(m)}$ be matrix that imposes the constraint at the m-th step. This matrix has two columns: 1st column is composed by the three director cosines of the tangent to the track in the point with curvilinear abscissa s and a 4th element fixed to zero. The 2nd column is constituted by three zeros and a 4th element fixed to one.

$$\mathbf{D}^{(m)} = \begin{pmatrix} \left.\frac{\delta X_x^{Train}}{\delta s}\right|_{s=\hat{s}^{(m)}} & 0 \\ \left.\frac{\delta X_y^{Train}}{\delta s}\right|_{s=\hat{s}^{(m)}} & 0 \\ \left.\frac{\delta X_z^{Train}}{\delta s}\right|_{s=\hat{s}^{(m)}} & 0 \\ 0 & 1 \end{pmatrix} \tag{50}$$

The constrained PVT solution for the m-th step can be evaluated by solving the system:

$$\Delta\underline{\rho}^{(m-1)} = \mathbf{H}^{(m-1)}\mathbf{D}^{(m-1)}\underline{z}^{(m)} + \underline{\upsilon} \tag{51}$$

Where $\underline{\upsilon}$ indicates the residuals vector. The set of equations can be solved by means of a weighted least square method or by means of an extended Kalman filter approach [7]. The corrections to be applied to the mileage and the satellite clock offset can be estimated as:

$$\underline{\hat{z}}^{(m)} = \mathbf{K}^{(m)}\Delta\underline{\rho}^{(m-1)} \tag{52}$$

Where the gain matrix $\mathbf{K}^{(m)}$ can be obtained as:

$$\mathbf{K}^{(m)} = \left(\mathbf{D}^{(m-1)T}\mathbf{H}^{(m-1)T}\mathbf{R}_v^{-1}\mathbf{H}^{(m-1)}\mathbf{D}^{(m-1)}\right)^{-1}\mathbf{D}^{(m-1)T}\mathbf{H}^{(m-1)T}\mathbf{R}_v^{-1} \tag{53}$$

Where $\mathbf{R}_v$ is the weight matrix

In absence of faults, according to [1], since υ can be modelled as a zero mean Gaussian m-variate random variable with covariance matrix $\mathbf{R}_\upsilon$, the estimation error $\Delta\underline{z} = \underline{\hat{z}} - \underline{z}$ is a zero

mean Gaussian random variable with covariance matrix:

$$\mathbf{R}_{\Delta\underline{z}} = E\left\{\Delta\underline{z}^T \Delta\underline{z}\right\} = \left(\mathbf{D}^T\mathbf{H}^T\mathbf{R}_v^{-1}\mathbf{H}\mathbf{D}\right)^{-1} \tag{54}$$

The variance of the estimated mileage can be then retrieved as:

$$\sigma_s^2 = \left[\mathbf{R}_{\Delta\underline{z}}\right]_{1,1} \tag{55}$$

In presence of satellite faults that have not been excluded by the integrity monitoring network, the expectation of $\Delta\underline{z}$ is no longer zero, but can be expressed as:

$$E\left\{\Delta\underline{z}\right\} = \mathbf{K}\boldsymbol{\beta} \tag{56}$$

Where $\boldsymbol{\beta}$ is the uncompensated range error vector.

4.4 TRACK CONSTRAINT IN RELATIVE POSITIONING

In a relative positioning system, a Reference Station (Master) forward to the OBU (Rover) its own raw data. By performing a double difference approach, the user is able to solve the navigation equations set by cancelling out all the biases due to the clock offsets. However, on the other side of the coin, the Rover can only estimate the baseline $\mathbf{b}$ between itself and the master station. By vector summing the estimated baseline to the Master station position is it possible to retrieve the absolute estimated Rover position. For sake of compactness, in the following the time dependence of the quantities is neglected. Let $\mathbf{e}_M^i$ be the vector line of sight between the Master station and the i-th satellite:

$$\mathbf{e}_M^i = r_M^i \cdot \hat{e}_M^i = \mathbf{X}^i - \mathbf{X}_M \tag{57}$$

Where:

r_M^i is the geometric distance between the i-th satellite and the Master station

$\hat{e}_M^i$ is the unit vector which elements are the director cosines of the line of sight between the i-th satellite and the Master station

$\mathbf{X}^i$ is the position of the i-th satellite

$\mathbf{X}_M$ is the Master station position

Similarly, the vector line of sight between the train and the i-th satellite $\mathbf{e}_{Train}^i$ can be defined as:

$$\mathbf{e}_{Train}^i = r_{Train}^i \cdot \hat{e}_{Train}^i = \mathbf{X}^i - \mathbf{X}_{Train}(s) \tag{58}$$

r_{Train}^i is the geometric distance between the i-th satellite and the Train

$\hat{e}_{Train}^i$ is the unit vector which elements are the director cosines of the line of sight between the i-th satellite and the Train

$\mathbf{X}^i$ is the position of the i-th satellite

$\mathbf{X}_{Train}$ is the train position that depends on the curvilinear abscissa of the track s

The baseline $\mathbf{b}$ can be written as:

$$\mathbf{b} = b \cdot \hat{e}_b = \mathbf{X}_{Train}(s) - \mathbf{X}_M \tag{59}$$

Where:

b is the magnitude of the baseline

$\hat{e}_b$ is the unit vector which elements are the director cosines of the baseline

A schematic representation of differential positioning is depicted in Figure 25.

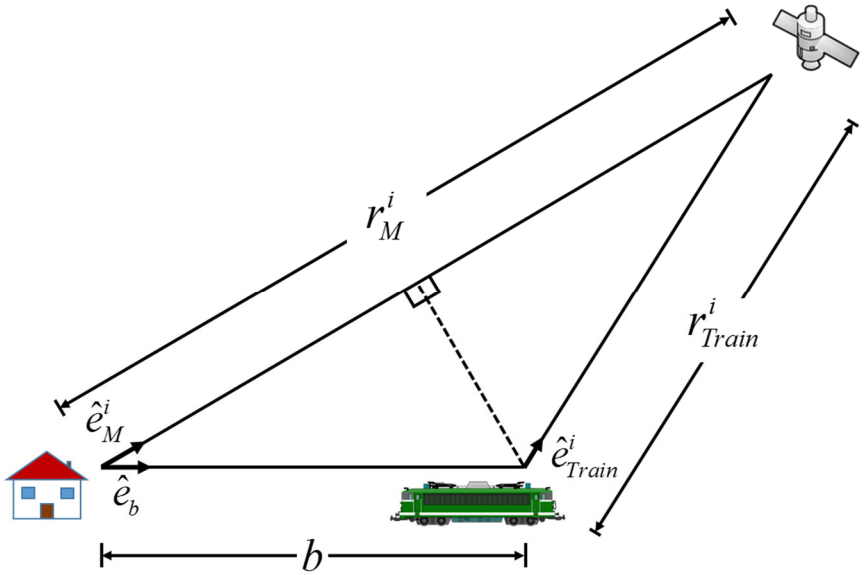

Figure 25. Differential Positioning scheme

According to [45], the single difference among the geometric distance between the i-th satellite and the train with respect to the geometric distance between the i-th satellite the Master $r_{Train,M}^i$ can be expressed as:

$$r_{Train,M}^i = r_{Train}^i - r_M^i = r_{Train}^i\left[1-\left\langle \hat{e}_{Train}^i, \hat{e}_M^i \right\rangle\right] - \left\langle b\cdot\hat{e}_b, \hat{e}_M^i \right\rangle \tag{60}$$

Where:

$\langle\bullet\rangle$ is the scalar product operator

The double difference that involves the satellites i-th and j-th with respect to the Master and the train $r_{Train,M}^{i,j}$ can be expressed as:

$$\begin{aligned} r_{Train,M}^{i,j} &= r_{Train,M}^i - r_{Train,M}^j = \\ &= \left\{ r_{Train}^i\left[1-\left\langle \hat{e}_{Train}^i, \hat{e}_M^i \right\rangle\right] - \left\langle b\cdot\hat{e}_b, \hat{e}_M^i \right\rangle \right\} - \left\{ r_{Train}^j\left[1-\left\langle \hat{e}_{Train}^j, \hat{e}_M^j \right\rangle\right] - \left\langle b\cdot\hat{e}_b, \hat{e}_M^j \right\rangle \right\} = \\ &= r_{Train}^i\left[1-\left\langle \hat{e}_{Train}^i, \hat{e}_M^j \right\rangle\right] - r_{Train}^j\left[1-\left\langle \hat{e}_{Train}^j, \hat{e}_M^j \right\rangle\right] - \left\{ \left\langle b\cdot\hat{e}_b, \hat{e}_M^i \right\rangle - \left\langle b\cdot\hat{e}_b, \hat{e}_M^j \right\rangle \right\} = \\ &= r_{Train}^i\left[1-\left\langle \hat{e}_{Train}^i, \hat{e}_M^j \right\rangle\right] - r_{Train}^j\left[1-\left\langle \hat{e}_{Train}^j, \hat{e}_M^j \right\rangle\right] - \left\langle b\cdot\hat{e}_b, \hat{e}_M^i - \hat{e}_M^j \right\rangle \end{aligned} \tag{61}$$

In the track constrained relative positioning there is only one unknown, the curvilinear abscissa. The solution can be obtained by an iterative approach based on the first order Taylor's series expansion around a train curvilinear abscissa estimation. Let $s^{(m)}$ be the curvilinear abscissa at the m-th step. The initial estimate, as in [7], is obtained by performing a track free PVT estimation and then selecting the nearest track point as the initial point for the iterations. Without loss of generality, let the pivot be the first satellite. Indicating the double differences between the reduced pseudoranges as $\Delta\rho^{i,j}_{Train,M} = \Delta\rho^{i}_{Train} - \Delta\rho^{j}_{Train} - \Delta\rho^{i}_{M} + \Delta\rho^{j}_{M}$, the vector $\overline{DD}^{(m)}$ obtained rearranging column-wise those values at the m-th iteration can be written as

$$\overline{DD}^{(m)} = \left(\Delta\rho^{2,1}_{Train,M}{}^{(m)} \quad \Delta\rho^{3,1}_{Train,M}{}^{(m)} \quad \cdots \quad \Delta\rho^{N_{Sat},1}_{Train,M}{}^{(m)}\right)^T \tag{62}$$

Let $\mathbf{H}^{(m)}$ be the design matrix at the m-th step that would have been evaluated in case of unconstrained PVT estimation. In this case, $\mathbf{H}^{(m)}$ can be expressed as:

$$\mathbf{H}^{(m)} = \begin{pmatrix} e^{2}_{Train,x}{}^{(m)} - e^{1}_{Train,x}{}^{(m)} & e^{2}_{Train,y}{}^{(m)} - e^{1}_{Train,y}{}^{(m)} & e^{2}_{Train,z}{}^{(m)} - e^{1}_{Train,z}{}^{(m)} \\ e^{3}_{Train,x}{}^{(m)} - e^{1}_{Train,x}{}^{(m)} & e^{3}_{Train,y}{}^{(m)} - e^{1}_{Train,y}{}^{(m)} & e^{3}_{Train,z}{}^{(m)} - e^{1}_{Train,z}{}^{(m)} \\ \cdots & \cdots & \cdots \\ e^{N_{Sat}}_{Train,x}{}^{(m)} - e^{1}_{Train,x}{}^{(m)} & e^{N_{Sat}}_{Train,y}{}^{(m)} - e^{1}_{Train,y}{}^{(m)} & e^{N_{Sat}}_{Train,z}{}^{(m)} - e^{1}_{Train,z}{}^{(m)} \end{pmatrix} \tag{63}$$

Where the elements of each row of the $\mathbf{H}^{(m)}$ represents the difference between the directors cosines of the line of sight between the OBU and the corresponding satellite with respect to those of the line of sight between the OBU and the pivot satellite. Let $\mathbf{D}^{(m)}$ be vector that imposes the track constraint at the m-th step. The elements of $\mathbf{D}^{(m)}$ are the director cosines of the tangent to the track in the point with curvilinear abscissa s

$$\mathbf{D}^{(m)} = \begin{pmatrix} \left.\frac{\delta X^{Train}_{x}}{\delta s}\right|_{s=\hat{s}^{(m)}} \\ \left.\frac{\delta X^{Train}_{y}}{\delta s}\right|_{s=\hat{s}^{(m)}} \\ \left.\frac{\delta X^{Train}_{z}}{\delta s}\right|_{s=\hat{s}^{(m)}} \end{pmatrix} \tag{64}$$

The constrained PVT solution for the m-th step can be evaluated by solving the system:

$$\overline{DD}^{(m-1)} = \mathbf{H}^{(m-1)}\mathbf{D}^{(m-1)}\Delta s^{(m)} + \underline{\upsilon} \tag{65}$$

Where $\underline{\upsilon}$ indicates the residuals vector. The set of linear equation can be solved by means of a weighted least square method or by means of an extended Kalman filter approach:

$$\hat{s}^{(m)} = \hat{s}^{(m-1)} + \mathbf{K}^{(m)}\overline{DD}^{(m-1)} \tag{66}$$

Where the gain matrix $\mathbf{K}^{(m)}$ can be obtained as:

$$\mathbf{K}^{(m)} = \left(\mathbf{D}^{(m-1)T}\mathbf{H}^{(m-1)T}\mathbf{R}_{\nu}^{-1}\mathbf{H}^{(m-1)}\mathbf{D}^{(m-1)}\right)^{-1}\mathbf{D}^{(m-1)T}\mathbf{H}^{(m-1)T}\mathbf{R}_{\nu}^{-1} \tag{67}$$

Where $\mathbf{R}_{\nu}$ is the weight matrix

4.5 SIMULATION RESULTS

In this section, the main results of the track-constrained estimation will be presented. A simulator developed by RadioLabs in the framework of the ESA Artes-20 3InSat and H2020 ERSAT projects have been used to process part of the results shown. In order to emulate a train performing a ride on a single track, a car travelling on a highway environment has been used. Particularly, the scenario design foresees a car travelling on the GRA (Grande Raccordo Anulare), a highway that surrounds the city of Rome in Italy. Two Reference and Integrity Monitoring (RIM) stations have been deployed near the path followed by the car. Both RIMs and OBU have been equipped with two single frequency COTS receivers developed by two different manufacturers (nvs and ubox). In the simulation, only the GPS constellation has been enabled. Figure 26 depicts the path followed by the car and the location of the RIMs. In the simulation results, only a part of the entire measurement campaign has been exploited. This information is depicted in Figure 26 by the colour of the line. The blue line indicates the part of the path used in the simulation while the red line represents the portion of data discarded by the simulations. The same dataset has been processed in the differential GPS approach and in

relative positioning approach; in this way, it is possible to carry out a performance analysis in terms of estimated mileage accuracy. To construct the Ground Truth, an additional multi-frequency and multi-constellation receiver produced by Septentrio has been installed in the OBU. Measurements coming from this higher-grade sensor have been processed by means of an external RTK (Real Time Kinematic) service[3]. Figure 27 and Figure 28 respectively show the temporal trend of the mileage estimation error for differential positioning approach and code double difference approach. The histograms of the positioning errors in both approaches are respectively depicted in Figure 29 and Figure 30. Finally, Figure 31 and Figure 32 show the Stanford Plots respectively for differential mode and for code double difference mode.

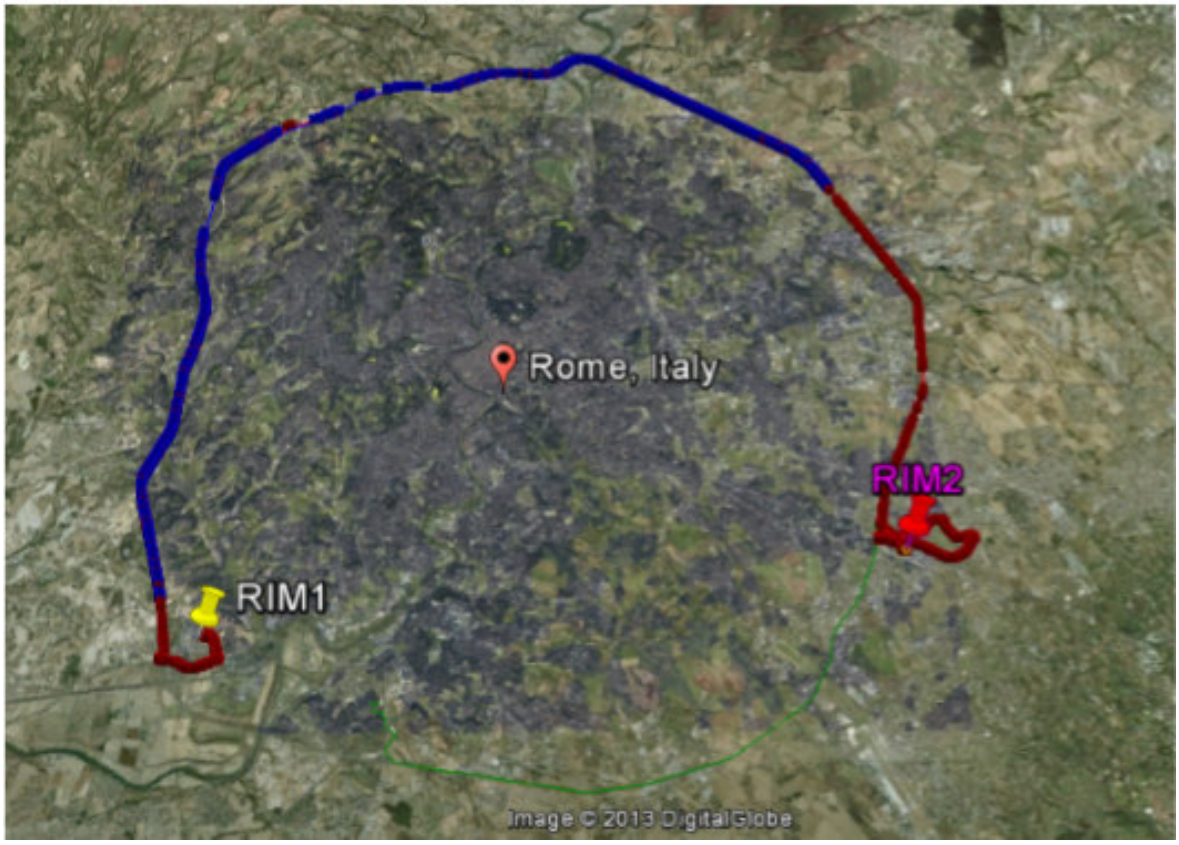

Figure 26. Ground truth of GRA highway in Rome (Italy). The blue line is the portion of the track taken into account in the simulations; the red line is the discarded section

[3] The Ground Truth has been provided by RadioLabs.

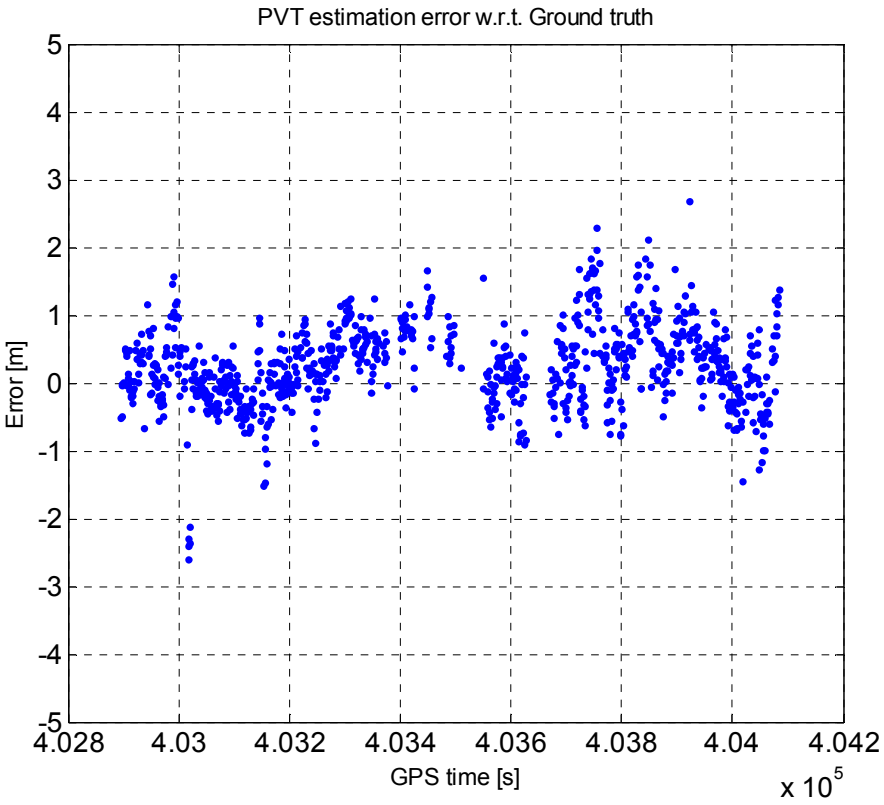

Figure 27. Error temporal trend in Differential GPS Mode

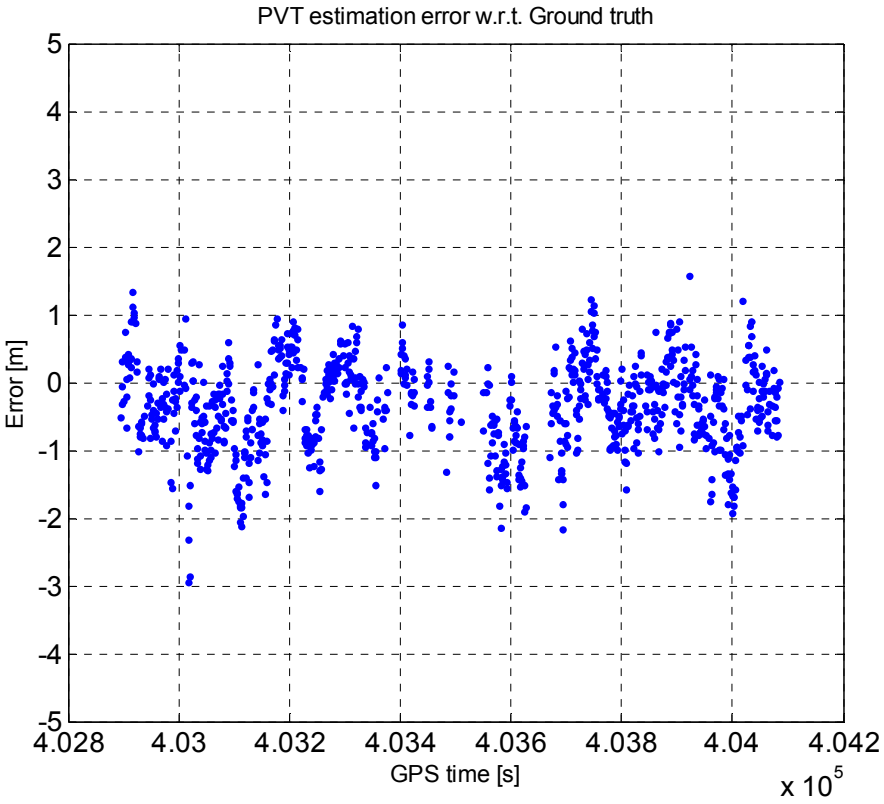

Figure 28. Error temporal trend in code Double difference mode

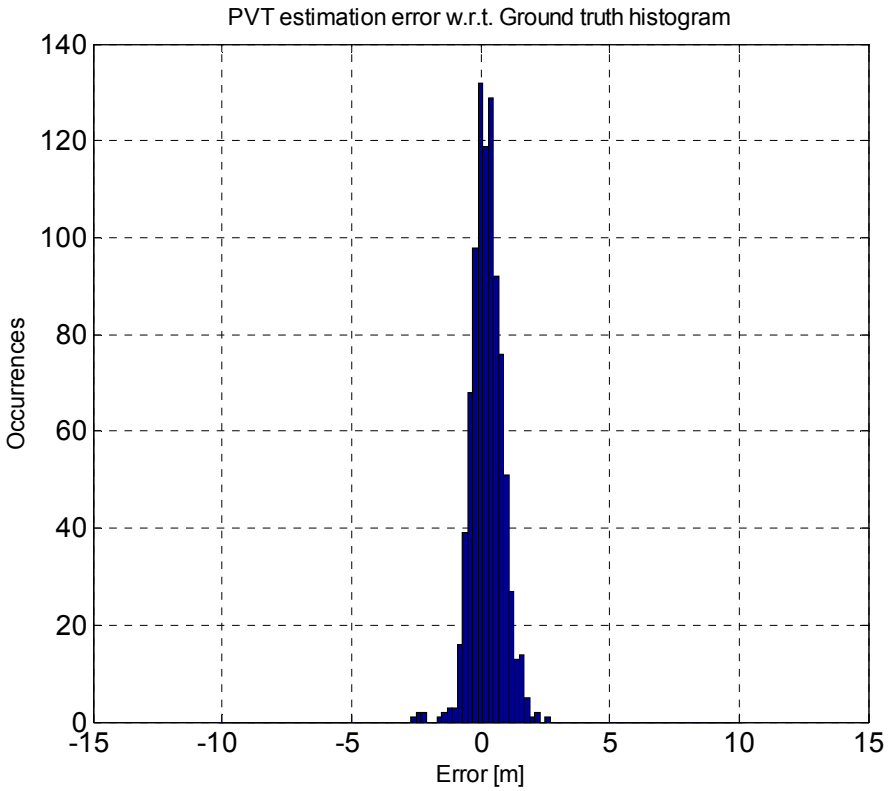

Figure 29. Histogram of the positioning error in differential mode

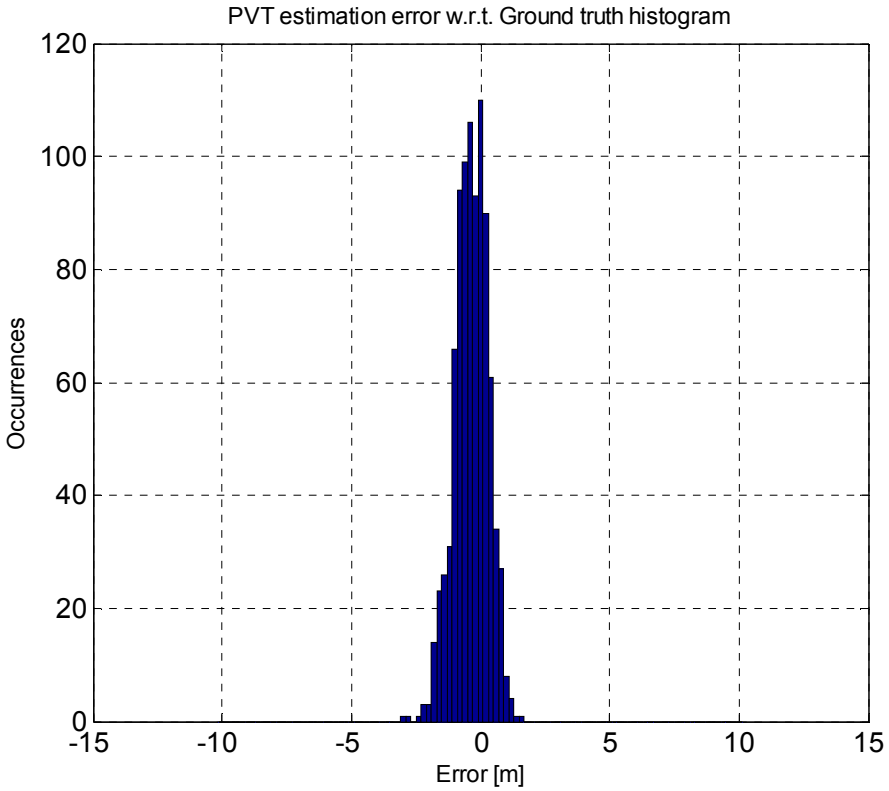

Figure 30. Histogram of the positioning error in code double difference mode

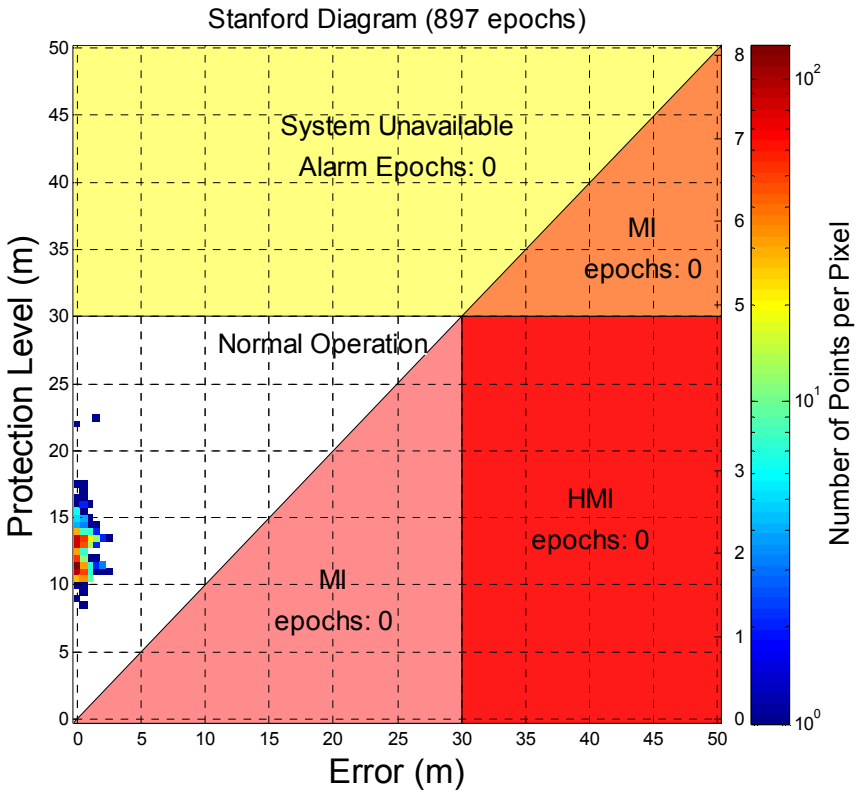

Figure 31. Stanford plot in differential mode

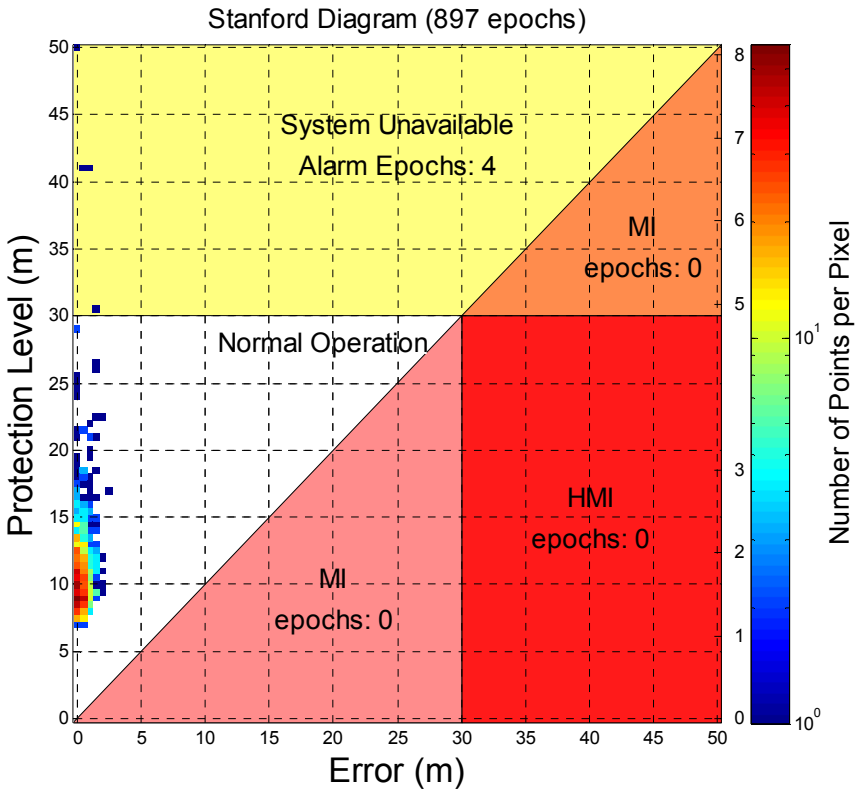

Figure 32. Stanford plot in code double difference mode

As it can be seen from the figures, the performance of the two approaches are similar. The magnitude of the position error for both approaches, in this scenario, is mostly lower than 2 meters. The main benefit of using the double difference approach is the removal of clocks issues from the navigation solution. In fact, the component of a satellite fault that affects the satellite clock offset will be completely compensated by the double difference approach. As it can be seen in the Stanford plot, the double difference approach, in this scenario, has been slightly more conservative; in fact, the protection level is over bounding the estimation error giving origin to 4 false alarms. Both the presented techniques, as it will be explained in the next section, can perform the position estimation even in case of multiple tracks.

5 TRACK DISCRIMINATION BY USING GNSS

In this section, the train positioning in case of multiple track will be described. As mentioned in section 4, this problem can be analysed separately from the positioning along the line. This problem, according to [46], is far more challenging than the PVT estimation alone; in fact, the inter-track separation is smaller compared to the confidence interval needed for the mileage estimation.

5.1 TRACK DISCRIMINATION: PROBLEM STATEMENT

In ERTMS L2, track side equipment like the track circuits allow to determine which track the train is lying on; by consequence of this, manufacturers and scientists have paid their attention on estimating the current train mileage (in mathematical terms the curvilinear coordinate) with respect to the known track [5]. The outcomes of several European projects indicated that the jointly use of multi-constellation receivers and next generation Wide Area Augmentation Systems should allow to guarantee the accuracy required for a safe and cost-effective train control system, when the train itinerary (i.e., the ordered sequence of tracks) is known by other means [5],[18],[43],[47]. However, at the start of mission, even with the current trackside technology there are some cases in which is not possible to determine the track with an acceptable confidence interval. The train in this phase proceeds in SRM (Staff Responsible Mode) until it meets the first balise group; after that it passes in Full Supervision and it is taken in charge by the RBC. As introduced in section 1, in SRM, the train is limited to a ceiling speed implying low average speed as well as low accelerations. If we were able to reduce the time, and ideally to remove it, spent in SRM, the operators would be able to increase the efficiency of the line. As in [5], GNSS based solutions are under study to determine the actual occupied track without the need of physical balises. Due to small inter-distance between parallel tracks, that can even be about 2.4 meters, the confidence interval required is one order of magnitude smaller than the one required for the train mileage (on known track). Some solutions have been studied to solve the track detection problem. In [48], authors provide a model based on HMM (Hidden Markov Model), a signal model widely used in speech processing and control. The basic idea behind a Markov chain is that the state of the system at time t depends on the state of the system depends at time $t-1$. The HMM is an extension of the concept of Markov models that includes the case where the observation is a probabilistic function of the state [49]. Other

two interesting approaches have been provided in [50] and [51], where authors suggested algorithms respectively based on switch curve information and based on LTS-Hausdorff distance. In [46], authors provided a method based on differential GNSS code positioning to perform the PVT estimation in presence of multiple tracks. In presence of multiple tracks, the single track PVT estimate is combined with track detection. The mileage is a continuous random variable; this means that determining the train position along the line is an estimation problem. On the other hand, determining on which track the train is lying on is a decision problem; in fact, in this case the variable object of determination can assume one out of N values, where N is the number of tracks. Let H_k be the hypothesis that the train is lying on the k-th track. As authors have suggested in [46], let $\Lambda_k\left(\rho_{Train}^i\right)$ be the generalized likelihood ratio given by the condition probability function of the observations ρ_{Train}^i with respect to the k-th hypothesis H_k divided by any arbitrary function that does not depend on H_k:

$$\Lambda_k\left(\rho_{Train}^i\right)=\frac{p_{P_{Train}^i/H_k}\left(P_{Train}^i/H_k\right)}{w\left(P_{Train}^i\right)} \tag{68}$$

Under the assumption that the hypotheses are uniformly distributed, the Bayesian (optimal) track detection rule selects the hypothesis corresponding the largest $\Lambda_k\left(\rho_{Train}^i\right)$, or equivalently to the largest $\ln\left[\Lambda_k\left(\rho_{Train}^i\right)\right]$ being the logarithm a monotonic increasing function.

5.2 TRACK DISCRIMINATION: STAND ALONE OR DIFFERENTIAL GNSS

According with the method proposed in [46], following the approach explained in section 4, the PVT estimation can be performed for each hypothesis H_k by solving the system:

$$\Delta\underline{\rho}_{H_k}^{(m-1)}=\mathbf{H}_{H_k}^{(m-1)}\mathbf{D}_{H_k}^{(m-1)}\underline{z}_{H_k}^{(m)}+\underline{\upsilon} \tag{69}$$

According to [46] and to [52], an estimation of $\underline{z}$ is performed for each hypothesis H_k assuming that H_k is true. Finally, a likelihood ratio test is applied to determine which

hypothesis is the most plausible. The selected hypothesis is the one which correspond to the largest generalized log-likelihood ratio.

$$\ln \tilde{\Lambda}_k(\boldsymbol{\rho}) = \underset{z_{H_k}}{Max}\left\{ \ln\left[\frac{p_{\boldsymbol{\rho}/H_k}\left(\mathbf{P}/\hat{z}_{H_k}\right)}{w(\mathbf{P})} \right] \right\} \tag{70}$$

Conditioned to the H_k hypothesis, $\boldsymbol{\rho}$ is a Gaussian distributed random variable with expectation and covariance matrix equal to:

$$\begin{aligned} E\left\{\boldsymbol{\rho}/\hat{z}_{H_k}, H_k\right\} &= \hat{\boldsymbol{\rho}}_{H_k} + \mathbf{H}_{H_k}\mathbf{D}_{H_k}\underline{\hat{z}}_{H_k} \\ Cov\left\{\boldsymbol{\rho}/\hat{z}_{H_k}, H_k\right\} &= \mathbf{R}_{\upsilon} \end{aligned} \tag{71}$$

Where the estimated pseudorange is defined as

$$\hat{\boldsymbol{\rho}}_{H_k} = \hat{\mathbf{r}}_{H_k} - c\delta\hat{\mathbf{t}}^{sat} + c\Delta\hat{\boldsymbol{\tau}}^{ion}_{H_k} + c\Delta\hat{\boldsymbol{\tau}}^{trop}_{H_k} \tag{72}$$

Where:

$\hat{\mathbf{r}}_{H_k}$ is the vector of the estimated geometric distance between the satellites and the receiver position at the final iteration when the train is assumed to be located along the k-th track

$c\delta\hat{\mathbf{t}}^{sat}$ is the vector of the estimated satellite clock offsets

$c\Delta\hat{\boldsymbol{\tau}}^{ion}_{H_k}$ is the vector of the estimated ionospheric incremental delay between the satellites and the receiver position at the final iteration when the train is assumed to be located along the k-th track

$c\Delta\hat{\boldsymbol{\tau}}^{trop}_{H_k}$ is the vector of the estimated tropospheric incremental delay between the satellites and the receiver position at the final iteration when the train is assumed to be located along the k-th track

The conditioned probability can be written as:

$$p_{\boldsymbol{\rho}/H_k}\left(\mathbf{P}/\hat{z}_{H_k}\right)=$$
$$=\frac{1}{\left[\left(2\pi\right)^{N_{sat}}\det\left(\mathbf{R}_{\upsilon}\right)\right]^{1/2}}\exp\left\{-\frac{1}{2}\left[\boldsymbol{\rho}-\hat{\boldsymbol{\rho}}_{H_k}-\mathbf{H}_{H_k}\mathbf{D}_{H_k}\underline{\hat{z}}_{H_k}\right]^{T}\mathbf{R}_{\upsilon}^{-1}\left[\boldsymbol{\rho}-\hat{\boldsymbol{\rho}}_{H_k}-\mathbf{H}_{H_k}\mathbf{D}_{H_k}\underline{\hat{z}}_{H_k}\right]\right\} \tag{73}$$

Let the function $w\left(\boldsymbol{\rho}\right)$ be defined as:

$$w\left(\boldsymbol{\rho}\right)=\frac{1}{\left[\left(2\pi\right)^{N_{sat}}\det\left(\mathbf{R}_{\upsilon}\right)\right]^{1/2}} \tag{74}$$

The log-likelihood ratio can be then expressed as:

$$\begin{aligned}\ln\tilde{\Lambda}_k\left(\boldsymbol{\rho}\right)&=\underset{z_{H_k}}{Max}\left\{\ln\left[\frac{p_{\boldsymbol{\rho}/H_k}\left(\mathbf{P}/\hat{z}_{H_k}\right)}{w\left(\mathbf{P}\right)}\right]\right\}=\\&=\underset{z_{H_k}}{Max}\left\{-\frac{1}{2}\left[\boldsymbol{\rho}-\hat{\boldsymbol{\rho}}_{H_k}-\mathbf{H}_{H_k}\mathbf{D}_{H_k}\underline{\hat{z}}_{H_k}\right]^{T}\mathbf{R}_{\upsilon}^{-1}\left[\boldsymbol{\rho}-\hat{\boldsymbol{\rho}}_{H_k}-\mathbf{H}_{H_k}\mathbf{D}_{H_k}\underline{\hat{z}}_{H_k}\right]\right\}\end{aligned} \tag{75}$$

The residuals vector corresponding to the k-th hypothesis $\breve{\boldsymbol{\upsilon}}_{H_k}$ can be expressed as:

$$\hat{\boldsymbol{\upsilon}}_{H_k}=\Delta\breve{\boldsymbol{\rho}}_{H_k}-\breve{\mathbf{H}}_{H_k}\breve{\mathbf{D}}_{H_k}\underline{\hat{z}}_{H_k} \tag{76}$$

Where:

$\Delta\breve{\boldsymbol{\rho}}_{H_k}$ is the reduced pseudo range at the final iteration when the train is assumed to be located along thek-th track;

$\breve{\mathbf{H}}_{H_k}$ is the design matrix at the final iteration when the train is assumed to be located along the k-th track

$\breve{\mathbf{D}}_{H_k}$ is the matrix that imposes the track constraint when the train is assumed to be located along the k-th track

$\underline{\hat{z}}_{H_k}$ the estimated mileage and receiver clock offset vector at the final iteration when the train is assumed to be located along the k-th track;

Finally, the log-likelihood ratio can be written as:

$$\ln \tilde{\Lambda}_k(\boldsymbol{\rho}) = -\frac{1}{2}\left\|\zeta_{H_k}\right\|^2 \tag{77}$$

Where:

$$\left\|\zeta_{H_k}\right\|^2 = \boldsymbol{\upsilon}_{H_k}^T \mathbf{R}_{\upsilon}^{-1} \boldsymbol{\upsilon}_{H_k}$$

The selected track is the one for which is minimum the weighted squared L2 norm of the residuals. The probability of each track can be then evaluated as:

$$\Pr\{H_k\} = \frac{\exp\left\{-\frac{1}{2}\left\|\zeta_{H_k}\right\|^2\right\}}{\sum_{n=1}^{N}\exp\left\{-\frac{1}{2}\left\|\zeta_{H_n}\right\|^2\right\}} \tag{78}$$

5.3 TRACK DISCRIMINATION: MULTI STATION DOUBLE DIFFERENCE

In a railway scenario, as it has been shown in section 2, the use of an augmentation network is highly recommended. Having a set of reference stations deployed trackside, it is possible to exploit measurements provided by more than one station to determine the track on which the train is lying among a set of N parallel tracks. In [53], authors describe a solution to this issue that jointly uses code and carrier phase raw measurements provided by a subset of RS belonging to a Local Area Augmentation Network. This local network can be also considered as a dedicated AIMN or as the 2nd layer of a "2-tiers" augmentation network. Similarly to the approach presented in [46], the proposed approach split the location along the track problem by the track detection problem. The first step of the algorithm performs a mileage estimation separately on each track assuming that the train is lying on that track, then the second step perform the track selection function. The mileage estimation is carried out by exploiting a coarse to fine procedure as shown in Figure 33. The first operation is a standard code double difference positioning selecting one RS belonging to the network. The aim of this coarse estimation is to provide an initialization for the track constrained algorithm presented in section

4. Let N be the number of tracks and H_k be the hypothesis that the train is lying on the k-th track. For each hypothesis H_k, the point of the k-th track nearest to the coarse estimation is individuated. A track constrained double difference approach is then applied to perform the fine estimation. To select which RS is more suitable to perform this step it is important to consider the baseline vector between the RS and the train position. A schematic representation of the geometry projection of the baselines on the tracks is depicted in Figure 34. If the baseline is parallel to the track, a small variation on the estimated mileage will produce an effect on the baseline; on the other hand, if the baseline is orthogonal to the track, small variation on the estimated mileage will produce very little variations on the baseline. In the track detection problem, the position on two adjacent tracks will produce small difference on a baseline parallel to the track while it will produce higher effect on a baseline orthogonal to the tracks. In essence, a baseline lying along the tracks gives more information on mileage determination than one lying at the cross-over. On the other side of the coin, a baseline orthogonal to the tracks gives more information on the track determination problem. The RS with the most parallel baseline among the others is selected to perform the mileage estimator step. Once, for each track, a position has been estimated, a check among the data provided by all the stations will be carried out to evaluate the probability associated with all the hypotheses. Then, the hypothesis corresponding to the highest probability will be selected.

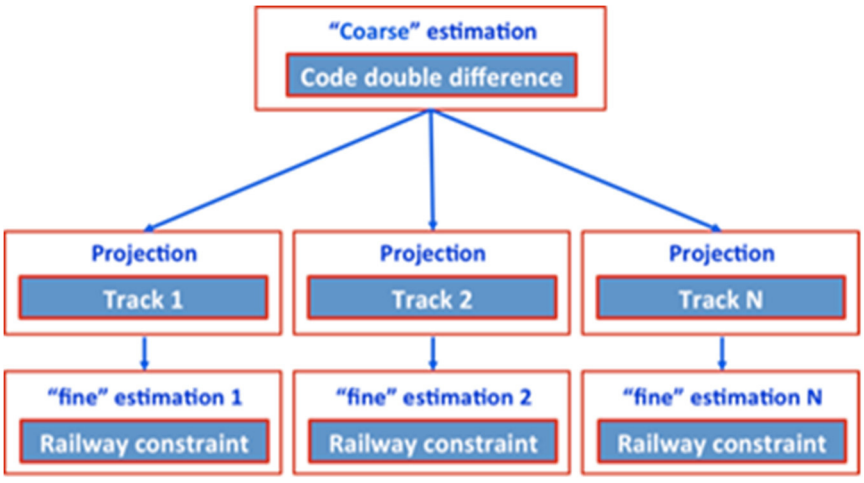

Figure 33. Coarse to fine mileage estimator

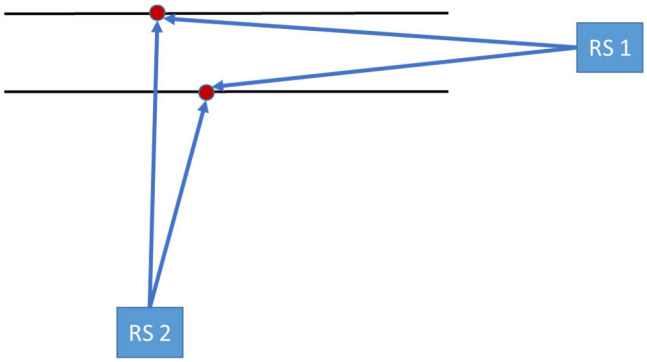

Figure 34. Geometry projections of the baseline on the track

Let $\underline{X}_{Train,k}(s_k)$ be the train position estimation obtained considering the hypothesis H_k as the true one. For both frequencies L1 and L2 it is possible to predict a theoretical carrier range measurement double difference vector by using the i-th and the j-th satellite with respect to the k-th position and the n-th Reference Station:

$$\Delta\nabla \mathbf{DD}_{n,k}^{i,j}\Big|_{\phi,f} = \Delta\nabla r_{n,k}^{i,j} + \Delta\nabla c\Delta t_{i,j,n,k}^{tropo} - \Delta\nabla c\Delta t_{i,j,n,k}^{iono}\Big|_f + \lambda_f \Delta\nabla N_{n,k}^{i,j}\Big|_f \tag{79}$$

where:

$\Delta\nabla r_{n,k}^{i,j}$ is the double difference of the geometric distance

c is the speed of the light in the vacuum

$\Delta\nabla c\Delta t_{i,j,n,k}^{tropo}$ is the double difference of the tropospheric incremental delay

$\Delta\nabla c\Delta t_{i,j,n,k}^{iono}\Big|_f$ is the double difference of the ionospheric incremental delay corresponding to the f-th frequency $f = L1, L2$

λ_f is wavelength corresponding to the f-th frequency $f = L1, L2$

$\Delta\nabla N_{n,k}^{i,j}\Big|_f$ is the double difference of carrier phase ambiguities corresponding to the f-th frequency $f = L1, L2$

Concerning phase ambiguity estimation, it can be initialized as:

$$\lambda_f \, \Delta\nabla N_{n,k}^{i,j}\Big|_f = \lambda_f \, \mathbf{DD}_{n,k}^{i,j}\Big|_{\phi,f} - \mathbf{DD}_{n,k}^{i,j}\Big|_{\rho,f} \tag{80}$$

where:

$\mathbf{DD}_{n,k}^{i,j}\Big|_{\phi,f}$ is the double difference of receivers carrier phase raw data corresponding to the f-th frequency $f = L1, L2$

$\mathbf{DD}_{n,k}^{i,j}\Big|_{\rho,f}$ is the double difference of receivers pseudoranges raw data corresponding to the f-th frequency $f = L1, L2$

Without loss of generality, let the first satellite be the pivot. For each satellite and for each track it is possible to write an indicator υ_k^i defined as:

$$\upsilon_k^i = \sum_{n=1}^{N_{RS}} \sum_{f=1}^{2} \left(\mathbf{DD}_{n,k}^{i,1}\Big|_{\phi,f} - \Delta\nabla \mathbf{DD}_{n,k}^{i,1}\Big|_{\phi,f} \right)^2 \tag{81}$$

Then for each track, the Dr_k indicator is evaluated as follows:

$$Dr_k = \sum_{i=2}^{N_{Sat}} \upsilon_k^i \tag{82}$$

The decision rule foresees that among the hypothesis, the one corresponding to the lowest Dr_k is selected. The probability associated to the k-th hypothesis can be expressed as:

$$\Pr\{H_k\} = \frac{e^{-Dr_k}}{\sum_{tr=1}^{N_{track}} e^{-Dr_{tr}}} \tag{83}$$

5.3.1 Simulation Results

To verify the system performance, a synthetic scenario has been created. Particularly raw data coming from the IGS station WTZR (Bad Koetzting – Bavaria – Germany) has been used to emulate a train still at a railway station. At this aim, a synthetic track (indicated with

#1) has been created assuming that the WTZR station lies in the middle of the track. The map view of the synthetic track is shown in Figure 35. Then a second track (labelled as #2), parallel to the first one, has been generated assuming a constant gap of 4 meters. Other two stations belonging to the IGS network have been selected to act as Master Stations. More in details the selected stations are: BZRG station (located in Bolzano – Italy) and GOPE (located in Ondrejov – Bohemia – Czech Republic). The BZRG station has also been used as the Master for first step of the algorithm. The footprint of the station network is shown in Figure 36.

Figure 35. WTZR synthetic track

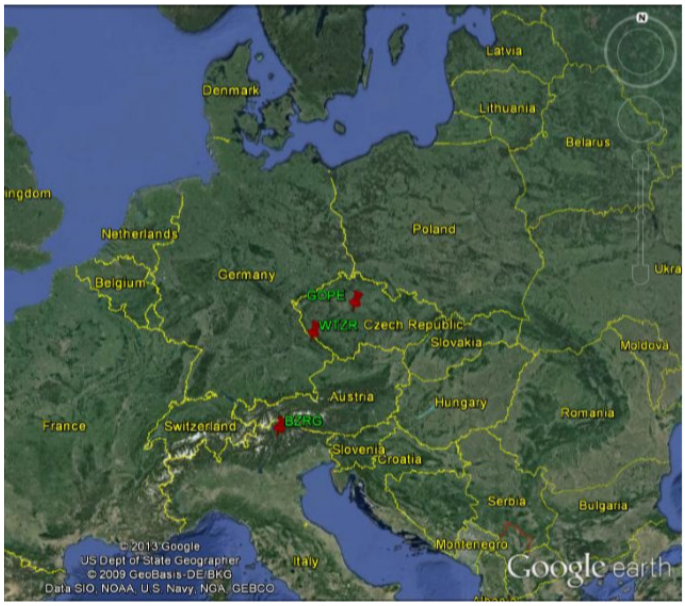

Figure 36. WTZR, BZRG and GOPE location

Both multi station double difference approach and the differential algorithm shown in the previous section have been tested with the same dataset acquired at 1Hz. The simulations have been carried out by considering only the L1 raw data. Both algorithms correctly identified the occupied track as the track number one. Figure 38 and Figure 39 show respectively the probabilities associated with the tracks in the differential approach and in the multi-station double difference. As it is possible to perceive by the pictures, the multi station double difference based approach performed much better than the differential approach. However, for both approaches, the use of sliding windows in which perform the estimation can improve the performance. The integration can be performed coherently (in the range or carrier phase domain) or incoherently (in the estimated track domain). The wider is the window, the higher will be the accuracy; however, the drawback of a wider window is the increasing of the time required to take the decision.

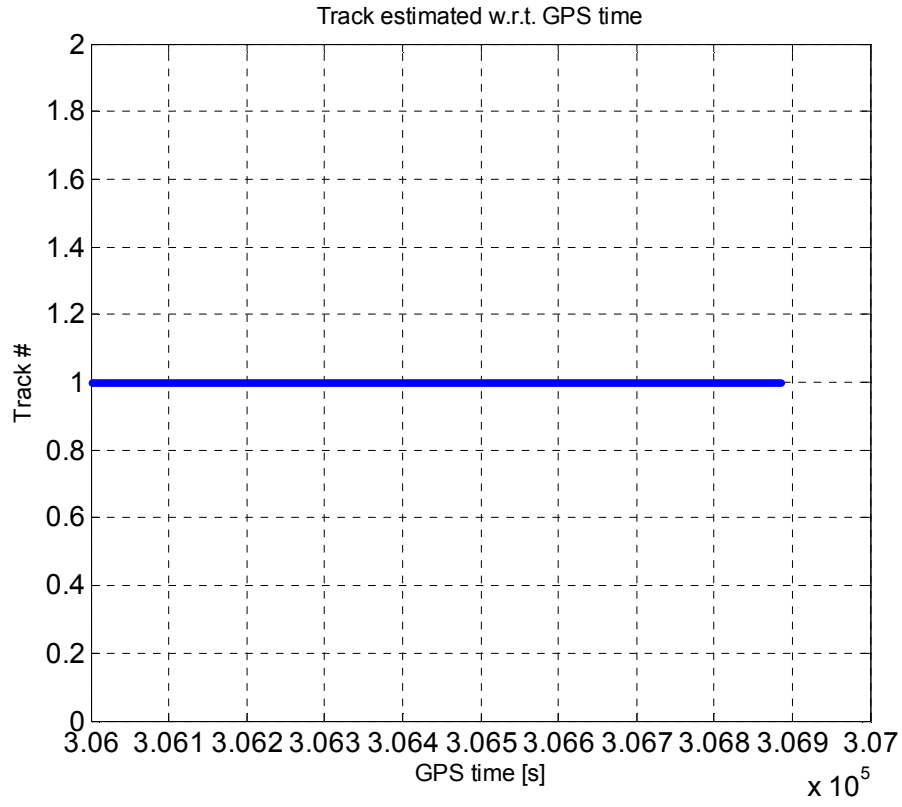

Figure 37. Identified occupied track with Differential and Multiple Station approach

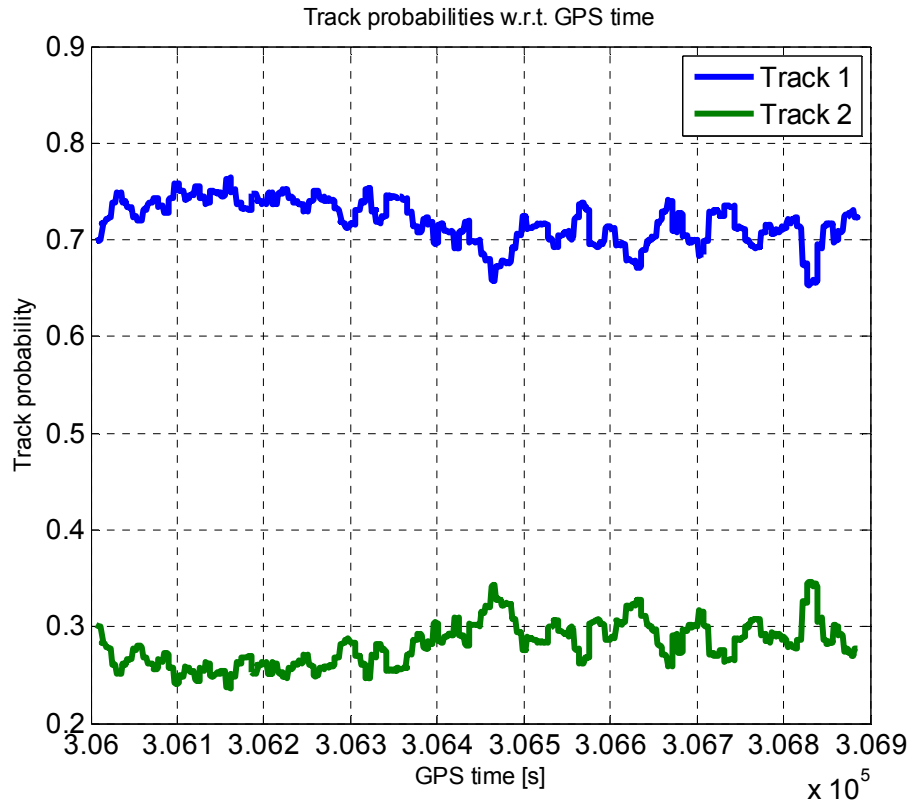

Figure 38. Track probabilities for differential approach

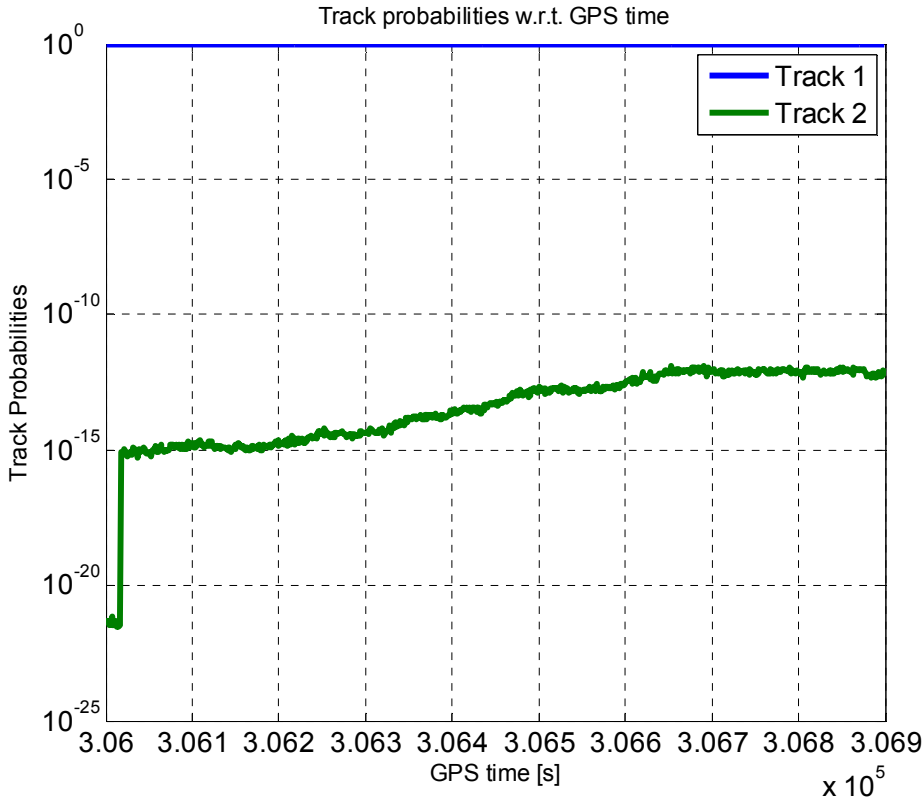

Figure 39. Track probabilities for multi station double difference approach

5.4 TRACK DISCRIMINATION: PHASE DOUBLE DIFFERENCE

A highly promising solution for track determination in the start of mission procedure has been presented in [5]. In this contribution, authors have made use of a carrier phase raw measurement double difference approach. The carrier phase raw measurement observed by either the train or the master station for the i-th satellite for the f-th frequency, for a generic epoch, can be written as:

$$\lambda_f \phi_o^i = r_o^i + c\left(\delta t_o - \delta t_i^{Sat}\right) - c\Delta\tau_{i,o}^{ion,f} + c\Delta\tau_{i,o}^{trop} + N_{i,o}^f \lambda_f + \upsilon_o^i\Big|_{\phi,f} \quad o \in \{Train, M\} \tag{84}$$

Where:

λ_f is the wavelength corresponding to the f-th frequecy;

ϕ_o^i is the measured carrier phase cycles for the i-th satellite by the o-th receiver;

r_o^i is the true range between the i-th satellite and the o-th receiver;

c is the speed of light in the vacuum;

δt_o is the o-th receiver clock offset;

δt_i^{sat} is the clock offset of the i-th satellite;

$c\Delta\tau_{i,o}^{ion,f}$ is the ionospheric incremental delay on the Line of Sight between the i-th satellite and the o-th receiver at the f-th frequency;

$c\Delta\tau_{i,o}^{trop,o}$ is the tropospheric incremental delay on the Line of Sight between the i-th satellite and the o-th receiver;

$N_{i,o}^f$ is the carrier phase ambiguity in the observation of the i-th by the o-th receiver at the f-th frequency;

$\upsilon_o^i\Big|_{\phi,f}$ is the error on the Line of Sight between the i-th satellite and the o-th receiver at the f-th frequency that has not been explicitly expressed. This term contains the receiver thermal noise, interferences and so on.

For sake of compactness, let $\nabla\Delta\underline{\rho}_f$ be the vector of double difference reduced

pseudoranges at the f-th frequency. In a similar way, let $\nabla\Delta\underline{L}_f = \lambda_f \nabla\Delta\underline{\phi}_f$ be the vector whose components are the double difference reduced carrier phase measurements at the f-th frequency. As it has been shown in section 4.4, it is possible to perform the PVT estimation by iteratively solving a set of equations. In case of using code measurement, the equation constrained system at the m-th step can be written as:

$$\nabla\Delta\underline{\rho}_f^{(m-1)} = \mathbf{H}^{(m-1)}\mathbf{D}^{(m-1)}\Delta\hat{s}^{(m)} + \underline{\upsilon}_f^{\rho} \quad f = 1,2 \tag{85}$$

Where:

$\nabla\Delta\underline{\rho}_f^{(m)}$ is the vector of double difference reduced pseudoranges st the f-th frequency at the m-th step;

$\mathbf{H}^{(m)}$ is the design matrix for the unconstrained PVT solution at the m-th step[4];

$\mathbf{D}^{(m)}$ is the vector that imposes the track constraint at the m-th step[5];

$\Delta\hat{s}^{(m)}$ is the estimated correction to be applied to the train mileage at the m-th step;

$\underline{\upsilon}_f^{\rho}$ is the residuals vector for code measurements at the f-th frequency;

In a similar way, in case of carrier phase observations the phase vector can be written as:

$$\nabla\Delta\underline{L}_f^{(m-1)} = \mathbf{H}^{(m-1)}\mathbf{D}^{(m-1)}\Delta\hat{s}^{(m)} + \lambda_f\nabla\Delta\mathbf{N}_f^{(m)} + \lambda_f\underline{\upsilon}_f^{\phi} \quad f = 1,2 \tag{86}$$

Where:

$\nabla\Delta\mathbf{N}_f^{(m)}$ is the vector whose components are the estimated double difference for carrier phase ambiguities at the m-th step;

Following the analytical model illustrated by authors in [5], both carrier phase and

[4] See section 4.4 for more details
[5] See section 4.4 for more details

pseudorange equations can be rearranged in a unique set of equations:

$$\begin{bmatrix} \nabla\Delta\underline{\rho}_1^{(m-1)} \\ \nabla\Delta\underline{\rho}_2^{(m-1)} \\ \nabla\Delta\underline{L}_1^{(m-1)} \\ \nabla\Delta\underline{L}_2^{(m-1)} \end{bmatrix} = \begin{bmatrix} \mathbf{H}^{(m-1)}\mathbf{D}^{(m-1)} & 0 & 0 \\ \mathbf{H}^{(m-1)}\mathbf{D}^{(m-1)} & 0 & 0 \\ \mathbf{H}^{(m-1)}\mathbf{D}^{(m-1)} & \lambda_1\mathbf{I} & 0 \\ \mathbf{H}^{(m-1)}\mathbf{D}^{(m-1)} & 0 & \lambda_2\mathbf{I} \end{bmatrix} \begin{bmatrix} \Delta\hat{s}^{(m)} \\ \nabla\Delta\mathbf{N}_1^{(m)} \\ \nabla\Delta\mathbf{N}_2^{(m)} \end{bmatrix} + \begin{bmatrix} \underline{\upsilon}_1^{\rho} \\ \underline{\upsilon}_2^{\rho} \\ \lambda_1\underline{\upsilon}_1^{\phi} \\ \lambda_2\underline{\upsilon}_2^{\phi} \end{bmatrix} \tag{87}$$

By considering the observation Narrow Lane and Wide Lane combinations of code and carrier phase, it is possible to write this equation set:

$$\begin{bmatrix} \nabla\Delta\underline{\rho}_{WL} \\ \nabla\Delta\underline{\rho}_{NL} \\ \nabla\Delta\underline{L}_{WL} \\ \nabla\Delta\underline{L}_{NL} \end{bmatrix} = \begin{bmatrix} \frac{f_1}{f_1-f_2} & -\frac{f_2}{f_1-f_2} & 0 & 0 \\ \frac{f_1}{f_1+f_2} & \frac{f_2}{f_1+f_2} & 0 & 0 \\ 0 & 0 & \frac{f_1}{f_1-f_2} & -\frac{f_2}{f_1-f_2} \\ 0 & 0 & \frac{f_1}{f_1+f_2} & \frac{f_2}{f_1+f_2} \end{bmatrix} \begin{bmatrix} \nabla\Delta\underline{\rho}_1 \\ \nabla\Delta\underline{\rho}_2 \\ \nabla\Delta\underline{L}_1 \\ \nabla\Delta\underline{L}_2 \end{bmatrix} \tag{88}$$

According to [5], the information carried by code wide lane combination can be neglected because of the high standard deviation with respect to the single frequencies observation; at the same time, the use of phase narrow lane combination requires an higher time for fixing the ambiguities, thus means that, performing a trade-off between time and accuracy, the choice will fall on code narrow lane and phase wide lane combinations. The PVT equation system at the m-th step of the iterative approach can be rewritten as:

$$\begin{bmatrix} \nabla\Delta\underline{\rho}_{NL}^{(m-1)} \\ \nabla\Delta\underline{L}_{WL}^{(m-1)} \end{bmatrix} = \begin{bmatrix} \mathbf{H}^{(m-1)}\mathbf{D}^{(m-1)} & 0 \\ \mathbf{H}^{(m-1)}\mathbf{D}^{(m-1)} & \lambda_{WL}\mathbf{I} \end{bmatrix} \begin{bmatrix} \Delta\hat{s}^{(m)} \\ \nabla\Delta\mathbf{N}_{WL}^{(m)} \end{bmatrix} + \begin{bmatrix} \underline{\upsilon}_{NL}^{\rho} \\ \lambda_{WL}\underline{\upsilon}_{WL}^{\phi} \end{bmatrix} \tag{89}$$

Where $\lambda_{WL} = \frac{\lambda_1\lambda_2}{\lambda_2 - \lambda_1}$ is the effective wide lane combination wavelength. The initial estimate of the phase ambiguities can be carried out by means of Melbourne-Wubbena approach:

$$\nabla\Delta\underline{B}_{MW} = \nabla\Delta\underline{L}_{WL} - \nabla\Delta\underline{\rho}_{NL} = \lambda_{WL}\nabla\Delta\mathbf{N}_{WL} + \lambda_{WL}\underline{\upsilon}^{\phi}_{WL} - \underline{\upsilon}^{\rho}_{NL} \tag{90}$$

By including the estimated carrier phase into the PVT system, the new equation set can be rewritten as:

$$\begin{bmatrix} \nabla\Delta\underline{\rho}_{NL}{}^{(m-1)} \\ \nabla\Delta\underline{L}_{WL}{}^{(m-1)} - \lambda_{WL}\nabla\Delta\hat{\mathbf{N}}^{(m-1)}_{WL} \end{bmatrix} = \begin{bmatrix} \mathbf{I} \\ \mathbf{I} \end{bmatrix}\mathbf{H}^{(m-1)}\mathbf{D}^{(m-1)}\Delta\hat{s}^{(m)} + \begin{bmatrix} \underline{\upsilon}^{\rho}_{NL} \\ \lambda_{WL}\underline{\upsilon}^{\phi}_{WL} \end{bmatrix} \tag{91}$$

By means of a least square estimator, the estimated mileage at the m-th step can be estimated as:

$$\Delta\hat{s}^{(m)} = \mathbf{K}^{(m)}\begin{bmatrix} \nabla\Delta\underline{\rho}_{NL}{}^{(m-1)} \\ \nabla\Delta\underline{L}_{WL}{}^{(m-1)} - \lambda_{WL}\nabla\Delta\hat{\mathbf{N}}^{(m-1)}_{WL} \end{bmatrix} \tag{92}$$

Where the gain matrix can be expressed as:

$$\mathbf{K}^{(m)} = \left(\mathbf{D}^{(m-1)T}\mathbf{H}^{(m-1)T}\begin{pmatrix}\mathbf{I} & \mathbf{I}\end{pmatrix}\mathbf{R}_{\upsilon}^{-1}\begin{pmatrix}\mathbf{I} \\ \mathbf{I}\end{pmatrix}\mathbf{H}^{(m-1)}\mathbf{D}^{(m-1)}\right)^{-1}\mathbf{D}^{(m-1)T}\mathbf{H}^{(m-1)T}\begin{pmatrix}\mathbf{I} & \mathbf{I}\end{pmatrix}\mathbf{R}_{\upsilon}^{-1} \tag{93}$$

$\mathbf{R}_{\upsilon}$ is a block matrix that can be defined as:

$$\mathbf{R}_{\upsilon} = \begin{pmatrix} \mathbf{R}_{\underline{\upsilon}^{\rho}_{NL}} & 0_{N_{Sat}-1} \\ 0_{N_{Sat}-1} & \mathbf{R}_{\underline{\upsilon}^{\phi}_{WL}} \end{pmatrix} \tag{94}$$

Where:

$\mathbf{R}_{\underline{\upsilon}^{\rho}_{NL}}$ is the double difference narrow lane pseudorange residuals covariance matrix;

$\mathbf{R}_{\underline{\upsilon}^{\phi}_{WL}}$ is the double difference wide lane carrier phase residuals covariance matrix;

$0_{N_{Sat}-1}$ is a square matrix $N_{Sat}-1$ by $N_{Sat}-1$ whose elements are all zeros.

Let $\nabla\Delta\mathbf{R}$ be a vector defined as:

$$\nabla\Delta\mathbf{R} = \begin{bmatrix} \nabla\Delta\underline{\rho}_{NL} \\ \nabla\Delta\underline{L}_{WL} \end{bmatrix} \tag{95}$$

The track detection problem is then carried out by exploiting a generalized likelihood ratio. The approach followed is similar to the others presented in this section.

$$\Lambda_k(\nabla\Delta\mathbf{R}) = \frac{\sum_{\nabla\Delta\mathbf{N}_{WL}} p_{\nabla\Delta\mathbf{R}/H_k,\nabla\Delta\mathbf{N}_{WL}}(\nabla\Delta\mathbf{R}/H_k,\nabla\Delta\mathbf{N}_{WL})P(\nabla\Delta\mathbf{N}_{WL}/H_k)}{w(\nabla\Delta\mathbf{R})} \tag{96}$$

Since the occupied track is statistically independent, authors were able to write:

$$\Lambda_k(\nabla\Delta\mathbf{R}) = \frac{\sum_{\nabla\Delta\mathbf{N}_{WL}} p_{\nabla\Delta\mathbf{R}/H_k,\nabla\Delta\mathbf{N}_{WL}}(\nabla\Delta\mathbf{R}/H_k,\nabla\Delta\mathbf{N}_{WL})P(\nabla\Delta\mathbf{N}_{WL})}{w(\nabla\Delta\mathbf{R})} \tag{97}$$

Then for each track and for each ambiguity set, the position estimation is carried out by considering them as the correct ones. The likelihood functional Can be written as:

$$\tilde{\Lambda}_k(\nabla\Delta\mathbf{R}) = \underset{s_{H_k}}{Max} \frac{\sum_{\nabla\Delta\mathbf{N}_{WL}} p(\nabla\Delta\mathbf{R}/s_{H_k},H_k,\nabla\Delta\mathbf{N}_{WL})P(\nabla\Delta\mathbf{N}_{WL})}{w(\nabla\Delta\mathbf{R})} \tag{98}$$

Conditioned to the *k*-th hypothesis and to the phase ambiguity $\nabla\Delta\mathbf{N}_{WL}$, $\nabla\Delta\mathbf{R}$ is a Gaussian distributed random variable with expectation:

$$E\left\{\nabla\Delta\mathbf{R}/\hat{s}_{H_k,\nabla\Delta\mathbf{N}_{WL}},H_k,\nabla\Delta\mathbf{N}_{WL}\right\} = \begin{bmatrix} \mathbf{0} \\ \lambda_{WL}\mathbf{I} \end{bmatrix}\nabla\Delta\mathbf{N}_{WL} \tag{99}$$

The covariance matrix is expressed as:

$$Cov\left\{\nabla\Delta\mathbf{R} / \hat{s}_{H_k,\nabla\Delta\mathbf{N}_{WL}}, H_k, \nabla\Delta\mathbf{N}_{WL}\right\} = \mathbf{R}_{\mathbf{v}_{WL}} \tag{100}$$

Then, selecting $w(\nabla\Delta\mathbf{R}) = \dfrac{1}{\left[(2\pi)^{2(N_{sat}-1)}\det\left(\mathbf{R}_{v_{WL}}\right)\right]^{\frac{1}{2}}}$, the functional can be expressed as:

$$\tilde{\Lambda}_k(\nabla\Delta\mathbf{R}) = \underset{s_{H_k}}{Max}\sum_{\nabla\Delta\mathbf{N}_{WL}} \exp\left\{-\frac{1}{2}\mathbf{v}^T_{s_{H_k},\nabla\Delta\mathbf{N}_{WL}}\mathbf{R}^{-1}_{\mathbf{v}_{WL}}\mathbf{v}_{s_{H_k},\nabla\Delta\mathbf{N}_{WL}}\right\}P(\nabla\Delta\mathbf{N}_{WL}) \tag{101}$$

Where $\mathbf{v}_{s_{H_k},\nabla\Delta\mathbf{N}_{WL}}$ is defined as:

$$\mathbf{v}_{s_{H_k},\nabla\Delta\mathbf{N}_{WL}} = \nabla\Delta\mathbf{R} - E\left\{\nabla\Delta\mathbf{R} / \hat{s}_{H_k,\nabla\Delta\mathbf{N}_{WL}}, H_k, \nabla\Delta\mathbf{N}_{WL}\right\} \tag{102}$$

Since the mileage has been estimated by means of a weighted least square estimator, the functional can be expressed as:

$$\begin{aligned}\tilde{\Lambda}_k(\nabla\Delta\mathbf{R}) &= \sum_{\nabla\Delta\mathbf{N}_{WL}} \exp\left\{-\frac{1}{2}\hat{\mathbf{v}}^T_{\hat{s}_{H_k},\nabla\Delta\mathbf{N}_{WL}}\mathbf{R}^{-1}_{\mathbf{v}_{WL}}\hat{\mathbf{v}}_{\hat{s}_{H_k},\nabla\Delta\mathbf{N}_{WL}}\right\}P(\nabla\Delta\mathbf{N}_{WL}) = \\ &= \sum_{\nabla\Delta\mathbf{N}_{WL}} \exp\left\{-\frac{1}{2}\left\|\hat{\mathbf{v}}_{\hat{s}_{H_k},\nabla\Delta\mathbf{N}_{WL}}\right\|^2_{\mathbf{R}^{-1}_{\mathbf{v}_{WL}}}\right\}P(\nabla\Delta\mathbf{N}_{WL})\end{aligned} \tag{103}$$

Where:

$\hat{\mathbf{v}}_{\hat{s}_{H_k},\nabla\Delta\mathbf{N}_{WL}}$ are the residual corresponding to the estimated mileage on the k-th track and to the phase ambiguities;

$\left\|\bullet\right\|^2_{\mathbf{R}^{-1}_{\mathbf{v}_{WL}}}$ is the weighted L2 norm operator.

The track for which is maximum the generalized likelihood ratio is selected:

$$\hat{H}_k = Arg\left\{ \underset{k}{Max}\left[\tilde{\Lambda}_k(\nabla\Delta\mathbf{R}) \right] \right\} \tag{104}$$

The posterior probability associated with each track can be determined as:

$$\Pr\{H_k\} = \frac{\sum_{\nabla\Delta\mathbf{N}_{WL}} \exp\left\{ -\frac{1}{2} \left\| \hat{\mathbf{v}}_{\hat{s}_{H_k},\nabla\Delta\mathbf{N}_{WL}} \right\|^2_{\mathbf{R}^{-1}_{\mathbf{v}WL}} \right\} P(\nabla\Delta\mathbf{N}_{WL})}{\sum_{n=1}^{N_{Tracks}} \sum_{\nabla\Delta\mathbf{N}_{WL}} \exp\left\{ -\frac{1}{2} \left\| \hat{\mathbf{v}}_{\hat{s}_{H_n},\nabla\Delta\mathbf{N}_{WL}} \right\|^2_{\mathbf{R}^{-1}_{\mathbf{v}WL}} \right\} P(\nabla\Delta\mathbf{N}_{WL})} \tag{105}$$

5.4.1 Simulation results

To test the phase double difference algorithm, in [5], authors made use of raw data provided by Sogei GRDNet (GNSS R&D network) [68]. Particularly, data coming from the RSs of Sanluri and Villasor have been employed. These two stations are part of the network deployed for the European Horizon 2020 ERSAT EAV project in Sardinia (Italy). The baseline between the two stations is about 22 km [5]. The Villasor station has been selected to emulate a train still at the station. At this aim, a synthetic track (Track #1) centered in Villasor station has been generated. Then, a second track (Track #2) parallel to the first has been synthetized assuming an inter-axis of 2.4 meters. The procedure correctly indicated the correct track. The probability associated with the track are shown in Figure 40.

5.5 CONSIDERATIONS

In this section three approaches to determine on which track the train is lying on by using GNSS observation has been discussed. This capability is important in case of start of mission. If it were possible to define an approach to automatically discriminate the current track, there would be a return in term of drastically reduction of the time required every time a service start. The direct consequence of this time contraction is the higher traffic management efficiency. Indirect benefit obtained is the mitigation of those threats due to human error when the train is running in SRM. The performance assessment for the presented approaches can be found in the cited references.

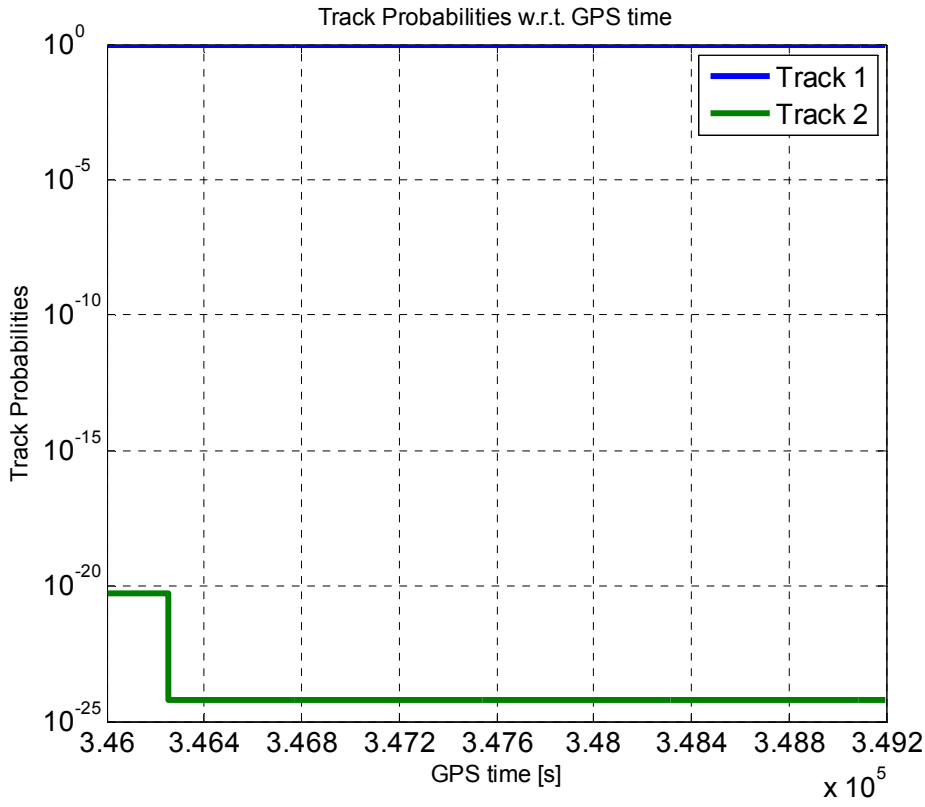

Figure 40. Track Probabilities in the phase double difference approach

6 TRAIN INTEGRITY AND SATELLITE TECHNOLOGY

This section deals with the introduction of ETCS L3. When this level will be operational, the traffic management will be dynamically managed increasing the capacity and the efficiency of the line. Train integrity as well as train separation are two issues that must be faced to perform the "moving block".

6.1 TOWARD THE MOVING BLOCK

As introduced in section 1, the ERTMS/ETCS standard foresees 3 different operational levels that differ among automation level provided: L1, L2 and L3. Beside these levels there is a fourth level called Level 0 that represents the situation under which an ETCS compliant train is travelling on a line that is not equipped with ETCS standard. L1 has been the first one to be deployed, defining a standard that is able to guarantee safety and interoperability. The control centre communicates with the train fleet by means of physical devices called balises. Through this communication link, the train receives the MA, a message that contains information on the authorization to proceed, the maximum speed that can be reached, the next breaking point and all those other data required by the train in order to be able to move. These instructions are then shown to the driver that has to put them into practice. In case of human error, the train is able to automatically correct the ride, mitigating the issues that could occur. The bottle neck of such an approach is the discontinuous link used to send the MAs to the trains. To increase the efficiency of the line management, L2 introduces the radio link communication; in this way, the train fleet and the control centre can rely on a channel to communicate even if the train is not over a balise. The main limitation in the traffic management of L1 and L2 is represented by the "fixed block" approach. The track is partitioned in a set of section which have a predetermined length called blocks; each block can be occupied by no more than one train at the same time. Following this approach, a convoy cannot enter in a block until it has been cleared by the previous train. This assumption determines the minimum separation between two consecutive train. L3 standard, that has only been conceptualized, foresees a more efficient rail management criterion that is called the "moving block". Under this approach, the block length is no more fixed, but can be changed dynamically according to the traffic and the network condition. The main challenge in the migration toward L3 and the moving block is represented by the block occupancy detection. In fact, under L1 and L2, each block is equipped with a track

circuit, a device that is able to detect the presence of rolling stocks on the section. This technology is well consolidated and fits perfectly with the fixed block approach. In the moving block approach, the block length is changed dynamically; this means that also the track circuits should be tuned based on the current block length. A possible solution has been presented by authors in [4] by defining the virtual track circuit. In essence, authors defined the space physically occupied by the train as delimited by the head and the tail of the train. The virtual track circuit length is obtained by considering the train length and two safety buffers located respectively at the front and at the rear of the train. Virtualizing the track circuits, two problems must be addressed: train integrity assessment and train separation.

6.1.1 Train Integrity Assessment

As it has been explained above, a train cannot enter in a block until the preceding train has cleared it. In case of a decoupling event, a portion of the convoy can be lost on the track. In this situation, if the line is L2 compliant, because the track circuits still detect the presence of a rolling stock on the section, the block will still be considered as busy. In this way, the train that comes after will not be allowed to come into the next block and there will not be any collision between the second train and the lost tail section of the previous one. On the other hand, if the line had been equipped with L3, there would have been no physical device to detect the presence of cars on the line. A schematic representation of the train integrity issue is depicted in Figure 41. This means that in L3 system the train must be able to assess its own integrity, determining if all the carriages are still coupled.

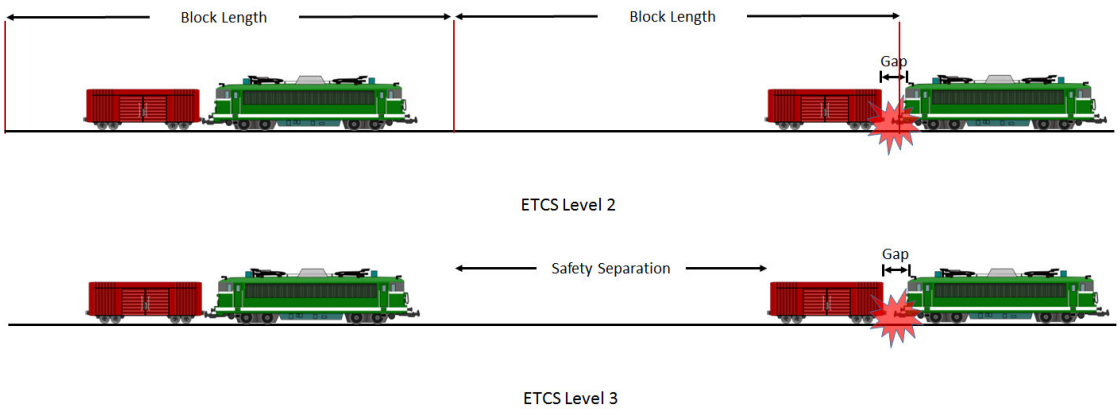

Figure 41. Train integrity issue

In case of decoupling event, an alert must be sent to the train control centre to prevent collisions and to start the procedure to recover the lost section. According to [3] and [4], the trains with pre-assembled configuration can implement the train integrity detector by connecting all the carriages with a cable (often already present for other purposes) and monitoring the electrical continuity on the cable. The main problem arises with the freight trains where the train composition changes potentially at each service requiring ad-hoc devices for the train integrity function. Some solutions foresee the installation of devices on all the coaches. In [54], authors proposed a solution that makes use of a distributed Wireless Sensor Network (WSN). The train composition is determined on the basis of the output of the sensors. To distinguish carriages belonging to different convoys authors proposed solutions based on localization or on dynamic group awareness. In case of unexpected train composition revealed by the WSN corresponding to a possible loss of carriages an alarm is arisen. Another system called TIMS (Train Integrity Monitoring System) which relies on a set of modules installed on each coach has been proposed in [55]. An interesting approach based on data fusion among several sensors including GNSS has been presented in [56], where authors presented a system to detect train integrity for the American train control system called PTC (Positive Train Control). The use of GNSS allow to assess the train integrity as well as to locate the position of the train.

6.2 TRACK CONSTRAINED DECOUPLING DETECTOR

In [4], authors presented a GNSS based approach to assess the train integrity by explicitly accounting for the fact that the train is constrained to lie on a railway line. The main idea is to jointly process observation retrieved by two GNSS receiver located respectively on the head and on the end of the train. In Figure 42, it is shown a schematic representation of the train equipped with pair of GNSS receivers. Authors proposed an approach based on double difference that explicitly account for the track constraint. Due to the short baseline, most of the atmospheric incremental delays are compensated as well as the clock offset contribution has been cancelled out. Moreover, the track constraint allows the reduction of the number of satellite required to perform the estimation.

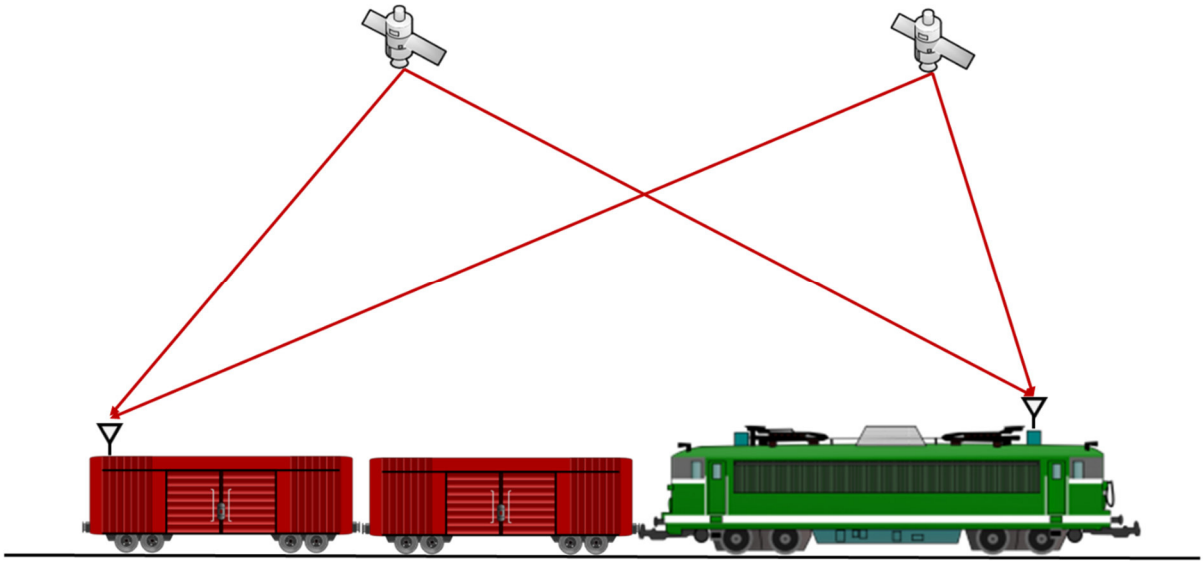

Figure 42. Schematic train with two receivers on board

The proposed algorithm is composed of two steps:

a) PVT estimation of the two GNSS receivers
b) Fine estimation of the baseline between the receivers

For each receiver, the first step is represented by the train positioning module performed by using one of the algorithms shown in section 4. In [4], authors used the constrained double difference approach by using one RS of a local area augmentation network. Performing the constrained PVT solution for both receivers, it is possible to obtain a coarse estimation of the train length as the difference between the mileages of the two receivers. The second step projects the baseline on the track performing an algorithm that is derived by the constrained double difference approach. If the estimated train length is bigger than the nominal one by more than a certain threshold the decoupling alert is arisen. The threshold is evaluated by exploiting the Neyman-Pearson criterion. Let $\mathbf{e}_H^i$ and $\mathbf{e}_E^i$ be respectively the vector line of sights between the i-th satellite and the receiver located at the head of the train and the vector line of sights between the i-th satellite and the receiver located at the end of the train:

$$\begin{aligned} \mathbf{e}_H^i &= r_H^i \cdot \hat{e}_H^i = \mathbf{X}^i - \mathbf{X}_H\left(s_H\right) \\ \mathbf{e}_E^i &= r_E^i \cdot \hat{e}_E^i = \mathbf{X}^i - \mathbf{X}_E\left(s_E\right) \end{aligned} \tag{106}$$

Where:

r_H^i is the geometric distance between the i-th satellite and the receiver located at the head of the train

$\hat{e}_H^i$ is the unit vector which elements are the director cosines of the line of sight between the i-th satellite and the receiver located at the head of the train

$\mathbf{X}^i$ is the position of the i-th satellite

$\mathbf{X}_H$ is the position of the receiver located at the head of the train that depends on the curvilinear abscissa of the track s_H

r_E^i is the geometric distance between the i-th satellite and the receiver located at the end of the train

$\hat{e}_E^i$ is the unit vector which elements are the director cosines of the line of sight between the i-th satellite and the receiver located at the end of the train

$\mathbf{X}^i$ is the position of the i-th satellite

$\mathbf{X}_E$ is the position of the receiver located at the end of the train that depends on the curvilinear abscissa of the track s_E

The baseline $\mathbf{b}$ between the two receivers can be written as:

$$\mathbf{b} = b \cdot \hat{e}_b = \mathbf{X}_H(s_E) - \mathbf{X}_E(s_H) \tag{107}$$

Where:

b is the magnitude of the baseline

$\hat{e}_b$ is the unit vector which elements are the director cosines of the baseline

A schematic representation of the proposed approach is depicted in Figure 43. Following an approach similar to the one presented in section 4, the single difference among the geometric distance between the i-th satellite and the receiver located at the head with respect to the geometric distance between the i-th satellite the other receiver $r_{H,E}^i$ can be expressed as:

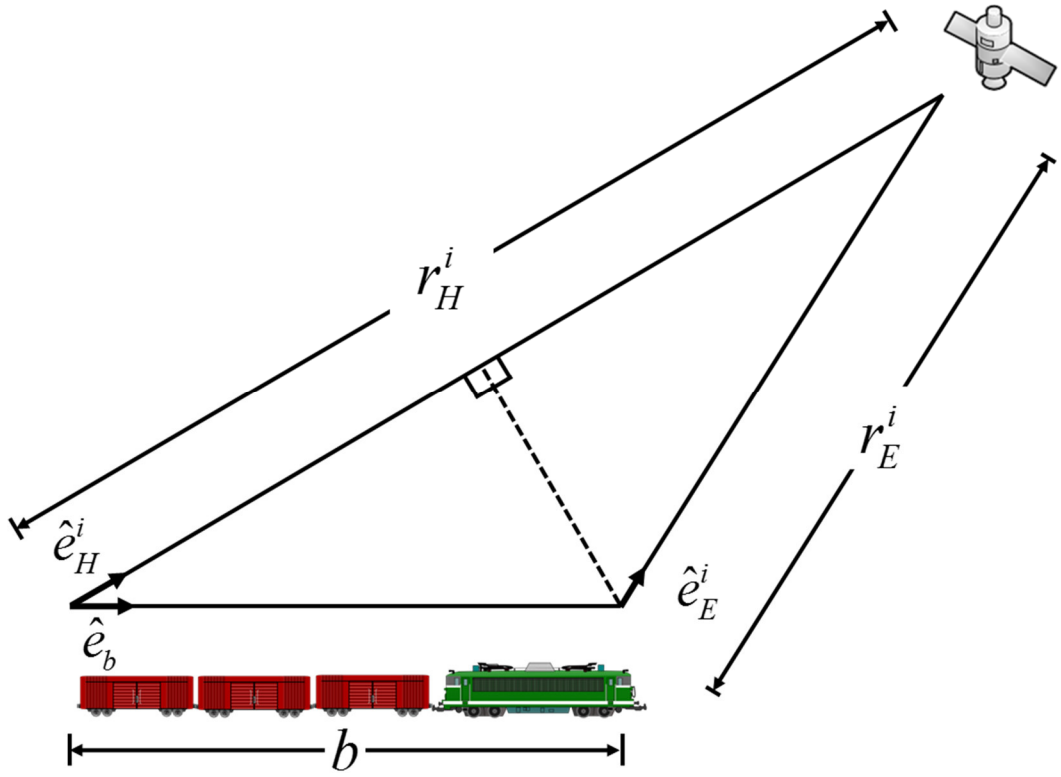

Figure 43. Baseline projection

$$r_{H,E}^i = r_H^i - r_E^i = r_H^i\left[1-\left\langle \hat{e}_H^i, \hat{e}_E^i \right\rangle\right] - \left\langle b\cdot\hat{e}_b, \hat{e}_E^i \right\rangle \tag{108}$$

Where:

$\langle\bullet\rangle$ is the scalar product operator

The double difference that involves the satellites i-th and j-th with respect to the on board receivers $r_{H,E}^{i,j}$ can be expressed as:

$$\begin{aligned} r_{H,E}^{i,j} &= r_{H,E}^i - r_{H,E}^j = \\ &= \left\{ r_H^i\left[1-\left\langle \hat{e}_H^i, \hat{e}_E^i \right\rangle\right] - \left\langle b\cdot\hat{e}_b, \hat{e}_E^i \right\rangle \right\} - \left\{ r_H^j\left[1-\left\langle \hat{e}_H^j, \hat{e}_E^j \right\rangle\right] - \left\langle b\cdot\hat{e}_b, \hat{e}_E^j \right\rangle \right\} = \\ &= r_H^i\left[1-\left\langle \hat{e}_H^i, \hat{e}_E^i \right\rangle\right] - r_H^j\left[1-\left\langle \hat{e}_H^j, \hat{e}_E^j \right\rangle\right] - \left\{ \left\langle b\cdot\hat{e}_b, \hat{e}_E^i \right\rangle - \left\langle b\cdot\hat{e}_b, \hat{e}_E^j \right\rangle \right\} = \\ &= r_H^i\left[1-\left\langle \hat{e}_H^i, \hat{e}_E^i \right\rangle\right] - r_H^j\left[1-\left\langle \hat{e}_H^j, \hat{e}_E^j \right\rangle\right] - \left\langle b\cdot\hat{e}_b, \hat{e}_E^i - \hat{e}_E^j \right\rangle \end{aligned} \tag{109}$$

Accounting for the track constraint it is possible to estimate the baseline between the receivers by using an iterative procedure. Let $s_H^{(m)}$ and $s_E^{(m)}$ be respectively the estimated mileage of the head and end of the train receivers at the m-th step. The estimated baseline between at the m-th step can be indicated as:

$$\mathbf{b}^{(m)} = \mathbf{b}^{(m-1)} + \Delta b_E^{(m)} \cdot \hat{e}_{b_E}^{(m)} - \Delta b_H^{(m)} \cdot \hat{e}_{b_H}^{(m)} \tag{110}$$

Where:

$\Delta b_E^{(m)}$ is the correction on the baseline due to the correction to be applied to the mileage of the receiver located at the end of the train at the m-th step

$\Delta b_H^{(m)}$ is the correction on the baseline due to the correction to be applied to the mileage of the receiver located at the head of the train at the m-th step

$\hat{e}_{b_E}^{(m)}$ is the unit vector corresponding to the tangents of the track in the position of the receiver located at the end of the train at the m-th step

$\hat{e}_{b_H}^{(m)}$ is the unit vector corresponding to the tangents of the track in the position of the receiver located at the head of the train at the m-th step

Let be $\overline{\mathbf{DD}}^{(m)}$ the vector of double-differences between the reduced pseudoranges obtained considering the on board receivers with respect to the i-th satellite and the pivot one at the m-th step. Without loss of generality let the pivot be the first satellite:

$$\overline{\mathbf{DD}}^{(m)} = \left(\Delta\rho_{H,E}^{2,1\,(m)} \quad \Delta\rho_{H,E}^{3,1\,(m)} \quad \cdots \quad \Delta\rho_{H,E}^{N_{sat},1\,(m)} \right)^T \tag{111}$$

Let $\mathbf{H}^{(m)}$ be the design matrix at the m-th step. This matrix is the same matrix that would have been evaluated in case of unconstrained PVT estimation for the receiver located at the end of the train. Each row of the $\mathbf{H}^{(m)}$ represents the difference between the directors cosines of the line of sight between the receiver and the corresponding satellite with respect to those of the line of sight between the receiver and the pivot satellite. $\mathbf{H}^{(m)}$ can be written as:

$$\mathbf{H}^{(m)} = \begin{pmatrix} e_{E,x}^{2\ (m)} - e_{E,x}^{1\ (m)} & e_{E,y}^{2\ (m)} - e_{E,y}^{1\ (m)} & e_{E,z}^{2\ (m)} - e_{E,z}^{1\ (m)} \\ e_{E,x}^{3\ (m)} - e_{E,x}^{1\ (m)} & e_{E,y}^{3\ (m)} - e_{E,y}^{1\ (m)} & e_{E,z}^{3\ (m)} - e_{E,z}^{1\ (m)} \\ \cdots & \cdots & \cdots \\ e_{E,x}^{N_{Sat}(m)} - e_{E,x}^{1\ (m)} & e_{E,y}^{N_{Sat}(m)} - e_{E,y}^{1\ (m)} & e_{E,z}^{N_{Sat}(m)} - e_{E,z}^{1\ (m)} \end{pmatrix} \tag{112}$$

Let $\mathbf{D}^{(m)}$ be vector that imposes the track constraint at the m-th step. The columns of $\mathbf{D}^{(m)}$ are respectively the director cosines of the tangent to the track in the points with curvilinear abscissa $s_H^{(m)}$ and $s_E^{(m)}$.

$$\mathbf{D}^{(m)} = \begin{pmatrix} \hat{e}_{b_H}^{\ (m)} & \hat{e}_{b_E}^{\ (m)} \end{pmatrix} = \begin{pmatrix} \left.\frac{\delta X_{H,x}}{\delta s}\right|_{s=\hat{s}_H^{(m)}} & \left.\frac{\delta X_{E,x}}{\delta s}\right|_{s=\hat{s}_E^{(m)}} \\ \left.\frac{\delta X_{H,y}}{\delta s}\right|_{s=\hat{s}_H^{(m)}} & \left.\frac{\delta X_{E,y}}{\delta s}\right|_{s=\hat{s}_E^{(m)}} \\ \left.\frac{\delta X_{H,z}}{\delta s}\right|_{s=\hat{s}_H^{(m)}} & \left.\frac{\delta X_{E,z}}{\delta s}\right|_{s=\hat{s}_E^{(m)}} \end{pmatrix} \tag{113}$$

The constrained PVT solution for the m-th step can be evaluated by solving the system:

$$\overline{DD}^{(m-1)} = \mathbf{H}^{(m-1)}\mathbf{D}^{(m-1)}\Delta b^{(m)} + \underline{\upsilon} \tag{114}$$

Where $\underline{\upsilon}$ indicates the residuals vector and $\Delta b^{(m)} = \begin{pmatrix} \Delta b_H^{\ (m)} \\ \Delta b_E^{\ (m)} \end{pmatrix}$.

The set of linear equation can be solved by means of a weighted least square method or by means of an extended Kalman filter approach:

$$\Delta\hat{b}^{(m)} = \Delta\hat{b}^{(m-1)} + \mathbf{K}^{(m)}\overline{DD}^{(m-1)} \tag{115}$$

Where the gain matrix $\mathbf{K}^{(m)}$ can be obtained as:

$$\mathbf{K}^{(m)} = \left(\mathbf{D}^{(m-1)T}\mathbf{H}^{(m-1)T}\mathbf{R}_v^{-1}\mathbf{H}^{(m-1)}\mathbf{D}^{(m-1)}\right)^{-1}\mathbf{D}^{(m-1)T}\mathbf{H}^{(m-1)T}\mathbf{R}_v^{-1} \tag{116}$$

Where $\mathbf{R}_v$ is the weight matrix. Once the correction to the baseline has been evaluated, the mileage of the two receivers can be updated as:

$$\begin{aligned} s_H^{(m)} &= s_H^{(m-1)} + \Delta b_H^{(m)} \cdot \hat{e}_{b_H}^{(m)} \\ s_E^{(m)} &= s_E^{(m-1)} + \Delta b_E^{(m)} \cdot \hat{e}_{b_E}^{(m)} \end{aligned} \tag{117}$$

The estimated train length is then evaluated as:

$$\begin{aligned} L^{(m)} &= s_H^{(m)} - s_E^{(m)} = s_H^{(m-1)} + \Delta b_H^{(m)} \cdot \hat{e}_{b_H}^{(m)} - s_E^{(m-1)} - \Delta b_E^{(m)} \cdot \hat{e}_{b_E}^{(m)} = \\ &= L^{(m-1)} + \Delta b_H^{(m)} \cdot \hat{e}_{b_H}^{(m)} - \Delta b_E^{(m)} \cdot \hat{e}_{b_E}^{(m)} \end{aligned} \tag{118}$$

6.3 TRAIN INTEGRITY SIMULATOR

To assess the performance of the algorithm by means of Monte Carlo simulations a simulation tool has been developed. Part of this simulation tool has been provided by RadioLabs consortium. The overall architecture of the simulator is depicted in Figure 44. The simulator description and the simulation results presented in this paragraph are discussed in more details in [4]. The first section of the simulator is responsible for the generation of the signals that the receiver would have received if it were present at a specific location at a certain time epoch.

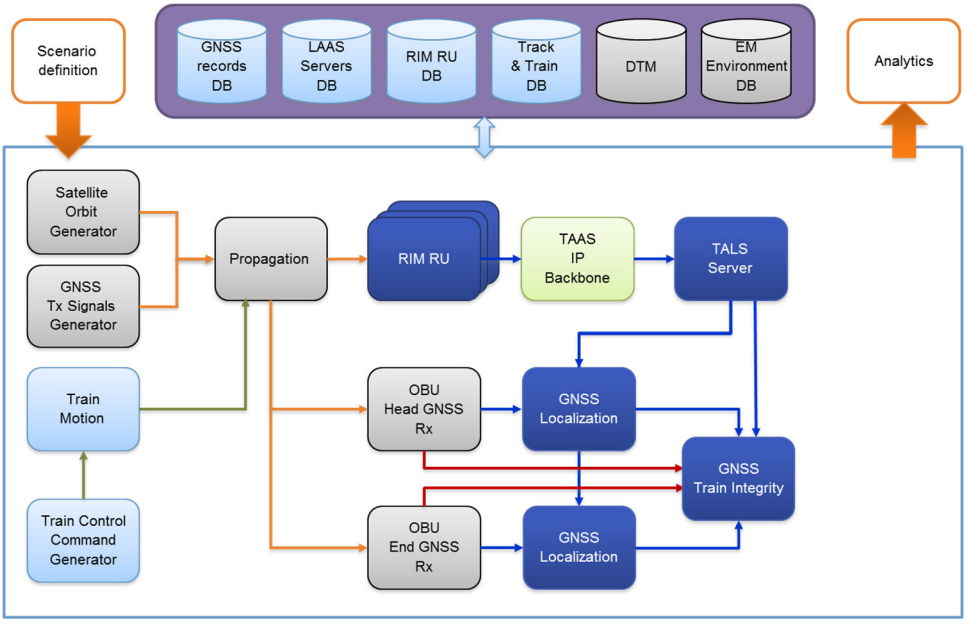

Figure 44. Simulator overall architecture

At this aim, it is important the scenario definition block which defines the number and location of the RSs as well as the train movement profile to be adopted during the simulations. In the simulation analysis, two kind of train have been considered: the first one, referred in the following as short train, has a nominal length of 500 meters, the second train, in the following referred as long train, has a 2500 meters nominal length. For both trains synthetic observations have been generated taking into account the movement profile. Both trains move at constant speed: 108 km/h for the short train and 80 km/h for the long train. Concerning the track, a portion of 30km of the line between "Roma Tuscolana" and "Zagarolo" has been considered. In Figure 45, it is shown the path followed by the train. In the simulations, the mechanical model has been simplified by using a conservative approach. The breaking system has been considered as not operating and the air resistance has been neglecting. The train, when all the carriages are still coupled, is considered as one fixed block; multiple decoupling have not been considered, so, after the decoupling, the train is modelled as two rigid blocks respectively representing the front section and the rear section. Particularly, in case of decoupling event, the front section continues its ride as if nothing happened while the rear section slows down by the only effect of the rolling resistance F_R. The friction between the wheel and the tracks originates rolling resistance. To determine the rolling resistance, two factors must be taken into account:

(i) Weight of the vehicle

(ii) the rolling resistance coefficient f_R which depends on the vehicle type

Figure 45. Roma Tuscolana to Zagarolo line

In a flat terrain, a vehicle with no deforming wheels, is subject to a rolling resistance that can be expressed as:

$$F_R = f_R \cdot m \cdot g \tag{119}$$

Where:

f_R is the rolling resistant coefficient

m is the mass of the vehicle in kg

g is the gravity acceleration

The motion equation for the decoupled section over a flat terrain is then expressed as:

$$s(t) = -\frac{1}{2}\frac{F_R}{m}t^2 + v_0 \cdot t = v_0 \cdot t - \frac{1}{2}g \cdot f_R \cdot t^2 \tag{120}$$

Where v_0 is the train speed when the decoupling occurs. To verify the correctness of the algorithm, for each train, two situations has been verified: nominal condition and decoupling event. In the first scenario, the trains are travelling with all the carriages coupled, while in the second case a decoupling event has been simulated. In both cases a Gaussian noise with an expectation of 10 cm and a standard deviation of 80 cm is added to the synthetic observation to model the receiver noise. In the following the first scenario will be addressed as Gap Free plus Receiver Noise (GF+RN) while the second case will be addressed as Gap Affected plus Receiver Noise (GA+RN). Figure 46 and Figure 47 depict respectively the probability density function and the normal probability plot of the empirical cumulative distributions of the estimation error of the mileage between receivers for the GF+RN case for both trains. By observing those pictures, it is possible to assume that in nominal condition the error can be approximated with a Gaussian distribution with no significant difference corresponding to the train different lengths. Concerning the gap affected scenario, the simulated decoupling event has been introduced after 100 seconds of travel. This means that in the first 100 seconds of the ride the GA+RN scenario is equivalent to the GF+RN case; after this moment the front section will continue its ride till the end of the simulation while the rear section will slow down with a

constant deceleration equal to 0.2 m/s^2. The temporal trend of the estimated baseline for both trains in the GA+RN scenario is depicted in Figure 48. In that picture, it is possible to verify how the train length estimation (blue curve) follows as expected the ground truth (green curve). Figure 49 and Figure 50 depict respectively the probability density function and the normal probability plot of the empirical cumulative distributions of the estimation error of the mileage between receivers for the GA+RN case for both trains. By observing those pictures, it is possible to verify how the error distribution can be approximated with a Gaussian only in the central part, presenting heavy tails [4]. In fact, the estimation error process depends on the number of visible satellites and on the geometry. A possible solution, as demonstrated in [4], can be the introduction of a median filter even if the drawback is a slight increase on the time to alert. Table 3 reports mean and variance of the estimation error.

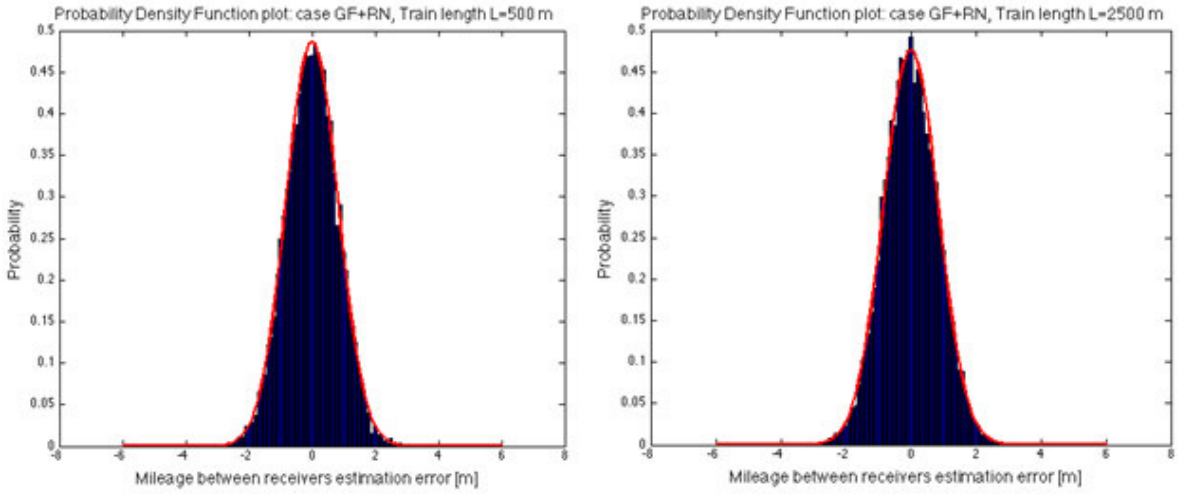

Figure 46. Probability Density Function of mileage between the receivers estimation error case GF+RN

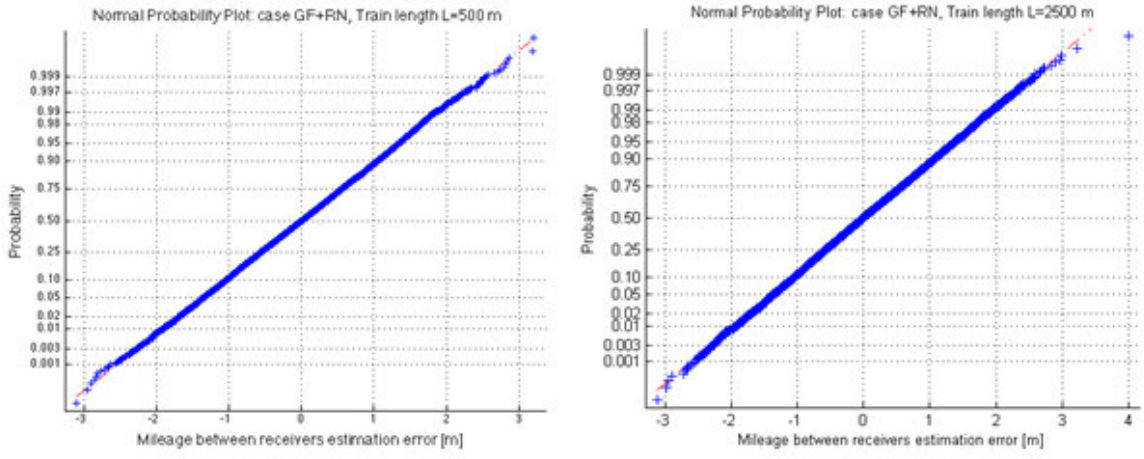

Figure 47. Normal probability plot of the estimation error on the mileage between the receivers case GF+RN

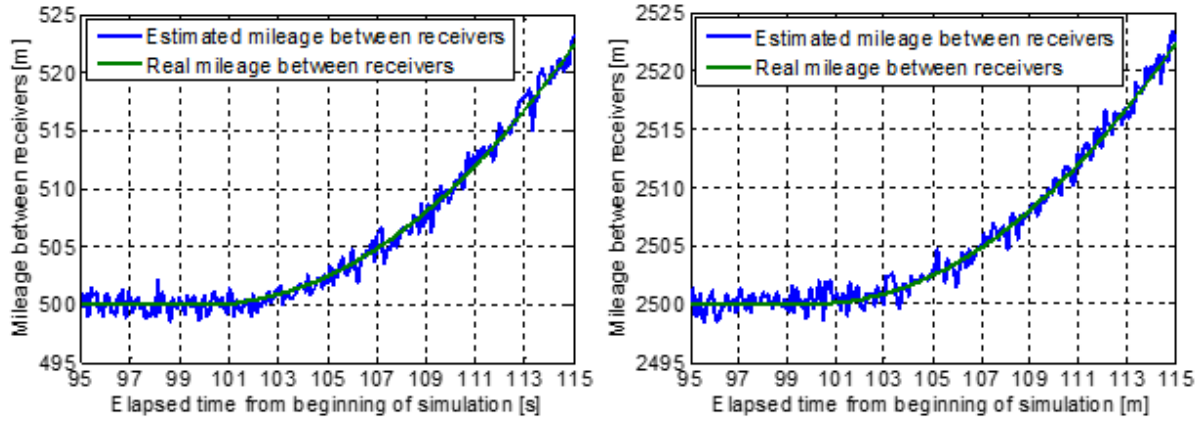

Figure 48. Estimated mileage between receivers w.r.t. elapsed time for short train (left) and long train (right)

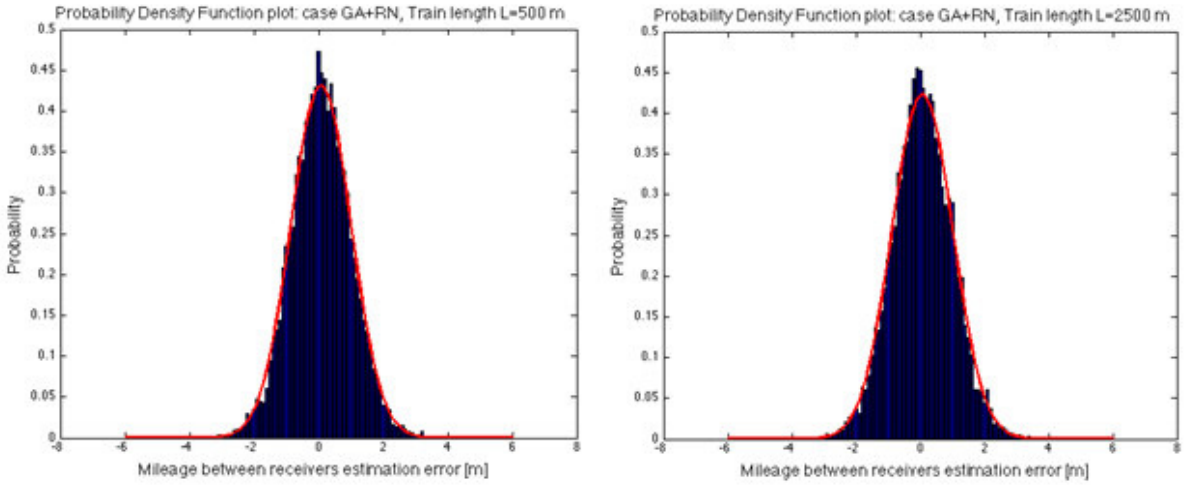

Figure 49. Probability Density Function of mileage between the receivers estimation error case GA+RN

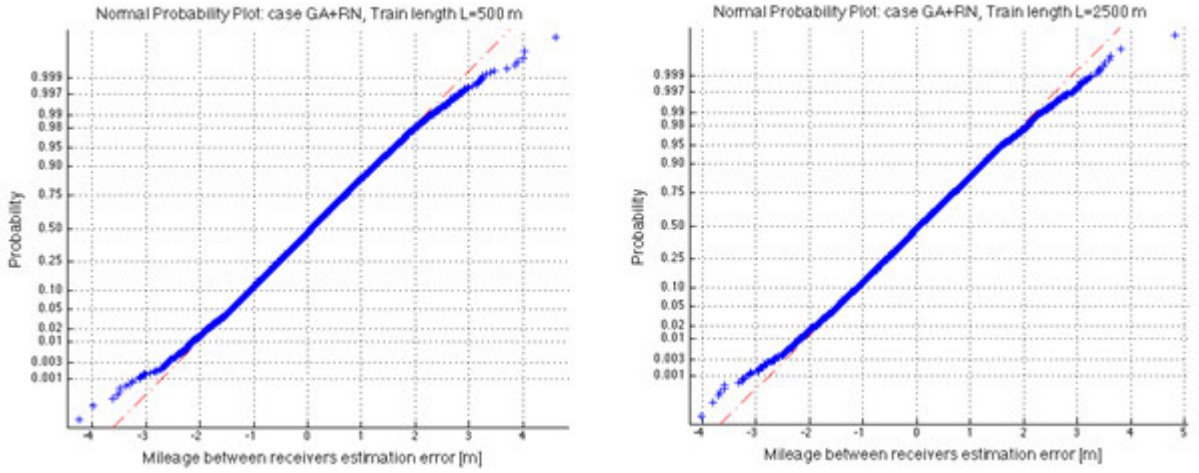

Figure 50. Normal probability plot of the estimation error on the mileage between the receivers case GA+RN

Table 3. Statistics of the estimation error on the mileage between the receivers

Case	GF+RN		GA+RN	
Train Length [m]	500	2500	500	2500
Mean [m]	-0.002	0.002	0.08	0.07
Std [m]	0.82	0.84	0.93	0.94

6.4 SINGLE CONSTELLATION DETECTOR PERFORMANCE

As observed in [4], in absence of fault, the train length estimation error can be considered as zero mean Gaussian distributed. The standard deviation of the distribution must be evaluated by means of on tuning and is function of the nominal baseline length [3]. Let $P_{fa,k}$ be the probability to declare a decoupling event while the coaches are still coupled by using the k-th constellation. The false alarm probability can be defined as:

$$P_{fa,k} = \frac{1}{2} erfc\left(\frac{Th_k}{\sigma_k \sqrt{2}} \right) \tag{121}$$

Where:

Th_k is the threshold for the k-th constellation

σ_k is the standard deviation of the length estimation performed by using the k-th constellation

$erfc(\cdot)$ is the complementary error function that can be expressed as:

$$erfc(x) = \frac{2}{\sqrt{\pi}} \int_x^{\infty} \mathrm{e}^{-t^2} dt \tag{122}$$

Following the Neyman-Pearson criterion, the decision threshold is set by imposing the target false alarm probability $\tilde{P}_{fa,k}$ as:

$$Th_k = \sqrt{2\sigma_k^2} \cdot erfc^{-1}\left(2\tilde{P}_{fa,k}\right) \tag{123}$$

When a decoupling occurs, the train length becomes larger than the nominal value by effect of the gap μ between the two parted sections. After the decoupling, the train length estimation error for the k-th constellation is still Gaussian distributed with expectation μ and standard deviation $\sigma_k^{dec}[\mu]$. Experimental results have shown how for gaps lower than 1km the dependence of the standard deviation from the gap can be neglected $\sigma_k^{dec}[\mu] \approx \sigma_k$ [3]. The detection probability, defined as the probability to detect a decoupling event, is function of the gap. In fact, the larger is the gap, the higher is the probability to detect the decoupling.

$$P_{D,k}[\mu] = \frac{1}{2} erfc\left(\frac{Th_k - \mu}{\sqrt{2} \cdot \sigma_k^{dec}[\mu]}\right) \simeq \frac{1}{2} erfc\left(\frac{Th_k - \mu}{\sqrt{2} \cdot \sigma_k}\right) \tag{124}$$

6.5 MULTI CONSTELLATION TRAIN INTEGRITY ASSESSMENT

6.5.1 Introduction

Train Integrity assessment is a decision problem. In fact, the typical output of the module is a Boolean value that represents the state of the train. When multi-constellation receivers are available there are mainly three approaches that can be followed. These approaches are similar to the ones for the position estimation presented in section 2. Particularly the possibilities are:

1) Performing unique decision by using a unique hybrid virtual constellation containing all the satellites in view
2) performing a decision for each constellation and then comparing the results
3) performing a set of decisions by using subsets of satellites not necessarily belonging to the same constellation and then comparing the results

The first case, in the following called coherent integration, increase the availability [18]. This enhancement is due to the better geometry of the system as well as to the higher number of satellites. Data fusion in this case is in the pseudorange domain. In the second approach, for

each constellation the train integrity assessment procedure is carried out producing a Boolean containing the output of the decision on whether the train is still integer or not. In this way the data fusion is performed directly in the Boolean domain. This approach is less prone to integrity issues[6]. The third case is a hybrid solution performing an incoherent integration of data obtained by a coherent integration. The third approach has not been considered in this work. In section 2 it is possible to find more details on data coming from more than one constellations.

6.5.2 Case of Study: Train Integrity Assessment by using GPS and GLONASS

In this subsection, a case of study related to train integrity is presented. The outcomes of such study can be found in [3]. In this analysis, it is considered the same test case presented in section 6.3. A synthetic scenario has been generated by using a 30km portion of track between "Roma Tuscolana" and "Zagarolo". On this track, synthetic observations for two trains with different length have been emulated in both hypotheses of nominal condition and decoupling event. For more details on the scenario see section 6.3. Simulations for all the four cases have been carried out by using three different approaches:

a) GPS data only
b) GLONASS data only
c) Coherent integration GPS and GLONASS

The results of the Monte Carlo simulations are depicted in Table 4. For sake of simplicity the coherent integration is considered as a virtual constellation. As it has been shown in [3], simulations have shown how the standard deviation of the Gaussian distribution is lower when the constellation obtained by using the coherent integration is selected. In the following the standard deviation of the train length estimation is assumed to be equal to 80 cm for a single constellation detector and equal to 60 cm for the coherently integrated double constellation. The trend of the decision threshold with respect to the target False Alarm Probability for both single and double constellation is depicted in Figure 51. As expected, by using a multi-constellation approach, because when all the satellites are healthy the standard deviation is lower, at the same target false alarm probability corresponds a lower detection threshold.

[6] See section 2 for further details

Table 4. Train length estimation error with GPS and GLONASS

	Case	GF+RN		GA+RN	
	Train Length [m]	500	2500	500	2500
GPS only	Mean [m]	-0.002	0.009	0.059	0.074
	Std [m]	0.831	0.830	0.934	0.933
GLONASS only	Mean [m]	-0.003	-0.006	-0.003	-0.002
	Std [m]	0.841	0.874	1.063	1.071
GPS + GLONASS	Mean [m]	-0.001	0.000	-0.010	-0.014
	Std [m]	0.572	0.580	0.680	0.677

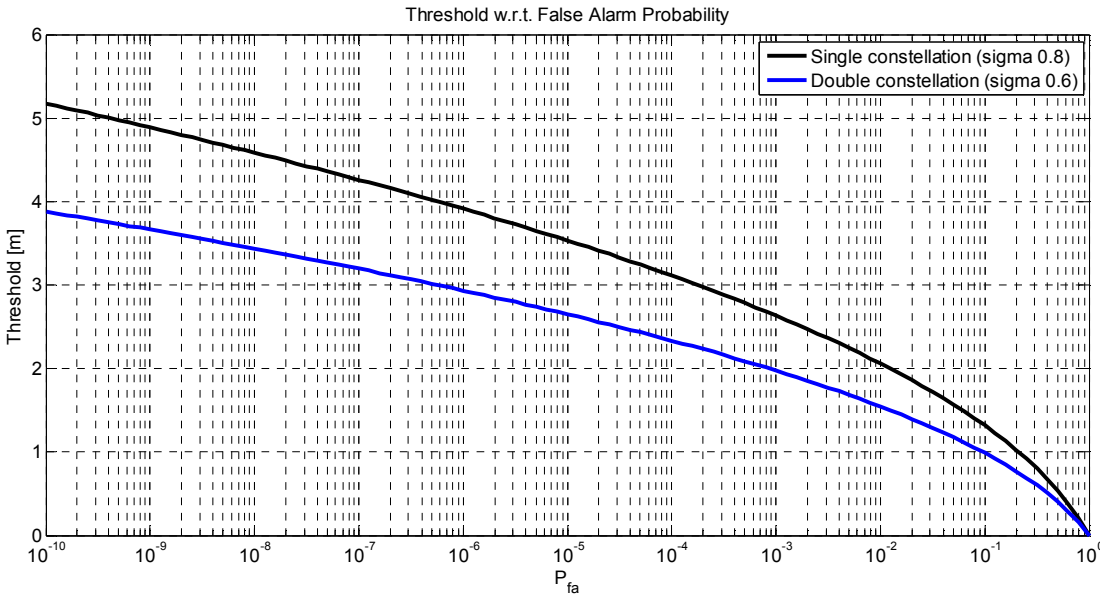

Figure 51. Threshold trend w.r.t. False Alarm Probability

In Figure 52, the trend of the detection probability as function of the gap between the parted sections for several values of threshold in presence of single constellation detector is depicted. Similarly, Figure 53 shows the trend of the detection probability as function of the gap between the parted sections for several values of threshold when the coherent integration between the two constellations is performed. As expected the detection probability is equal to 50% when the gap is equal to the threshold [3]. Fixed a gap, the lower is the threshold the higher is the detection probability. Figure 54 shows the detection error trade-off curve when the gap is 5 meters. This graph shows in a logarithmic scale the relationship between the false alarm probability and the miss detection probability.

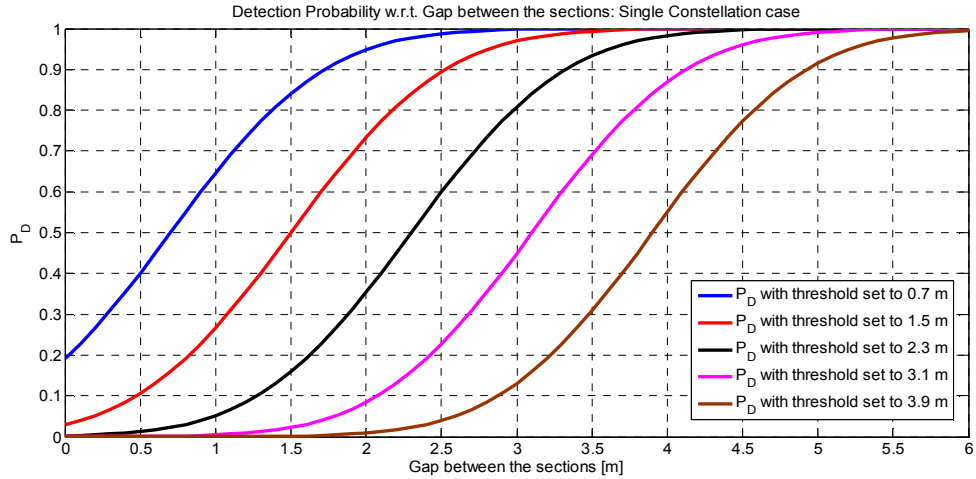

Figure 52. Detection Probability vs train gap for the generic single constellation

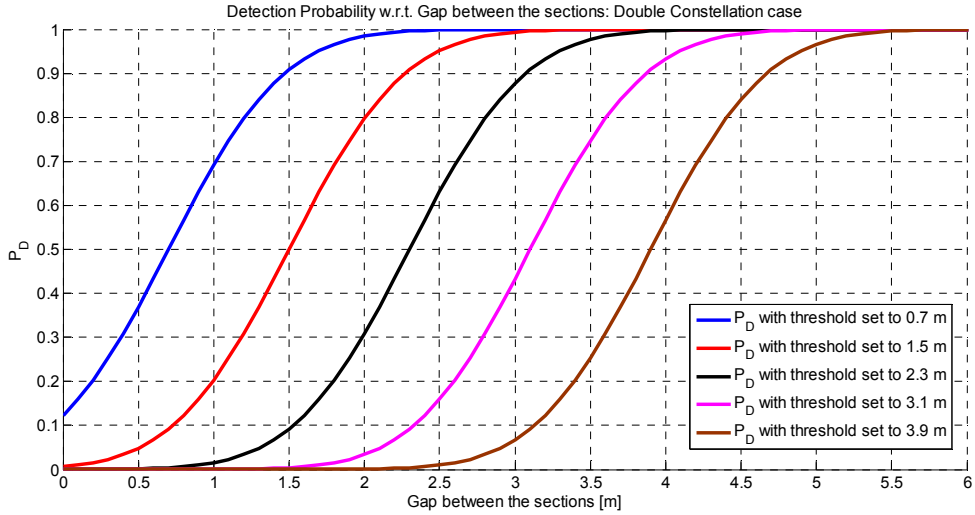

Figure 53. Detection Probability vs train gap for the double constellation

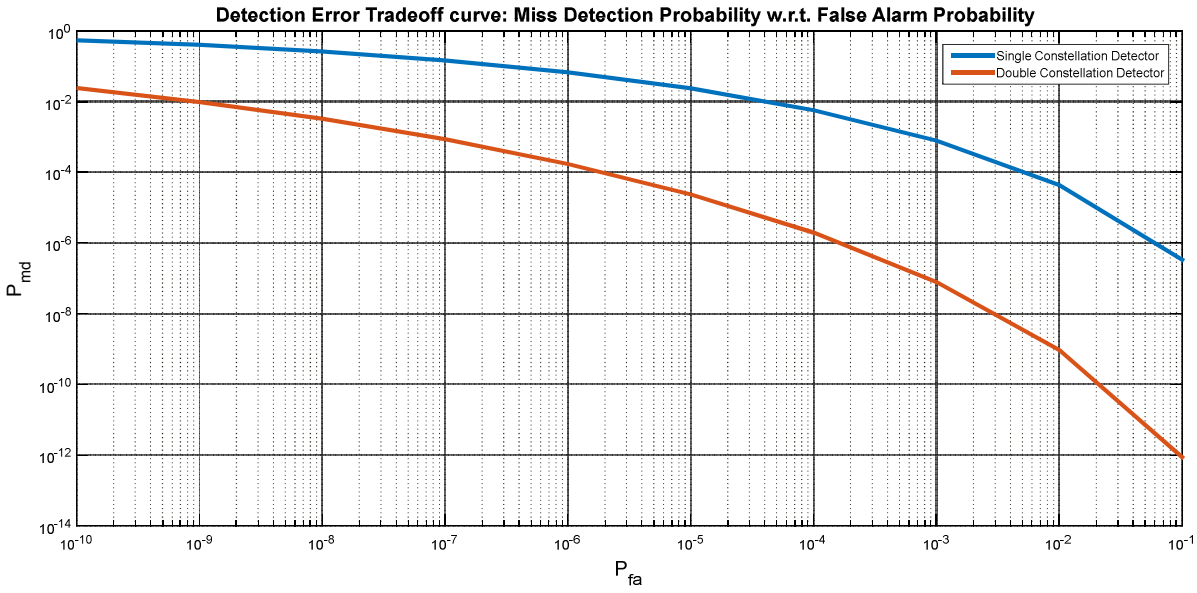

Figure 54. DET curve for a gap of 5 meters

The curves depicted in Figure 54, as expected, indicate how the use of multi-Constellation approach, when all the satellites are supposed to be healthy, guarantee a lower miss detection probability keeping constant the false alarm probability. However, in order to fulfil the stringent requirements imposed by SIL-4, the incoherent integration technique appears to be more appealing thanks to the fact that is more robust in terms of integrity.

6.5.3 Incoherent Multi-Constellation Integration

In [18], authors defined an analytical approach to perform the incoherent integration of multiple detectors. Let N be the number of independent detections obtained by processing data coming from N constellations. Three strategies can be implemented to detect the decoupling:

i) 1 out of N (1ooN);
ii) N out of N (NooN);
iii) M out of N (MooN).

In the 1ooN approach, the decoupling alarm is triggered when at least one of the detectors has indicated the presence of a decoupling. On the opposite, the NooN approach foresees that the decoupling has occurred when all the detectors detected such an event. In the MooN strategy the decoupling is detected when at least M out of the N detectors available have decided for the decoupling. If N is greater than 2, a single constellation anomalous detection can be identified [18].

6.5.3.1 1 out of N logic

In this strategy, the train integrity warning is set when at least one of the detectors has identified the decoupling. The main advantage of processing data separately by constellation is the independence in the estimation errors of the detectors. Being the errors independent, the detection probability of the decoupling event in the 1ooN logic can be written as:

$$P_{D,(1ooN)} = 1 - \prod_{i=1}^{N} (1 - P_{D,i}) \tag{125}$$

Where $P_{D,i}$ is the detection probability of the *i*-th estimator. The detection probability is function of the gap between the parted sections of the train. The bigger is the gap, the higher is the probability that the decoupling event is revealed by the detector [18]. The miss detection probability can be written as:

$$P_{md,(1ooN)} = 1 - P_{D,(1ooN)} = 1 - 1 + \prod_{i=1}^{N}(1 - P_{D,i}) = \prod_{i=1}^{N}(1 - P_{D,i}) = \prod_{i=1}^{N}(P_{md,i}) \tag{126}$$

In the 1ooN approach, the total miss detection probability is the product of the miss detection probability of the single detectors. This approach can be considered as conservative. Concerning the total false alarm probability, it is possible to write:

$$P_{fa,(1ooN)} = 1 - \prod_{i=1}^{N}\left(1 - P_{fa,i}\right) \tag{127}$$

When the Neyman-Pearson criterion is used, the major benefit of the 1ooN approach is the possibility to impose the total false alarm probability and evaluate threshold for each detector. Being all the decisions independent, this approach is not affected by the decoupling event masked by a faulty detector. The detection error trade-off curves for the 1ooN approach when 2,3 and 4 detectors are depicted in Figure 55. The curves depicted in Figure 55 are evaluated assuming a gap between the parted sections of 5 meters.

6.5.3.2 N out of N logic

In this strategy, the train integrity warning is set when all the detectors have identified the decoupling. This logic can be considered as the dual of the 1ooN approach; in fact, the expression of the false alarm probability and the miss detection probability are respectively:

$$P_{fa,(NooN)} = \prod_{i=1}^{N} P_{fa,i} \tag{128}$$

$$P_{md,(NooN)} = 1 - \prod_{i=1}^{N}\left(P_{D,i}\right) = 1 - \prod_{i=1}^{N}\left(1 - P_{md,i}\right) \tag{129}$$

Figure 56 shows the Detection Error Trade-off curves when respectively 2, 3, and 4 detectors are present and the gap between the parted sections is 5 meters obtained by using the NooN logic. As for the 1ooN logic, the higher is the number of available detectors; the lower is the achievable missing detection probability keeping constant the total false alarm probability [18].

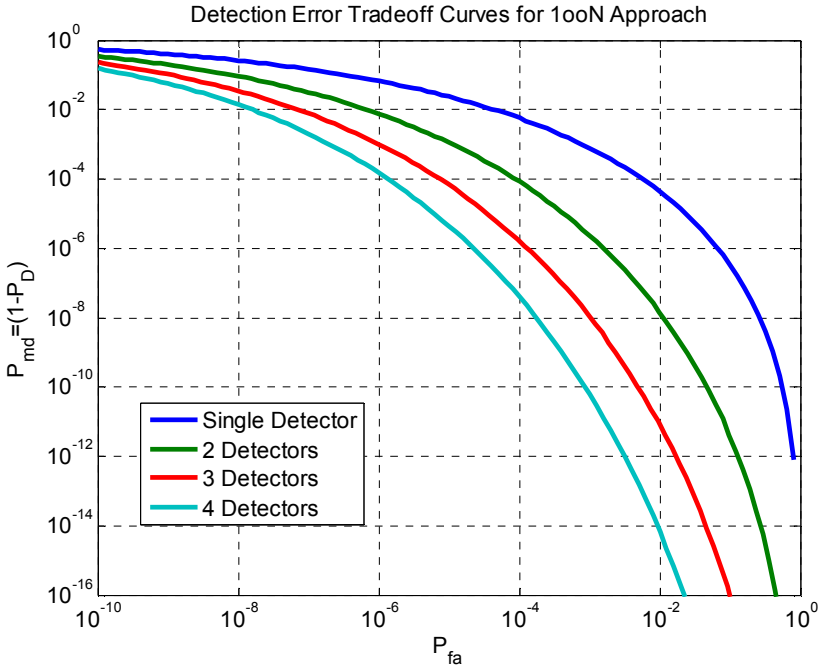

Figure 55. DET Curves for 1ooN Approach (gap 5 meters)

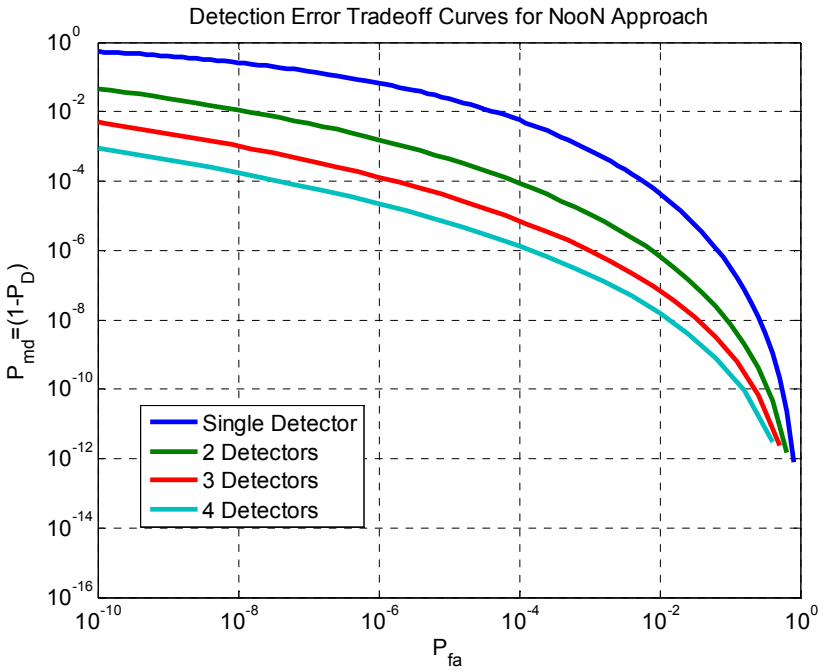

Figure 56. DET Curves for NooN Approach (gap 5 meters)

6.5.3.3 M out of N logic

In this strategy, the train integrity warning is set when at least M out of the N detectors has identified the decoupling. This strategy is the more general; in fact, both 1ooN and NooN logic can be retrieved as limit cases of this strategy. Assuming that the single constellation estimators have the same error budget, the performance of this logic can be written is a very compact form [18]. Analytical expressions for the miss detection probability and the false alarm probability can be written by means of the Bernoulli distribution:

$$P_{md,(MooN)} = \sum_{i=(N-M+1)}^{N} \binom{N}{i} P_{md,k}{}^{i} \cdot \left(1 - P_{md,k}\right)^{N-i} \tag{130}$$

$$P_{fa,(MooN)} = \sum_{i=M}^{N} \binom{N}{i} P_{fa,k}{}^{i} \cdot \left(1 - P_{fa,k}\right)^{N-i} \tag{131}$$

The main advantage of using this strategy is the higher robustness with respect to the outliers. Figure 57 shows the Detection Error Trade-off curves when respectively 2, 3, and 4 detectors are present and the gap between the parted sections is 5 meters obtained by using 2oo3, 2oo4 and 3oo4 approaches.

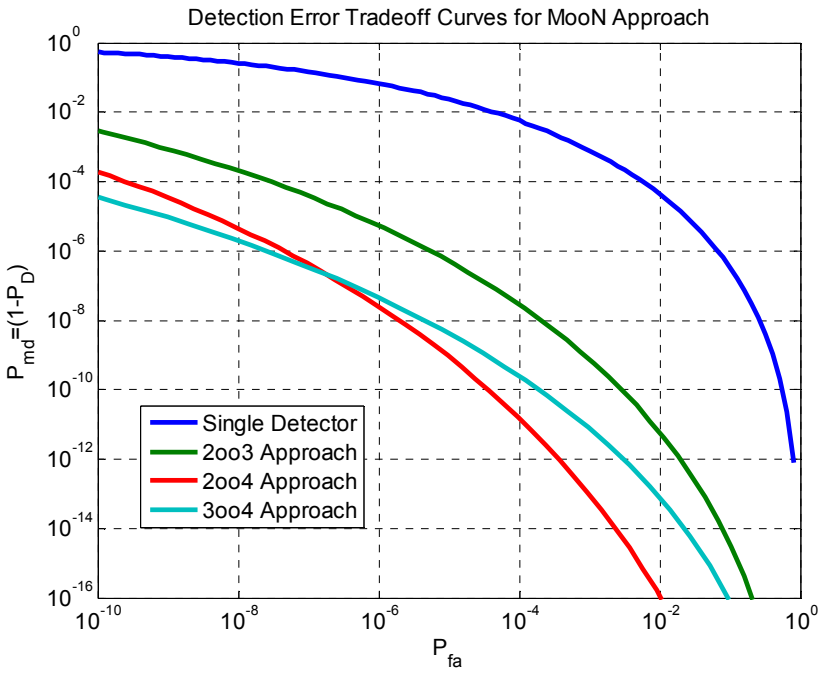

Figure 57. DET Curves for MooN Approach (gap 5 meters)

6.5.4 Case of study: Triple constellation train integrity detector

In a system that has three available independent detectors, as shown in the previous subsection, three strategies can be selected: 1oo3, 2oo3 and 3003. The 2oo3 logic represent the majority voting between the decisions taken separately by each detector at once [18]. The detection error trade-off curves for the three logics when the gap between the parted section is equal to 5 meters are depicted in Figure 58. As it is possible to see by that picture, if the target false alarm probability is between 10^{-10} and 10^{-2}, the majority voting approach is the one that guarantee the lower miss detection probability. Let the target false alarm probability be 10^{-4}; since the detection probability depends on the gap between the sections after the decoupling, it is possible to evaluate which is the minimum gap that guarantee a certain level of miss detection probability. An exemplum of this kind of information is presented in Figure 59. From the picture is it possible to appreciate how the use of multi-constellation benefit to the performance. However, the picture is only intended as a qualitative analysis; to evaluate the real benefit, the parameter of the statistics must be tuned with on-field acquisition sessions. Moreover, the impact of the multipath on such data has not been taken into account.

6.6 TRAIN SEPARATION

As introduced in the previous sub-sections, when L3 will be operational, there will be no physical device to protect the blocks. That means that the train must assess its own integrity and that the separation among two consecutives trains must be monitored. More in details, to avoid collisions, the separation among two adjacent convoys must be evaluated according the space needed to stop the second train and accounting the confidence interval of both train positions and breaking distance [43]. This consideration assumes great importance in the context of railway traffic management; the higher are the accuracies of the position and speed estimations, the smaller will be the confidence interval and therefore the denser can be the traffic. In [43], authors referred to three reference approaches to solve that issue:

i. Separation estimated on the basis of the position estimation of the two trains without data exchange among the trains (Non Coordinated Approach – NCA)
ii. Separation estimated on the basis of the position estimation of the two trains with data exchange to agree the list of satellites to be used (Coordinated Approach – CA)

iii. Relative positions among the trains (Joint Approach - JA).

In the first two approaches, the system will evaluate the gap between the trains as the difference of the positions of the two convoys. Let s_m and s_n be respectively the estimated mileage of the m-th train and the estimated mileage of the n-th train.

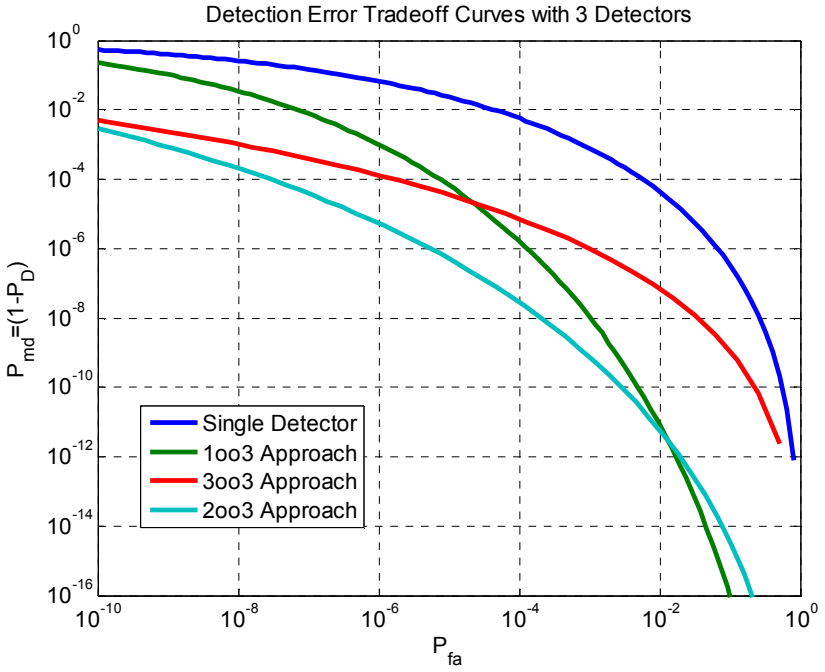

Figure 58. DET Curves for 3 detectors

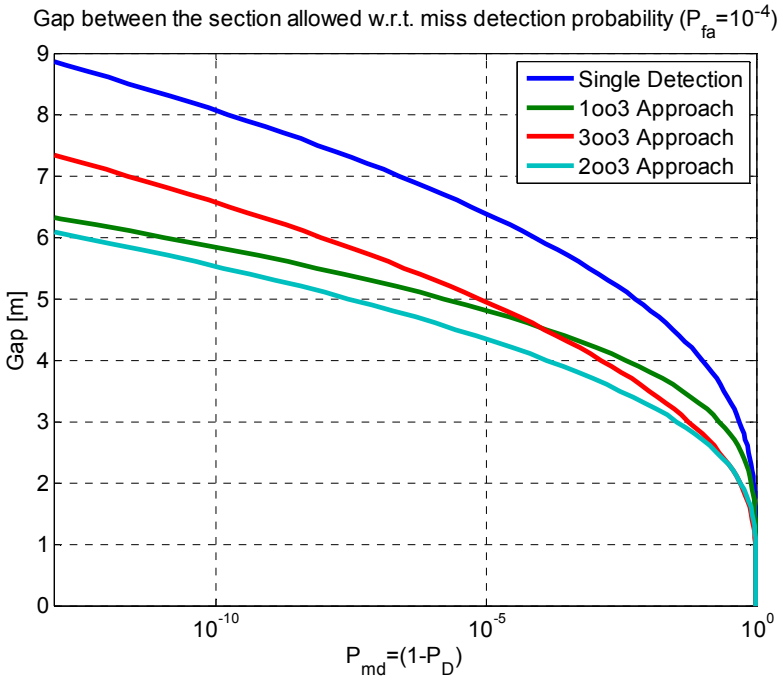

Figure 59. Gap between the sections allowed w.r.t. miss detection probability

The estimated separation among the convoys at the k-th epoch, assuming that the m-th is in advance with respect to the n-th, can be indicated as $\Delta s_{m,n}[k]$. This quantity can be expressed as:

$$\Delta s_{m,n}[k] = s_m[k] - s_n[k] - L_m[k] \tag{132}$$

Where:

$s_m[k]$ is the estimated mileage of the m-th train at the k-th epoch;

$s_n[k]$ is the estimated mileage of the n-th train at the k-th epoch;

$L_m[k]$ is the length of the m-th train at the k-th epoch (this length can be shortened if a portion of the m-th train decouples);

The third approach can be considered an extension of the train integrity algorithm shown is the previous sub-sections. In this case the algorithm will perform the estimated separation by accounting the knowledge of the track and compares it with the nominal separation. If the estimated separation is smaller than the nominal value by more than a certain threshold the inter-distance alert is arisen. Authors, in [43], analysed CA and JA approaches by means of Monte Carlo simulations on a synthetic scenario. On the track from "Roma Tuscolana" to "Zagarolo" that has already been shown in Figure 45, two trains, riding at a cruise speed set at 80 km/h, have been considered. The nominal train length has been considered of 500 meters and each train has been equipped with a GNSS receiver located at the head of the locomotive. In this simulation only GPS constellation has been considered. The nominal separation among the convoys has been set to 2 km. The larger is the nominal separation between the convoys, the lower will be the accuracy. On the other side of the coin, the smaller is the gap among two adjacent trains, the smaller is the tolerable error to avoid collisions. The histograms of the separation estimation errors for both CA and JA cases are depicted in Figure 60. As it is possible to see in the picture, in both scenarios the error is Gaussian distributed. The statistics of the error are reported in Table 5. As expected, the JA approach has a standard deviation of the estimation error smaller than the CA case.

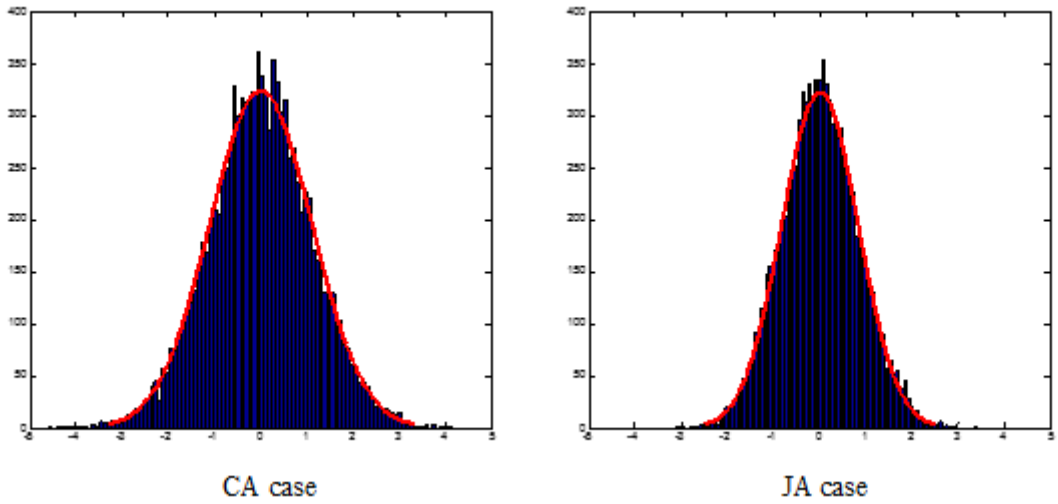

Figure 60. Histograms of separation estimation error for CA and JA cases

Table 5. Statistics of separation estimation error for CA and JA cases

Case	CA	JA
Mean [m]	0.0069	0,0095
Std [m]	1,1080	0,8306

6.7 CONSIDERATIONS

In this section, the train integrity assessment and the train separation issues have been analysed. The object of this chapter if crucial for the introduction of ETCS L3. The introduction of other sensors is foreseen in order to guarantee the continuity even in those areas where the GNSS signals are not available. The multi-sensor approach will be introduced in the next chapter.

7 MULTI-SENSOR TRAIN POSITIONING

The train control system based on GNSS technology is affected by two big issues: multipath and SIS denied areas (such as tunnels). These problems can drastically compromise the continuity and the availability of the system. This section intends to introduce to the possible use of other sensors to increase the system availability also in those situation in which the SIS is not available or it is too degraded to provide reliable solutions. The activities described in this section have been studied during my visit in Nottingham Geospatial Institute.

7.1 INTRODUCTION

In the railway context, there are several areas where the SIS is not available or it is strongly degraded: tunnels, urban canyon, side walls, platform roof and so on. These environmental characteristics can partly (or even totally) cover the sky, reducing drastically the number of satellite usable to perform the PVT estimation. In many of these situations, the use of multi-constellation, even when data are fused in a coherent way, is not enough to provide a geometry sufficient to provide reliable GNSS solutions. This problem affects, obviously, all the three functionalities presented in this work: train positioning, track determination and train integrity assessment. The possible solution is represented by exploitation of the output of external sensors like odometers, inertial units, imaging sensors and so on. The contribution of the data provided by those means can be taken into account either as a continuous information source (performing an integration) or as a backup information source. A schematic representation of the multisensory approach is depicted in Figure 61. When GNSS data are available, the information acquired can be used to compensate the eventual drift of the sensors of the subsidiary subsystem. When the GNSS signals are not available, an alternative navigation solution must be provided. It is important to investigate a set of candidate solutions to determine which one is better suited for the rail environment. According to [57], most navigation approaches rely on either position fixing or dead reckoning. The first category is represented by those systems that estimates current position by measuring distances or angles with respect to reference points of known position. On the other hand, dead reckoning is a navigation technique that estimates current position by means of the change in position from the previous location.

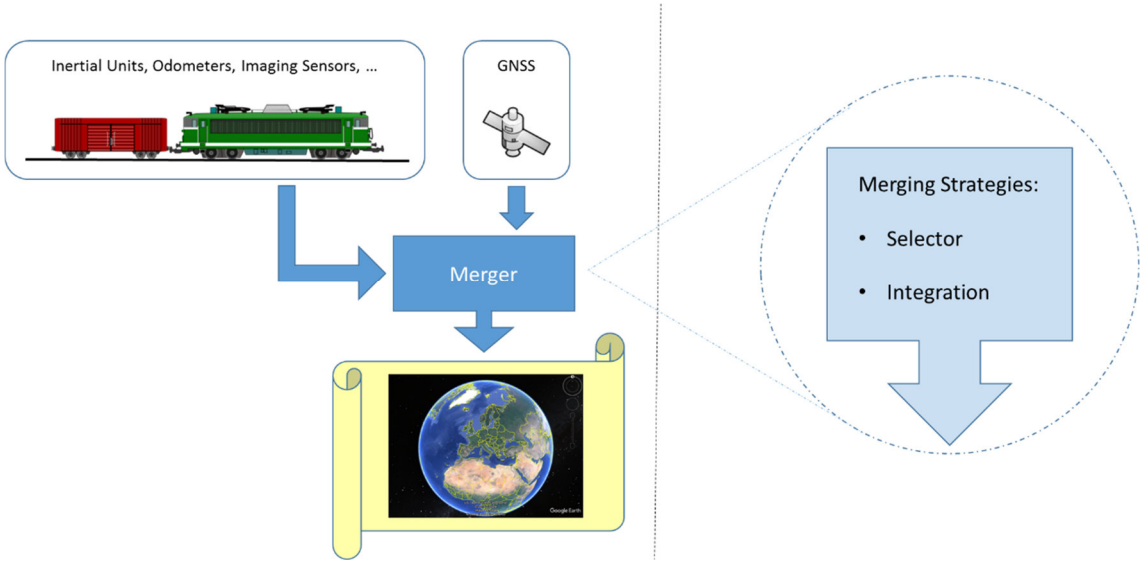

Figure 61. Multi-sensor Navigation System

The main limitation for the position fixing method is the fact that they rely on devices that are external to the user (like the GNSS satellites) which availability and continuity cannot be guaranteed. On the other hand, the dead reckoning, relying only on the equipment itself, is able to provide a continuous navigation solution (except for hardware failures) starting from a known position. On the other side of the coin, the main problems to face when dealing with dead reckoning systems is the error growth over the time. In fact, as explained in [57], the final position is obtained as the sum of a set of relative position measurements; each one of these contributions is effected by an error. As suggested in [57], since the characteristics of the two approaches are complementary, to get the benefit of both of them, a dead reckoning technique can be integrated with a position fixing technology. One of the most studied dead reckoning approach is the INS (Inertial Navigation System. An INS is composed by a set of inertial sensors called IMU (Inertial Measurement Unit) and a navigation processor. The IMU is generally constituted by accelerometers and gyroscopes. By integrating the output of the sensors, the navigation processor is able to estimate the position, the velocity and the attitude of the object. The accelerometers measure the accelerations of the body while the gyroscopes measure the angular rates. In a strapdown INS, the IMU is aligned with the navigation body. Another system that can be considered as dead reckoning is the rail odometer. The odometer estimates the travelled distance by observing the rotation of the wheels. In literature, many studies have addressed the data fusion problem. An interesting approach has been proposed in [58] where the jointly use of GPS, odometers and inertial sensors for train positioning has been described. Data fusion has been carried out by means of a Kalman Filter. In [59], authors exploited a

particle filter to perform the data fusion between GNSS and odometer data by exploiting the track constraints to improve the filter. Another approach has been provided in [60], where authors proposed an approach based on the combination between statistical pattern recognition techniques and multiple-model vehicle tracking. In [47], authors defined a method to integrate odometer with GNSS data making use of weighted median filters.

7.2 INERTIAL NAVIGATION SYSTEM

7.2.1 IMU Errors Model

As introduced in the introduction, an IMU is composed by a set of accelerometers and a set of gyroscopes (typically one accelerometer and one gyroscope for each of the three axes). As explained in [61], It is possible to address four main categories of IMUs. Some examples of error characteristics are shown in Figure 62. A it has been shown in [62] and [63], the output of an inertial sensor can be expressed as:

$$S_m = \left(1 - S_f\right) S_t + b \tag{133}$$

Where:

S_m is the sensor output or measurement

S_t is the true value that the sensor measures (i.e. true system accelerations or angular rates)

b is the bias

S_f is the scale factor of the sensor

More in detail, the bias term can be decomposed in the sum of different contributions:

$$b(t) = b_0 + b_1(t) + w(t) \tag{134}$$

IMU Grade	Example	Approximate Cost	Gyro Errors		Accelerometer Errors	
Consumer	Invensense ITG-3200 (gyro) STM LIS3LV02DL (acc)	Board ~38£ (gyro) Board ~31£ (acc)	Bias Scalefactor Noise	4 (°/s) n/a 22,8(°/√hr)	Bias Scalefactor Noise	<100 (mg) n/a n/a
Low-cost	Microstrain 3DM-GX3-25	~1.7k£	Bias Scalefactor Noise	0.2 (°/s) <2000 ppm 3.5 (°/√hr)	Bias Scalefactor Noise	<10 (mg) <2000 ppm n/a
Tactical	Honeywell HG1700	~14k£	Bias Scalefactor Noise	1-10 (°/hr) 150 ppm 0.125-0,5 (°/√hr)	Bias Scalefactor Noise	1-2 (mg) 300 ppm n/a
Navigation	Honeywell CIMU	~60k£	Bias Scalefactor Noise	0.0035 (°/hr) 5 ppm 0.0025(°/√hr)	Bias Scalefactor Noise	0.05 (mg) 100 ppm n/a

Figure 62. IMUs grades

Where:

b_0 is a null-shift bias that can be estimated online

$b_1(t)$ is a component of the bias that is function of the time

$w(t)$ is the sampling noise

According to [63], both b_0 and the sampling noise can be modelled by observing long term data acquired in zero input condition. More in details, the average of the long term data can be considered an estimation for b_0 while the standard deviation (provided that the sampling rate is much more higher than the maximum frequency content of the process $b_1(t)$) can represent the standard deviation of a band limited white noise that can be used to model the process $w(t)$. The most difficult component to model is the $b_1(t)$. As suggested in [62], this contribution can be modelled as a first order Markov process:

$$\dot{b}_1(t) = -\frac{1}{\tau} b_1(t) + w_{b1}(t) \tag{135}$$

τ is time constant

$w_{b1}(t)$ is the process driving noise

To described the process, as in [63], it is necessary to determine the time constant and the standard deviation; in fact, the power spectral density of the driving noise can be written as

$$Q_{w_{b1}-} = \frac{2}{\tau}\sigma_{b1}^2 \tag{136}$$

The time constant can be estimated by observing the autocorrelation of the detrended data. The detailed procedure can be found in [63].

7.2.2 Dead Reckoning with INS

In a strapdown system, the IMU is aligned with the body. The first problem to be solved is the attitude determination. In fact, the accelerometers and gyroscopes provide measurement in the body frame, a coordinate system that is defined to have these characteristics:

1) The origin is set in the centre of mass of the navigating object
2) Y axis (roll axis) is directed towards the forward direction
3) X axis (pitch axis) is directed along the transverse direction
4) Z axis (yaw axis) indicates the vertical direction closing the right handed tern

A schematic representation of body frame is depicted in Figure 63. The relative orientation of body frame and the reference frame is determined by solving the attitude. One possible approach is to make use of Euler angles. As in [64], the main idea behind Euler statement is that the relative orientation between two coordinate systems can be defined by means of three independent angles. These three angles, in navigation, are defined as yaw, pitch and roll.

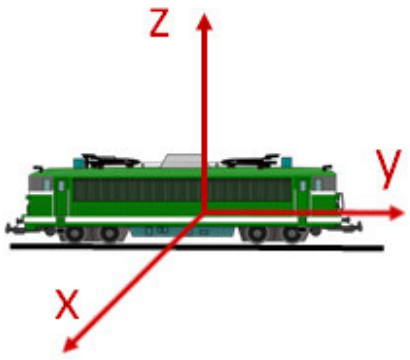

Figure 63. Body frame

According to [63] there are two main limitations in the use of Euler angles; in fact, the time evolution of the angles is described by means of non-linear differential equations containing transcendental functions. Moreover, if the pitch angle is 90 degrees (or equivalently -90 degrees), the yaw and the roll can be exchanged giving origin to a singularity situation. An alternative solution is constituted by the use of quaternions. As explained in [63], as a consequence of the Euler's theorem, the total effect of a series of rotation can be described by a single rotation around an axes $\hat{e}$ of magnitude Φ. The relative orientation of the body frame and the reference frame is known when both the magnitude of the rotation and the direction of the rotation axis are specified. Particularly, the quaternions are defined as:

$$\mathbf{q} = \begin{pmatrix} q_0 \\ \vec{q} \end{pmatrix} \tag{137}$$

Where:

$$\begin{aligned} q_0 &= \cos(\Phi) \\ \vec{q} &= \Phi \hat{e} \end{aligned} \tag{138}$$

In a strapdown inertial system, the accelerometers measure the accelerations components along the three axes of the body frame. The position increment (in the body frame), if the gravity has been correctly compensated, can be retrieved by integrating the accelerations twice.

$$\vec{p} = \int_o^t \int_o^t \vec{a}(\tau)\, d\tau \tag{139}$$

To express the position movement in the navigation frame, the output of the gyroscopes can be integrated to evaluate the current attitude. However, both accelerometers and gyroscopes have biases that can lead to error that grows with the time. Moreover, the local gravity effect must be estimated because it influences the measurement of the accelerometers. The analytical model can be found in more details in [63]. A schematic representation of the basic INS functioning is depicted in Figure 64. As it is possible to see in the picture, being a dead reckoning approach, the state of the system is derived by the state at the previous step.

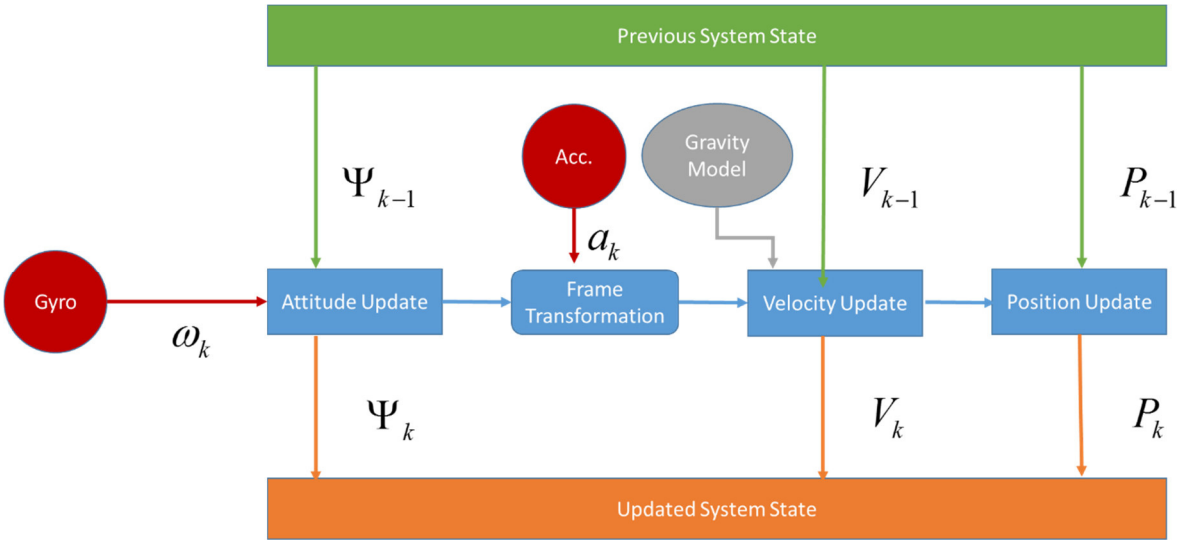

Figure 64. INS functioning scheme at a glance

This means that in order to be able to provide a navigation solution at the first step, the system must be initialized. As stated in [57], initial position and velocity must be provided by an external sensor (e.g. GNSS) while for the attitude initial pitch and roll can be estimated by observing inertial data (see [57] for description of the initialization procedure).

7.2.3 GNSS/INS Data Fusion

As stated in [57], since INS and GNSS technology have complementary characteristics both in terms of benefits and in terms of drawbacks, the integration between these two techniques is able to provide a solution that exploits the benefits of both approaches. Particularly, the drift of the INS can be mitigated by means of the GNSS observation while the continuity of the INS can be exploited to provide a solution even in those areas not covered by the signal in space. There are several kind of integration architectures. One possible solution is the loosely coupled approach where the GNSS data is used to provide a PVT solution that is the input for the data fusion block. Another possible approach is the tightly coupled integration where the input of the integration module is represented by the GNSS raw measurements. There is also a third solution called ultra-tightly coupled where the data fusion is performed at signal tracking level. The loosely coupled approach is the easiest because the GNSS block performs a PVT estimation regardless of the INS solution and its output is used to estimate and compensate the errors of the IMU. This solution is therefore appealing in case of system extension. In fact, just to give an exemplum, if a system has been designed to work only with GNSS, it is possible

to design a fusion block that takes as input the PVT estimation obtained with the GNSS and process INS data to provide a loosely couple integration. Generally, a modification in one of the blocks (e.g. new algorithms to perform the PVT or to assess the Signal in Space integrity) does not need to be propagated in the other block or in the fusion block.

7.3 DEAD RECKONING IN TRAIN POSITIONING

7.3.1 Introduction to Cardinal Heading

As it has been introduced in the previous sub-section, the INS relies on the dead reckoning approach. In fact, starting from a known point (estimated with an external sensor like a GNSS receiver) it is able to track the movements and the rotation of the object (the train in this case). The initial pitch and roll of the vehicle can be estimated by comparing the accelerometers output with the local gravity evaluation [65]. Anyway, for the initial heading (yaw) an external sensor is needed (like a magnetometer or a compass). Being aboard a train, there is an important simplification to the navigation problem. In fact, the rolling stock is constrained to ride along a curve which can be referred as 'Track'. This means that by the knowledge of the train position along the track, it is possible to predict the heading of the train. Particularly, the train heading will be equal to the track direction in the point where the train is. The ambiguity of π can be solved exploiting the other sensors (for example by the accelerometers). In other words, the problem of train positioning can be reduced to a mono-dimensional problem. This concept is quite similar to the track constraint approach used in the GNSS segment. The heading aiding in the INS technology is a technique already experimented in the pedestrian navigation field. In that framework, the CHAIN (Cardinal Heading Aided Inertial System) has been introduced [61],[65],[66]. The main assumption behind the cardinal heading technique is that looking at a building map, most of the environments have rectangular shapes with the corridors and rooms parallel to the external walls [61]. A schematic representation of a building plan is depicted in Figure 65. The user that is moving in such environment, as stated by authors in [66], is constrained to move parallel to one of the cardinal headings of the building. Then, representing the building as a set of polygons, it is possible to verify, among the four possibilities available in the selected polygon, which heading has a higher probability to be the correct one. Once the heading has been chosen, this information can be used in the Kalman filter. This approach can be used also in many urban areas (like Manhattan in New York) where the streets and avenues makes a rectangular mesh.

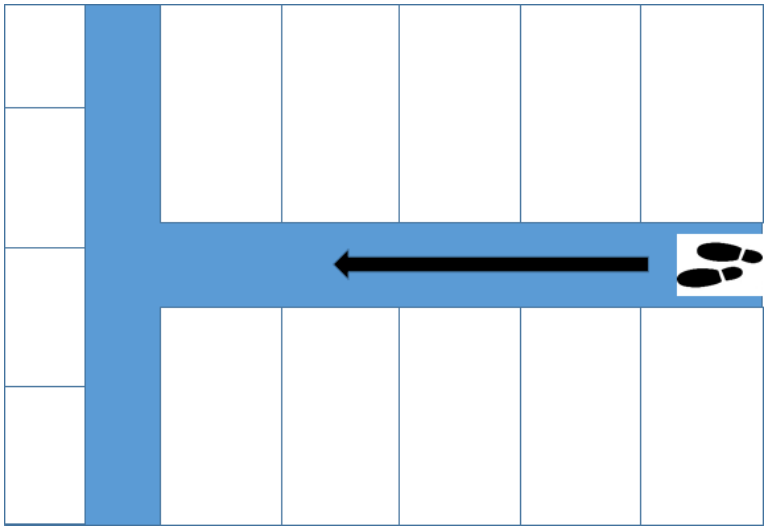

Figure 65. Building map

7.3.2 Cardinal Heading in a train environment

Considering a railway scenario, as it has been introduced above, the train heading in a certain epoch must be equal (with an ambiguity of 180° that can be solved by knowing motion verse) to the heading of the track in the point where the IMU is located at that epoch. In this scenario is possible to consider the track as a combination of straight segments and then build a set of polygons around the track. In essence, when the estimated position falls inside a polygon, the heading of the segment of track corresponding to that polygon is assumed as the correct one. Even in this case, the 180° ambiguity is resolved knowing the motion direction. The main part of the research has been focused on the definition of the procedure to automatically build a polygon map around the track. At this aim, the test track of The Nottingham Geospatial Building has been used. For many details on the test track, please refer to [67]. Figure 66 shows the plot of the track with the associated polygon map. In the figure, the black curve represents the track, while the coloured blocks are the polygons. In this particular scenario, the track used has the peculiarity to be closed loop. In this case, the last point of the track and the first one are consecutives. The polygons can be obtained following the following procedure:

1) Let $\vec{l}$ and $\vec{r}$ be two lines parallel to the track line $\vec{t}$ located respectively on the left side and of the right side at a distance w
2) A set of N points t_i belonging the track line $\vec{t}$ are selected

3) For each point t_i with $i \in \{1,2,...,N\}$, the vertex $v_{l,i}$ is determined by the intersection of $\vec{l}$ and the segment orthogonal to $\vec{t}$ passing through t_i
4) For each point t_i with $i \in \{1,2,...,N\}$, the vertex $v_{r,i}$ is determined by the intersection of $\vec{r}$ and the segment orthogonal to $\vec{t}$ passing through t_i
5) Each polygon is described by the four vertices $v_{l,i}$, $v_{r,i}$, $v_{r,i+1}$ and $v_{l,i+1}$ with $i = \{1,2,...,N-1\}$
6) If the track is a closed loop, an N-th polygon can be described by the four vertices $v_{l,N}$, $v_{r,N}$, $v_{r,1}$ and $v_{l,1}$

The procedure foresees two possibilities for the polygon selections: deploy by step and deploy by gap. In the first approach, firstly a set of points belonging to the track are acquired, and then, the polygons are built according to a subset of that points obtained by decimation. In the second approach, the polygons are built according to a fixed separation among them. The number of polygon considered as well as the lines displacement w must be tuned according to line characteristics. For example, in a curve area (where the heading changes) is more convenient to have more polygons than in a straight area where the heading remains constant.

7.4 CONCLUSIONS

The analysis of the techniques to guarantee the continuity in the areas where the GNSS signals are not available is still an on-going activity. The aim of this section was to highline the key points and the issues that must be faced addressing that problem. In this framework, the use of inertial sensors has been considered as one of the possible candidate solutions. A theoretical background about this technology has been drawn as well as a possible solution to export the results introduced by cardinal heading in the pedestrian navigation has been described. The analysis of the impact of such techniques in the railway environment is not been completed yet.

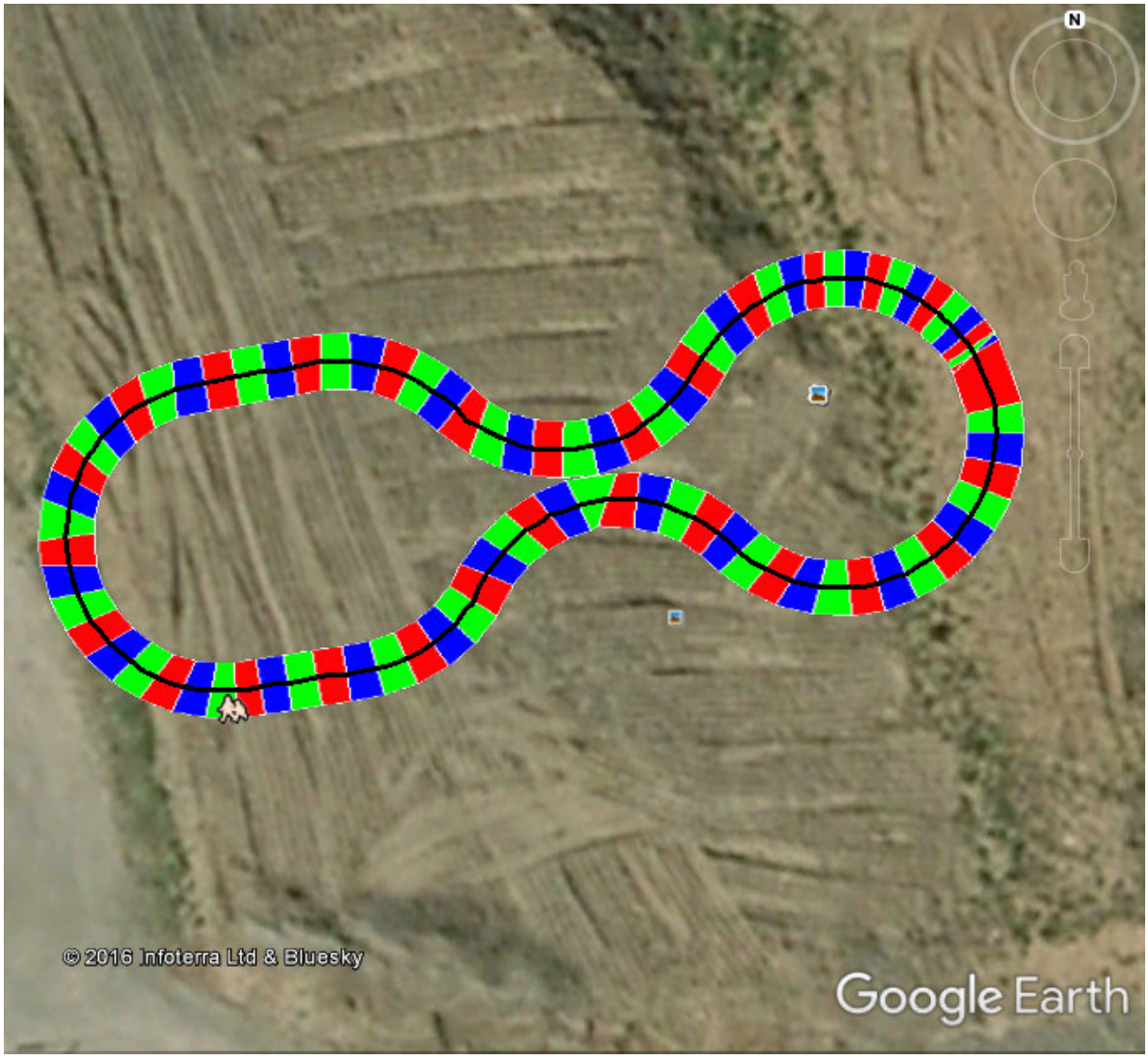

Figure 66. Polygon map around the track

8 CONCLUSIONS

8.1 FINAL CONSIDERATIONS

In this thesis, the introduction of GNSS technology into the ERTMS framework has been investigated. Particularly, the overall system architecture that has been addressed foresees: a space segment, a ground segment and a user segment. Space segment is constituted by the orbiting satellites (GNSS, SBAS, and so on), the Ground segment is essentially an augmentation network with integrity monitoring functions and finally the user segment is represented by the train fleet. This work has focused on ground segment and user segment. More in details, the object of the research has been the study of satellite navigation aspects as well as the analysis of typical issues concerning the railway environment and applications. Particularly, the theoretical aspects on GNSS that have been discussed are the comparison between local and wide architectures, the modelling of the ionospheric delay, the analysis and the definition of integrity monitoring techniques and the design of a "2-tier" augmentation network. Augmentation and integrity monitoring play a key role in the system due to the high requirements that must be fulfilled. In first analysis, it has been shown how a local area augmentation network, thanks to the high correlation of the local errors, can be used to increase system performance. On the other hand, the wide area augmentation, having a wider "footprint" has the opportunity to better identify non-local issues. To take advantage of both kinds of augmentation, a hybrid architecture (labelled as "2-tier") has been proposed. Concerning the integrity monitoring, techniques for the signal in space integrity assessment have been described. Moreover, a technique to assess a Reference Station integrity monitoring in the "2-tier" augmentation network has been analysed. For all these approaches, the exclusion thresholds have been determined according to Neyman-Pearson criterion and the performance analysis have been carried out in terms of miss detection probability. To simulate the behaviour of the procedures in presence of faults, synthetic anomalies have been produced and used. Simulation result highlighted the proposed approaches correctly assessed the SIS and RS integrity monitoring. Concerning railway application track, three main applications have been addressed: train positioning along the line, track discrimination and train integrity assessment. The first problem is the determination of the position of the train on the line (progressive mileage). This operation, according to [1], can be performed by explicitly considering that the train is constrained to lie on a line (i.e. the track). From the state of the art, two techniques have

been selected: track constrained differential GNSS and track constrained relative positioning. Both techniques have been described and a dataset acquired during a car measurement campaign has been used to compare the performance of the two estimators in terms of position estimation error. Simulation results have shown as the magnitude of the position error in both approaches, in the considered scenario, has been mostly lower than 2 meters with a similar temporal trend. By using the double difference approach, it is possible to cancel out all the issues related to the satellite clock offset. In presence of multiple tracks, the track determination problem can be separated by the mileage estimation problem. Inspired by an approach at the state of the art, two methodologies have been proposed. Heading for L3, a problem that assumes fundamental relevance is the train integrity. In this study, the train integrity problem has been described and a solution for the detection of decoupling event has been provided for both single and multi-constellation environments. By means of Monte Carlo simulations it has been shown how the information provided by more than one constellation can be fused in both coherent and incoherent ways. The performance analysis has been carried out for all of the approaches. In the last section of the thesis, the problem of grating system continuity even in those area where the GNSS signals are either not present or too degraded to be used to provide reliable solutions. This analysis has focused on the introduction of a multi-sensor approach. An introduction on the dead reckoning as well as on the inertial navigation systems has been performed. Finally, an approach to exploit the track constraint in the inertial navigation framework has been illustrated.

8.2 Wrap up and Future works

The analysis carried out in this thesis has shown how the introduction of the GNSS technology into the railway sector represents a high promising innovation. The research that has been followed and that has been presented here looks toward both L2 and L3 levels of ETCS. The main perspective of this work is to realize cost-effective solutions for the modernization of the railway line. The market slice that can benefit of this study is quite huge if it is considered that in Europe there are many low traffic regional lines. The aspect that needs more investigation up to now is the introduction of the alternative navigation system to provide solutions even in those areas where the GNSS technology cannot guarantee a reliable solution. The kind of sensors selected as well as the data fused approach can be different depending on the application. In parallel to this research track, there are some ongoing activities related to the

design of new integrity monitoring algorithms as well as the definition of augmentation strategies.

9 REFERENCES

[1] A. Neri, A. Filip, F. Rispoli, and A.M. Vegni, "An Analytical Evaluation for Hazardous Failure Rate in a Satellite-based Train Positioning System with reference to the ERTMS Train Control Systems", ION GNSS 2012, Nashville, TN, U.S.A.

[2] Website: http://www.ertms.net/?page_id=40.

[3] A. Neri, F. Rispoli, and P. Salvatori, "AN ANALYTICAL ASSESSMENT OF A GNSS-BASED TRAIN INTEGRITY SOLUTION IN TYPICAL ERTMS LEVEL 3 SCENARIOS", ENC 2015, Bordeaux, France.

[4] A. Neri, F. Rispoli, P. Salvatori, and A.M. Vegni, "A Train Integrity Solution based on GNSS Double-Difference Approach", ION GNSS+ 2014, Tampa, FL, U.S.A.

[5] A. Neri, S. Sabina, R. Capua, P. Salvatori, "Track Constrained RTK for Railway Applications", ION GNSS+ 2016, Portland, OR, U.S.A.

[6] A. Basili, L. Ghisu, F. Rispoli, B. Buttarazzi, A. Neri and F. Senesi, "A roadmap for the adoption of space assets for train control systems: The Test Site in Sardinia", *2012 IEEE First AESS European Conference on Satellite Telecommunications (ESTEL)*, Rome, 2012, pp. 1-6

[7] A. Neri, C. Stallo, A. Coluccia, V. Palma, M. Ruggieri, F. Toni, P. Salvatori and F. Rispoli, On Board Unit Design For Train Positioning by GNSS, Eusipco 2013, Marrakech, Morocco.

[8] V. Palma, P. Salvatori, C. Stallo, A. Coluccia, A. Neri and F. Rispoli, "Performance evaluation in terms of accuracy positioning of local augmentation and integrity monitoring network for railway sector,"Metrology for Aerospace (MetroAeroSpace), 2014 IEEE , vol., no., pp.394,398, 29-30 May 2014

[9] A. Filip, F. Rispoli, "SIL 4 Compliant Train Location Determination System Based on Dual-Constellation EGNOS-R Interface for ERTMS/ETCS", CERGAL 2014, Dresden, 8-9 July 2014.

[10] A. Filip, and F. Rispoli, “Safety concept of GNSS based train location determination system SIL 4 compliant for ERTMS/ETCS,” in *Proc. of ENC-GNSS 2014*, Rotterdam, Netherlands.

[11] A. Filip, J. Beugin, and J. Marais, “Safety Concept of Railway Signaling Based on

Galileo Safety-of-Life Service," *COMPRAIL*, Toledo, Spain, Sept 15-17, 2008, pp. 103-112.

[12] A. Neri, R. Capua, and P. Salvatori, "High Integrity Two-tiers Augmentation Systems for Train Control Systems," ION Pacific PNT 2015, Honolulu, HI, U.S.A.

[13] P. K. ENGE, R. M. KALAFUS AND M. F. RUANE, "DIFFERENTIAL OPERATION OF THE GLOBAL POSITIONING SYSTEM," IN IEEE COMMUNICATIONS MAGAZINE, VOL. 26, NO. 7, PP. 48-60, JULY 1988

[14] E. D. KAPLAN, C. J. HEGARTY. UNDERSTANDING GPS, PRINCIPLES AND APPLICATIONS, SECOND EDITION. ISBN-10: 1-58053-894-0.

[15] J. A. Klobuchar, "Ionospheric Time-Delay Algorithm for Single-Frequency GPS Users," in *IEEE Transactions on Aerospace and Electronic Systems*, vol. AES-23, no. 3, pp. 325-331, May 1987.

[16] J. Blanch, T. Walter and P. Enge, "Satellite Navigation for Aviation in 2025," in *Proceedings of the IEEE*, vol. 100, no. Special Centennial Issue, pp. 1821-1830, May 13 2012.

[17] K. BORRE ET AL. A SOFTWARE-DEFINED GPS AND GALILEO RECEIVER A SINGLE-FREQUENCY APPROACH. ISBN-10: 0-8176-4390-7.

[18] A. Neri, F. Rispoli, P. Salvatori, "A GNSS based solution for supporting virtual block operations in train control systems," in Navigation World Congress (IAIN), 2015 International Association of Institutes of , Prague, Czech Rebublic, vol., no., pp.1-6.

[19] P. Enge, "Local area augmentation of GPS for the precision approach of aircraft," in Proceedings of the IEEE, vol. 87, no. 1, pp. 111-132, Jan 1999

[20] P. Enge, T. Walter, S. Pullen, Changdon Kee, Yi-Chung Chao and Yeou-Jyh Tsai, "Wide area augmentation of the Global Positioning System," in *Proceedings of the IEEE*, vol. 84, no. 8, pp. 1063-1088, Aug 1996.

[21] P. Salvatori, A. Neri, C. Stallo, V. Palma, A. Coluccia and F. Rispoli, "Augmentation and Integrity Monitoring Network and EGNOS performance comparison for train positioning," *2014 22nd European Signal Processing Conference (EUSIPCO)*, Lisbon, 2014, pp. 186-190.

[22] S. Shanmugam, J. Jones, A. MacAulay and A.J. Van Dierendonck, "Evolution to modernized GNSS ionospheric scintillation and TEC monitoring", Position Location and Navigation Symposium (PLANS), 2012 IEEE/ION, vol., no., pp.265-273, 23-26

April 2012.

[23] J.A. Klobuchar, "Ionospheric Effects on GPS", GPS World April 1991.

[24] P. Salvatori, A. Neri, C. Stallo and F. Rispoli, "Ionospheric incremental delay models in railway applications," *Metrology for Aerospace (MetroAeroSpace), 2015 IEEE*, Benevento, 2015, pp. 251-255.

[25] J. Vukovic and T. Kos, "Ionospheric time-delay models for GNSS", ELMAR, 2011 Proceedings, vol., no., pp.191-194, 14-16 Sept. 2011.

[26] N. Jakowski and M.M. Hoque, "Ionospheric range error correction models", Localization and GNSS (ICL-GNSS), 2012 International Conference on , vol., no., pp.1,6, 25-27 June 2012

[27] S.M. RADICELLA, "THE NEQUICK MODEL GENESIS, USES AND EVOLUTION", ANNALS OF GEOPHYSICS VOL. 52, N. 3/4, AUGUST 2009.

[28] Website: http://sidc.oma.be/esww3/presentations/Session4/Arbesser.pdf

[29] N. CROCETTO, F. PINGUE, S. PONTE, G. PUGLIANO AND V. SEPE, "IONOSPHERIC ERROR ANALYSIS IN GPS MEASUREMENTS," ANNALS OF GEOPHYSICS, VOL. 51, N. 4 AUGUST 2008.

[30] B. Muhammad, E. Cianca and A.M. Salonico, "Multi GNSS Advanced RAIM: An availability analysis," in Metrology for Aerospace (MetroAeroSpace), 2014 IEEE , vol., no., pp.28-33, 29-30 May 2014

[31] M. Joerger and B. Pervan, "Solution separation and Chi-Squared ARAIM for fault detection and exclusion," in Position, Location and Navigation Symposium - PLANS 2014, 2014 IEEE/ION , vol., no., pp.294-307, 5-8 May 2014

[32] J. Blanch, T. Walter, P. Enge and V. Kropp, "A simple position estimator that improves advanced RAIM performance," in Aerospace and Electronic Systems, IEEE Transactions on , vol.51, no.3, pp.2485-2489, July 2015

[33] S. Paternostro, T. Moore, C. Hill, J. Atkin and H. P. Morvan, "Evaluation of advanced receiver autonomous integrity monitoring performance on predicted aircraft trajectories,"*2016 IEEE/ION Position, Location and Navigation Symposium (PLANS)*, Savannah, GA, 2016, pp. 842-856

[34] T. Walter, J. Blanch, M. Joerger and B. Pervan, "Determination of fault probabilities for ARAIM,"*2016 IEEE/ION Position, Location and Navigation Symposium (PLANS)*, Savannah, GA, 2016, pp. 451-461.

[35] M. Joerger and B. Pervan, "Fault detection and exclusion using solution separation and chi-squared ARAIM," in *IEEE Transactions on Aerospace and Electronic Systems*, vol. 52, no. 2, pp. 726-742, April 2016.

[36] S. Matsumoto, S. Pullen, M. Rotkowitz, and B. Pervan, “GPS Ephemeris Verification for Local Area Augmentation System (LAAS) Ground Stations”, in Proc. of ION GPS 2009, September 14-17, 2009, Nashville, TN, USA.

[37] J. Blanch, T. Walter, P. Enge., “Fast Multiple Fault Exclusion with a Large Number of Measurements”, in Proc. of Institute of Navigation (ION) International Technical Meeting, 2015, Dana Point, California., USA.

[38] H. Tang, S. Pullen, P. Enge, L. Gratton, B. Pervan, M. Brenner, J. Scheitlin, P. Kline, "Ephemeris type a fault analysis and mitigation for LAAS,"*Position Location and Navigation Symposium (PLANS), 2010 IEEE/ION*, Indian Wells, CA, USA, 2010, pp. 654-666.

[39] L. Heng, G. X. Gao, T. Walter and P. Enge, "GPS Signal-in-Space Integrity Performance Evolution in the Last Decade," in *IEEE Transactions on Aerospace and Electronic Systems*, vol. 48, no. 4, pp. 2932-2946, October 2012.

[40] B. Pervan and L. Gratton, "Orbit ephemeris monitors for local area differential GPS," in *IEEE Transactions on Aerospace and Electronic Systems*, vol. 41, no. 2, pp. 449-460, April 2005.

[41] L. Gratton, B. Pervan and S. Pullen, "Orbit ephemeris monitors for category I LAAS,"*Position Location and Navigation Symposium, 2004. PLANS 2004*, 2004, pp. 429-438.

[42] Y. C. Lee, "Receiver autonomous integrity monitoring (RAIM) capability for sole-means GPS navigation in the oceanic phase of flight," *Position Location and Navigation Symposium, 1992. Record. 500 Years After Columbus - Navigation Challenges of Tomorrow. IEEE PLANS '92., IEEE*, Monterey, CA, 1992, pp. 464-472.

[43] A. Neri, F. Rispoli, P. Salvatori, “The perspective of adopting the GNSS for the evolution of the european train control system (ERTMS): a roadmap for standardized and certifiable platform“, ION GNSS+ 2015, Tampa, FL, U.S.A

[44] V. D. Colceriu, T. Ştefănuţ, V. Bâcu and D. Gorgan, "Generating accuracy and integrity aware train movement maps using GNSS and MEMS sensors," *Intelligent Computer Communication and Processing (ICCP), 2015 IEEE International*

Conference on, Cluj-Napoca, 2015, pp. 441-446

[45] A. Neri, V. Palma, F. Rispoli and A. M. Vegni, "Track constrained PVT estimation based on the double-difference technique for railway applications," *21st European Signal Processing Conference (EUSIPCO 2013)*, Marrakech, 2013, pp. 1-5

[46] Neri, A.M. Vegni, and F. Rispoli, "A PVT Estimation for the ERTMS Train Control Systems in presence of Multiple Tracks" in Proc.of ION GNSS 2013, September 16-20, 2013, Nashville, TN, USA

[47] A. Neri, S. Sabina, U. Mascia, "GNSS and odometry fusion for high integrity and high available train controlsystems", ION GNSS+ 2015, Tampa, FL, U.S.A

[48] W. Jian, S. Wei, C. Bo-gen and C. De-wang, "The Algorithm of Track Occupied Identification Base on HMM," Computer Science and Information Engineering, 2009 WRI World Congress on, Los Angeles, CA, 2009, pp. 493-497

[49] L. R. Rabiner, "A tutorial on hidden Markov models and selected applications in speech recognition," in *Proceedings of the IEEE*, vol. 77, no. 2, pp. 257-286, Feb 1989

[50] W. Jian, L. Jiang, S. Wei and C. Bai-gen, "Track occupied identification method based on switch curve information," Intelligent Vehicles Symposium, 2009 IEEE, Xi'an, 2009, pp. 994-997

[51] Y. Xi-Hui, W. Jian, C. Bai-gen and S. Wei, "A novel automatic track identification algorithm based on LTS-Hausdorff distance," *2011 14th International IEEE Conference on Intelligent Transportation Systems (ITSC)*, Washington, DC, 2011, pp. 1984-1988

[52] Van Trees, Detection, Estimation, and Modulation Theory, Part III, John Wiley & Sons, 2001

[53] A. Neri, F. Rispoli and P. Salvatori, " A CENELEC SIL-4 compliant approach for discriminating railway parallel tracks based on EGNOS-GALILEO receivers," ENC-GNSS 2014, Rotterdam, The Netherlands, 2014

[54] H. Scholten, R. Westenberg, and M. Schoemaker, "Sensing train integrity," in Proc. of IEEE Sensors, pages 669-674, Los Alamitos, Oct. 2009

[55] S. Oh, Y. Yoon, K. Kim, and Y. Kim, "Design of Train Integrity Monitoring System for Radio based Train Control System," in Proc. of 12th International Conference on Control, Automation and Systems, Oct. 17-21, 2012, Jeju Island, Korea

[56] K. M. Betts, T.J. Mitchell, D.L. Reed, S. Sloat, D.P. Stranghoener, and J.D. Wetherbee,

"Development and Operational Testing of a Sub-meter Positive Train Localization System," in Proc. of IEEE/ION PLANS 2014, Monterey, CA, May 2014, pp. 452-461

[57] P. D. Groves, Principles of GNSS, Inertial, and Multisensor Integrated Navigation Systems, ISBN-13: 978-1-58053-255-6

[58] P. Ernest, R. Mazl and L. Preucil, "Train locator using inertial sensors and odometer," IEEE Intelligent Vehicles Symposium, 2004, 2004, pp. 860-865

[59] J. Liu, B. g. Cai and J. Wang, "Track-constrained GNSS/odometer-based train localization using a particle filter," 2016 IEEE Intelligent Vehicles Symposium (IV), Gothenburg, 2016, pp. 877-882

[60] C. Chen, J. Ibanez-Guzman and O. Le-Marchand, "Low-cost loosely-coupled GPS/odometer fusion: a pattern recognition aided approach," 2008 11th International Conference on Information Fusion, Cologne, 2008, pp. 1-6

[61] Abdul Rahim, Khairi "Heading drift mitigation for low-cost inertial pedestrian navigation". [Ph. D. diss.], University of Nottingham, 2012

[62] Warren S. Flenniken IV, John H. Wall, David M. Bevly, " Characterization of Various IMU Error Sources and the Effect on Navigation Performance", ION GNSS 2005, Long Beach, CA, U.S.A.

[63] Demoz, Gebre-Eqziabher, "Design and Performance Analysis of a Low-Cost Aided Dead Reckoning Navigator", [Ph. D. diss.], Stanford University, 2004

[64] R. Pio, "Euler angle transformations," in IEEE Transactions on Automatic Control, vol. 11, no. 4, pp. 707-715, Oct 1966

[65] K. Abdulrahim, C. Hide, T. Moore and C. Hill, "Aiding MEMS IMU with building heading for indoor pedestrian navigation," 2010 Ubiquitous Positioning Indoor Navigation and Location Based Service, Kirkkonummi, 2010, pp. 1-6

[66] J. Pinchin, C. Hide and T. Moore, "A particle filter approach to indoor navigation using a foot mounted inertial navigation system and heuristic heading information," 2012 International Conference on Indoor Positioning and Indoor Navigation (IPIN), Sydney, NSW, 2012, pp. 1-10

[67] Website: https://www.nottingham.ac.uk/grace/facilities/testtrack.aspx

[68] Website: http://www.sogei.it/flex/cm/pages/ServeBLOB.php/L/IT/IDPagina/780